DOE/MC/30098 -- 5235
(DE96011328)

FT-IR Spectroscopic Investigation Of Fireside Deposits In A Pilot-Scale Combustor

Topical Report
December 1995

February 23, 1996

Work Performed Under Contract No.: DE-FC21-93MC30098

For
U.S. Department of Energy
Office of Fossil Energy
Morgantown Energy Technology Center
Morgantown, West Virginia

By
University of North Dakota
P.O. Box 9018
Grand Forks, ND 58202

DISCLAIMER

DOE/MC/30098 -- 5235
(DE96011328)
Distribution Category UC-103

FT-IR spectroscopic Investigation Of Fireside Deposits In A Pilot-Scale Combustor

Topical Report
December 1995

Work Performed Under Contract No.: DE-FC21-93MC30098

For
U.S. Department of Energy
Office of Fossil Energy
Morgantown Energy Technology Center
P.O. Box 880
Morgantown, West Virginia 26507-0880

By
University of North Dakota
Energy & Environmental Research Center
P.O. Box 9018
Grand Forks, N.D. 58202-9018

TABLE OF CONTENTS

LIST OF FIGURES

IR SPECTROSCOPIC INVESTIGATION OF FIRESIDE DEPOSITS IN A PILOT-SCALE COMBUSTOR

EXECUTIVE SUMMARY

Successful operation of conventional, as well as advanced, coal combustion systems depends on controlling and minimizing the development of ash fouling and slagging, i.e., fireside deposits. The development of these deposits depends not only on combustion design and operating conditions, but also on the composition and quantity of inorganic species in the coal. The increasing demand for control and mitigation of ash deposition in combustion boilers necessitates refined and advanced technologies. As a means of optimizing the control strategy, a distinct need exists to obtain improved and faster identification of imminent ash deposition. New advanced spectroscopic techniques offer the potential to achieve this goal.

An accessory for a Fourier transform infrared (FT-IR) spectrometer was designed to monitor deposit formation in the convective pass of a pilot-scale combustor. This accessory, the infrared emission sampling probe (IESP), provides a means to monitor infrared emissions produced inside the furnace duct. The probe is designed to fit into a standard optical access while still providing operator viewing through the port.

Tests involving the collection of emission spectra of ash deposits on the furnace duct and deposition probes under coal-fired operating conditions of the combustor were conducted on two coals using the IESP probe. The IR monitoring of ash deposits was evaluated using Antelope subbituminous and Illinois No. 6 bituminous coals.

Data collected using the IESP indicate that the current instrument configuration offers promise for application as a deposit thickness monitor. No information could be obtained on deposit chemistry during formation using this configuration of the IESP; however, several improvements in the instrument can be made that will make it more effective in the measurement of deposit chemistry.

The capability of FT-IR for remotely monitoring deposit thickness has been demonstrated. After some refinement of the optical interface and development of turnkey software, further investigation of the infrared emissions of ash deposits can be done. The development of the FT-IR technique coupled with the IESP can be continued to advance the capabilities for determining deposit chemistries in situ. In addition, for the application of remote IR measurements to deposit thickness, a simple optical instrument can be developed using the concept of a two-wavelength measurement. The new instrument will be much less complicated to construct and operate than an FT-IR spectrometer and may be a hand-held device similar to an optical pyrometer.

IR SPECTROSCOPIC INVESTIGATION OF FIRESIDE DEPOSITS IN A PILOT-SCALE COMBUSTOR

1.0 INTRODUCTION

Successful operation of conventional as well as advanced coal combustion systems depends on controlling and minimizing the development of ash fouling and slagging, i.e., fireside deposits. The development of these deposits depends not only on combustion design and operating conditions, but also on the composition and quantity of the inorganic species in the coal.

Coals contain several minerals, and low-rank coals contain organically associated cations that vary in their association, size, and position relative to one another and in their composition. In the course of combustion, the major inorganic constituents directly affect chemical and physical transformations, such that inorganic species are initially partitioned into gaseous, liquid, and solid intermediates. The state of these intermediates depends on temperature, time, and their location in the combustion system, which also affect the nature and the extent of their deposition. Thus the type of deposit varies throughout the boiler system. For example, silicates will be deposited in the section containing the secondary superheater and suspended surfaces (900°–1200°C, 1650°–2200°F), whereas sulfates will be deposited later in the cooler region (<900°C, <1650°F) of the reheater and primary superheater section. The silicate and sulfate phases affect initiation, growth, and strength development of deposits.

The increasing demand for control and mitigation of ash deposition in combustion boilers requires refined and advanced technologies. As a means to optimize the control strategy, a distinct need exists to obtain improved and faster identification of imminent ash deposition. New advanced spectroscopic techniques offer the potential to achieve this goal.

Various researchers have reported for several decades the dependence of the radiative properties of ash deposits on deposit morphology and chemistry (1, 2). In addition, it is known that many chemical species found in deposits emit in characteristic bands. Recent spectroscopic studies on samples of fly ash and deposits, together with in situ measurements at laboratory, pilot, and industrial scale now indicate the technical possibilities for monitoring deposits (3–13). The spectroscopic information relates to aspects of deposit chemistry, its physical structure, and radiative heat-transfer properties. This information may be used to monitor the progressive character of deposits in utility boilers as they initiate, grow, and develop strength and to assist in decisions related to boiler operation, such as sootblowing.

Baxter and coworkers (10) demonstrated that Fourier transform infrared (FT-IR) spectroscopy can be applied to monitoring the formation of ash and slag deposits in a laboratory-scale combustion system. The focus of this program is to extend the work of Baxter and others by applying the technique of FT-IR emission spectroscopy to a more practical setting. An instrument has been designed at the Energy & Environmental Research Center (EERC) to allow monitoring of combustion deposits in a viewing geometry similar to one common in conventional combustion systems.

During the course of this project, Professor Terry Wall (Department of Chemical Engineering, University of Newcastle, NSW, Australia), acting as consultant, produced a literature review on the radiative properties of ash deposits. This review is included as Appendix D.

2.0 OBJECTIVES

The goal of the work was to assess the feasibility of applying FT-IR spectroscopy to determine the mineral species responsible for fouling and slagging deposits in a pilot-scale coal-fired combustor.

Specific objectives were as follows:

- To design and construct an optical transfer system to focus the infrared emissions from the slag deposit as it forms on the heat-transfer surface in the furnace on to the FT-IR emission sampling port
- To monitor and record the infrared emissions from the ash deposits as they form on the heat-transfer surface
- To analyze the infrared spectra collected from emissions of ash deposits
- To determine the physical significance of infrared spectra collected as a result of ash deposition on the heat-transfer surface of the furnace
- To identify a positive correlation between ash buildup and infrared emission, which will determine the viability of developing FT-IR spectroscopic monitoring as a control technology for minimizing ash buildup in furnace ducts of full-scale coal-fired boilers at power generation utilities

3.0 EXPERIMENTAL

3.1 Design and Construction of the Infrared Emission Sampling Probe

An accessory for a Bomem MB-100 FT-IR spectrometer was designed to monitor deposit formation in the convective pass of a pilot-scale combustor. The accessory, i.e., the infrared emission sampling probe (IESP), provides a means to monitor the infrared emissions produced inside the furnace duct. The probe is designed to fit into a standard optical access while still providing operator viewing through the port. This was accomplished by modifying the optical access mounting plate to incorporate a compression fitting, which mounts the IESP and has a 25.4-mm quartz window mounted to allow a view offset of 38.1 mm along the central axis of the IESP. A mirror is mounted at 45 degrees to the quartz window surface to facilitate viewing access. A drawing of the optical access is shown in Appendix B.

Figure 1 shows an overhead view of the viewing geometry for the deposit in the high-temperature section. The three circles represent the deposition probes that collect ash and

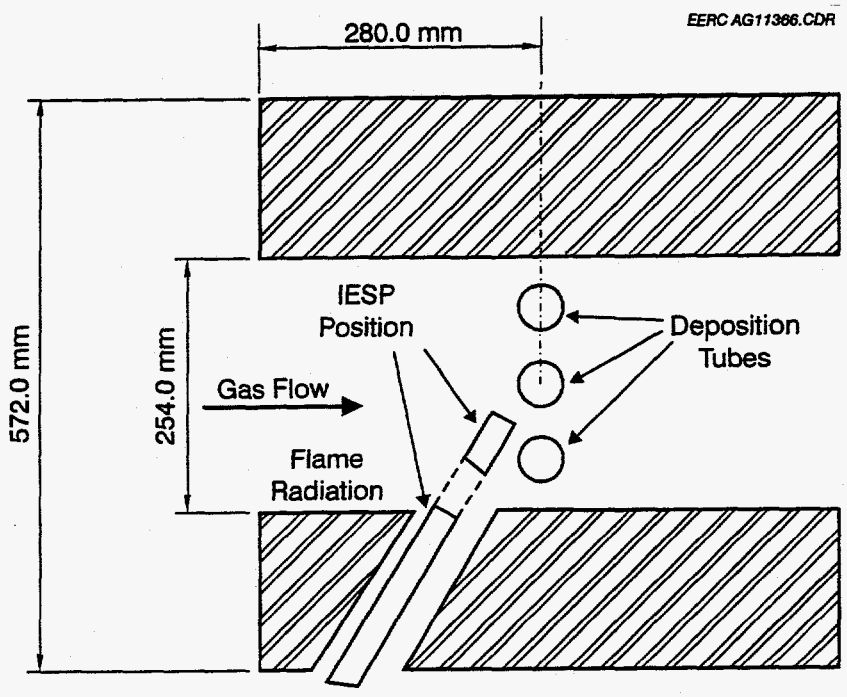

Figure 1. Overhead view of furnace duct with deposition tubes.

slag deposits during furnace operation. The optical access is shown in the lower left portion of the figure. The line extending from the optical access to the deposition probe bank is coincident with the IESP axis.

The IESP consists of the optical section and the outer jacket, which protects the infrared optics when the unit is inserted into the harsh environment of the furnace duct. The following description of the optical portion of the IESP will begin at the input (furnace) end:

The objective lens, commercially fabricated from cadmium telluride, is a 12.5-mm-diameter planoconvex lens with a 125-mm effective focal length. The lens focuses the view of the FT-IR onto the heat-transfer tube, where ash and slag deposits are collected. Mounted in a specially designed holder, the lens is bathed by a constant flow of nitrogen across that face of the lens exposed to the furnace duct. The purpose of the nitrogen flow is to cool the surface of the lens and to sweep contacting particles from the surface. The lens assembly is attached to an 8-mm- diameter gold-surface light pipe 1 m in length, and that pipe is connected to a 1:4 beam expander to adapt the 8-mm-diameter light pipe to a 32-mm section. The 32-mm light pipe, in turn, is connected directly to the Bomem FT-IR spectrometer emission port. The lens focuses the view of the IR spectrometer onto the heat-transfer tube, where ash and slag deposits are collected.

During tests, the entire optical path of the assembly from spectrometer to lens is under constant nitrogen purge. The protective jacket consists of two concentric tubes that encase the 8-mm light pipe and lens assembly. The innermost tube, 24 mm in diameter, is designed to be under continuous nitrogen purge. This nitrogen flow passes between the lens assembly and the

innermost tube to provide positive pressure at the lens assembly to keep deposits from forming on the probe end. Between the inner and outer protective jacket tubes is a constant flow of cooling water to maintain the temperature of the instrument optics. Two thermocouples are incorporated into the probe; the first monitors the back face of the objective lens, and the second monitors probe cooling water temperature.

The overall function of the IESP is to focus the spectrometer optics on the slag deposit as it forms on the heat-transfer surface in the furnace for the narrow-field collection of emissions from the ash deposit. Engineering drawings of the IESP are given in Appendix B. Figure 2 depicts the IESP and Bomem FT-IR during operation in the pilot plant.

3.2 Collection of Emission Spectra from Thermally Excited Authentic Mineral Samples

Spectra of authentic quartz, barite, and kaolinite mineral samples were obtained at four temperatures: 200°, 400°, 600°, and 800°C (390°, 750°, 1100°, and 1470°F) using a graphite furnace with a platinum sample support and the prototype of the IESP. The sample support and graphite furnace were configured and samples treated in manner similar to that described in Vassallo et al. (12). The spectra collected are shown in Appendix C. The collected spectra correspond to those reported by Vassallo et al. (12) and also on a structural basis agree with published transmission spectra of mineral standards. Note that there are shifts in specific peak frequencies when the reference spectra are compared to those collected in the laboratory, since the emission spectra are taken at elevated temperatures.

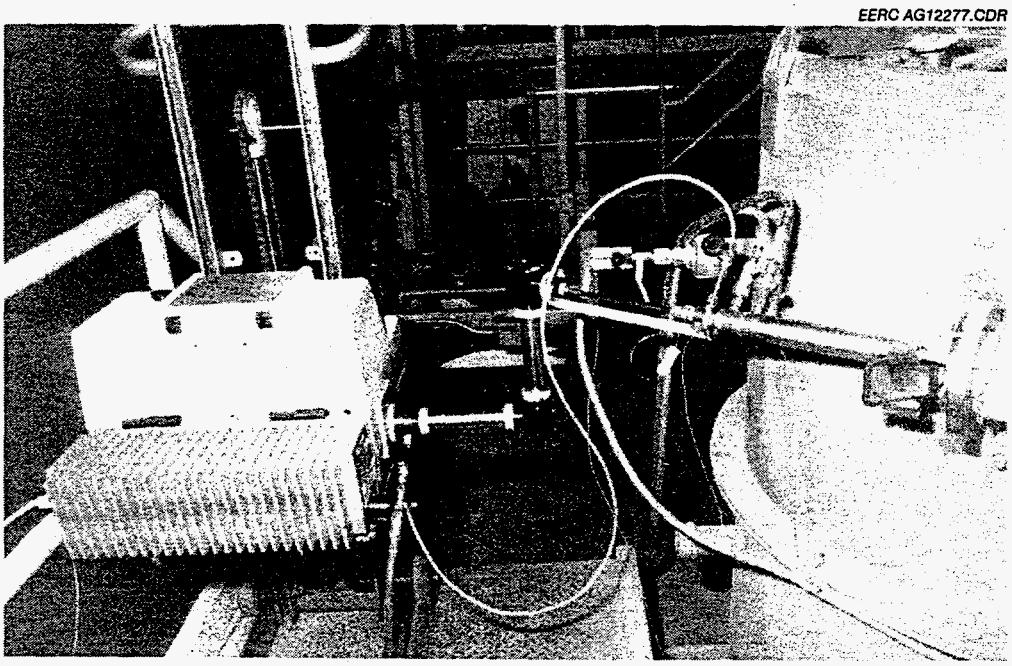

Figure 2. Photograph of IESP during pilot plant operation.

3.3 Collection of Emission Spectra from Pilot-Scale Combustion of Coal

Real-time analytical data on the formation of ash deposits on heat-exchange surfaces were obtained from in situ monitoring of infrared emissions from coal combustion deposits during their development in the convective section of a pilot-scale combustor under full-load conditions. A specially designed accessory, the IESP, allows the radiation from deposits to be transferred for collection by an IR spectrometer. The probe, consisting of an optical section and a protective outer jacket, fits into a standard optical access of a furnace duct but still permits operator viewing through the port.

Tests involving the collection of emission spectra of ash deposits on the furnace duct and deposition probes under coal-fired operating conditions of the combustor were conducted on two coals using the IESP probe described in Section 3.1. The IR monitoring of ash deposits was evaluated using Antelope subbituminous and Illinois No. 6 bituminous coals.

An isometric drawing of the EERC combustion test facility (CTF) is shown in Figure 3. The furnace capacity is approximately 34 kg/hr (75 lb/hr, 550,000 Btu/hr) of pulverized coal. The combustion chamber is 760 mm (30 in.) in diameter, 2.4 m (8 ft) high, and refractory-lined for combustion testing. A detailed description of the CTF is given in Appendix A.

Coal is pulverized remotely in a hammer mill pulverizer, targeted to a size of 70% less than 200 mesh. A detailed description of the combustion parameters for the test is given in Appendix A.

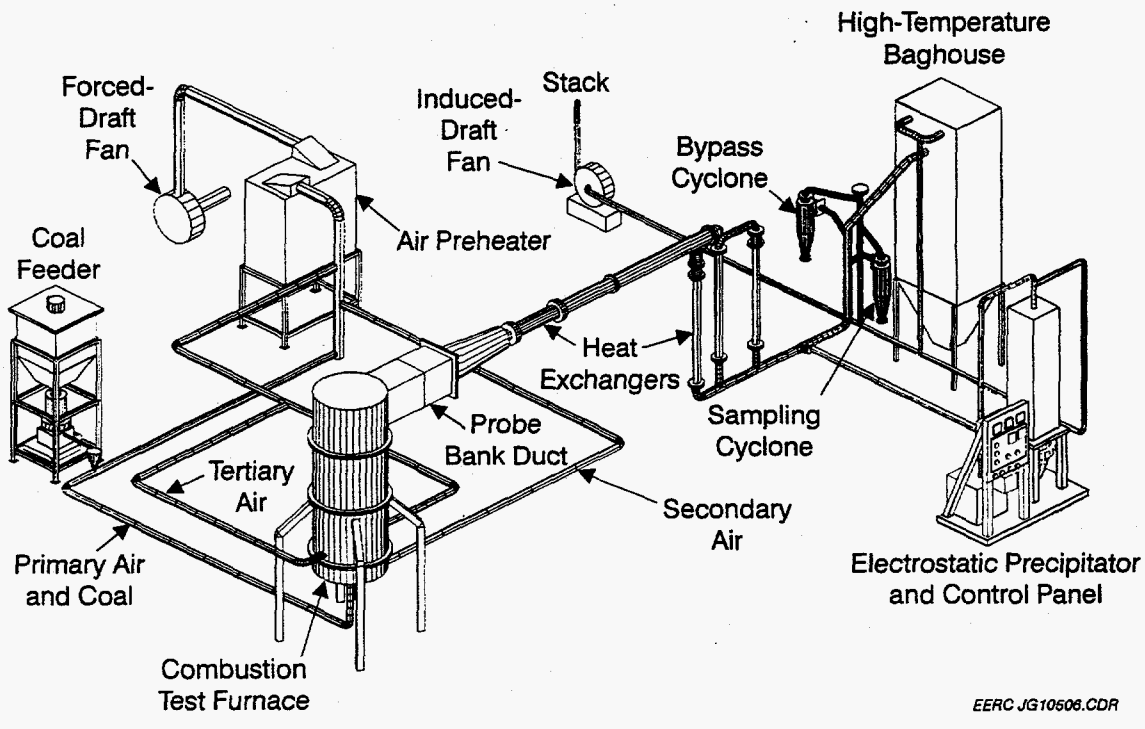

Figure 3. Combustion test facility and auxiliary systems.

Figure 4 shows the structure of the ash-fouling test probe bank on which the IR-emitting deposits formed. The IESP is focused on the center probe. The probe bank is located on a hinged door to facilitate its removal from the furnace for inspection and cleaning. The three fouling probes used during this combustion test were constructed of 42-mm (1.66-in.)-outside-diameter Type 304 stainless steel pipe and were cooled with compressed air. Each probe has two thermocouples embedded in its upstream edge to measure metal temperature. One of the thermocouples on each probe is attached to a temperature recorder–controller that regulates the cooling air to the probe. The surface temperature of each probe was maintained at 530°C (1000°F). The gas velocity between the tubes is normally about 7.6 m/s (25 ft/s) when low-rank coals are fired. The gas temperature entering the probe bank is normally maintained at 1090°C (2000°F).

Additional information on the CTF, including the general test method, can be found in Appendix A.

3.4 Feed Coal

Pilot-scale testing of IR monitoring of ash deposition on heat-exchange probes was carried out using coals of two different ranks. Antelope subbituminous coal and a typical Illinois No. 6 bituminous coal were burned under the conditions mentioned in Appendix A. Proximate and ash composition analyses of the coals burned in the CTF to produce the deposits are shown in Appendix E, Table 1. The ash content of the Ante Appendix E lope subbituminous coal from the Powder River Basin in Wyoming is typical of coals from that region. Likewise, the ash content of

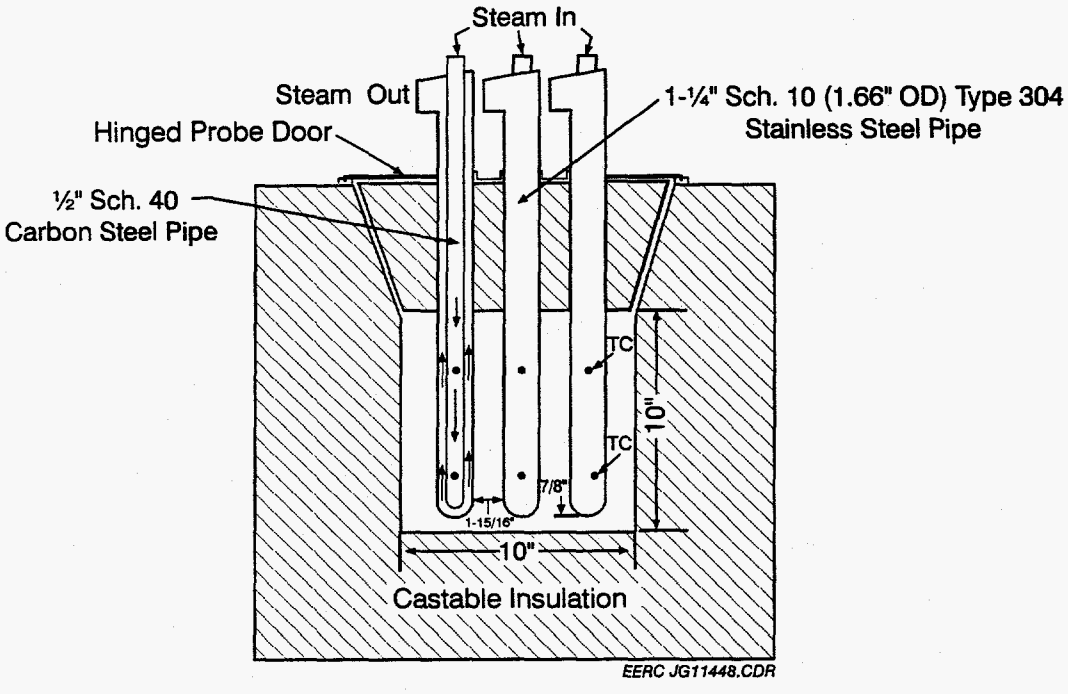

Figure 4. Detail of probe bank construction.

the Illinois No. 6 bituminous coal is typical of coals from Illinois and Indiana. The big difference in the ash composition of the two coals is largely related to the relative amounts of calcium and magnesium (higher in the Antelope coal) and the iron (higher in the Illinois No. 6). Also contained in Appendix E are XRD and XRF analyses of the deposits formed during combustion and observed by the FT-IR–IESP.

4.0 RESULTS

4.1 Preliminary Tests of IESP

Preliminary tests using the IESP were conducted involving the collection of emission spectra of the furnace duct and deposition probes under gas-fired operating conditions of the combustor. For these tests, the planoconvex CdTe lens had not been fabricated, but, instead, a CdTe optical flat was employed, which gave the IESP an acceptance cone half angle of 1.5°. These baseline tests demonstrated the level of background infrared radiation as well as the efficiency of the protective housing of the IESP optics. The combustor (fireside) temperature during gas firing was approximately 1200°C, and the gas temperature in the probe region was 550°C. Figure 5 shows two emission spectra resulting from the FT-IR–IESP probe monitoring. The upper spectrum was taken with the IESP 203 mm from the deposition probe, whereas the lower spectrum was recorded with the IESP 51 mm from the deposition probe. The spectra have the general shape of the Planck blackbody curve. Riding on top are absorbing carbon dioxide gas peaks in the 2200–2350 cm^{-1} region and the water vapor peaks in the regions of 3100–4000 cm^{-1} and 1100–2000 cm^{-1}. Note that

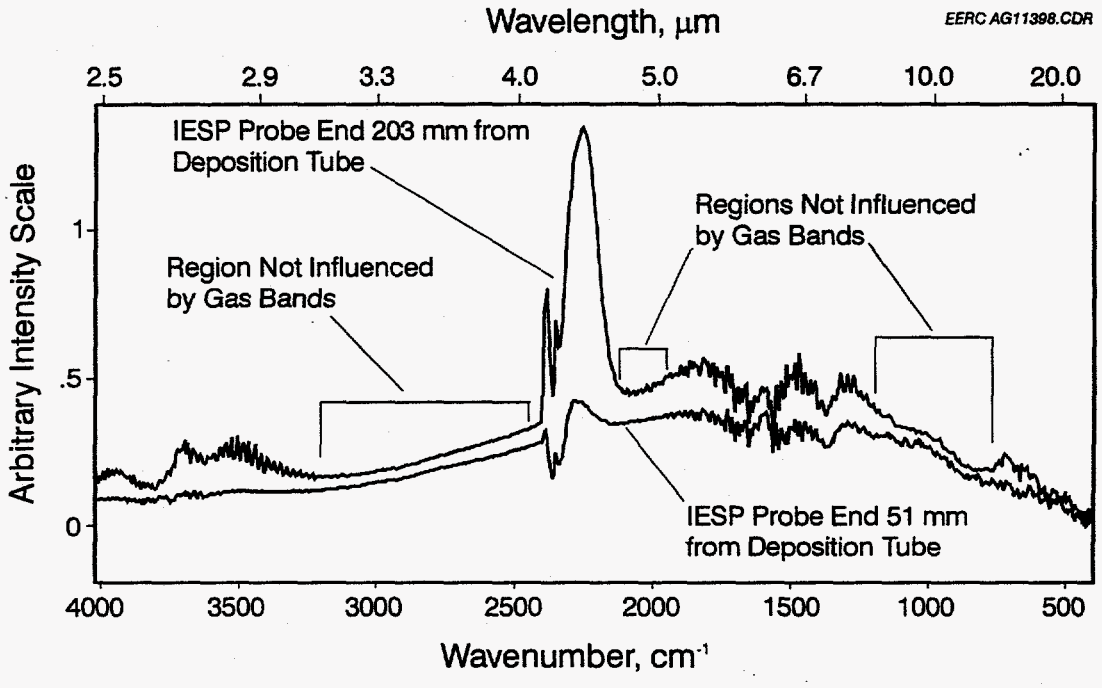

Figure 5. FT-IR spectra of furnace duct under natural gas firing conditions.

as the IESP was moved further from the deposition probe, more of the furnace duct was viewed, allowing collection of more radiant energy, and the overall IR intensity increased. Additionally, as more duct-emanating gases came into view, the intensity of the infrared absorbance for CO_2 and water vapor peaks increased.

4.2 Infrared Emissions from Ash Deposition

The FT-IR–IESP was assembled for measurements in the CTF combustor using coal at full-load conditions. Spectral data were collected from ash deposited on the furnace probes during combustion of Antelope subbituminous coal and Illinois No. 6 bituminous coal. Accumulations of 64 scans were collected at 15-minute intervals over 6 hours of the combustion test. Data reduction included analysis of individual raw spectra and individual IR bands as a function of time. Figure 6 shows the emission infrared spectra of (a) inside of the furnace with deposition tubes removed, (b) clean deposition tubes, and (c) mature deposit on deposition tubes.

Analysis of the data collected with the FT-IR–IESP revealed spectroscopic information indicative of deposit formation and thickness. The results indicate that the instrument is capable of remotely sensing the thickness of deposits by monitoring two wavelengths in the mid-infrared range. The designated wavelengths are: $\lambda_1 = 10\ \mu m$ (1000 cm^{-1}), which shows little variation in intensity over the course of the test (an inactive region to be used as a baseline), and $\lambda_2 = 4.4\ \mu m$ (2272 cm^{-1}), which has intense bands present when the deposition tubes are clean. By taking the

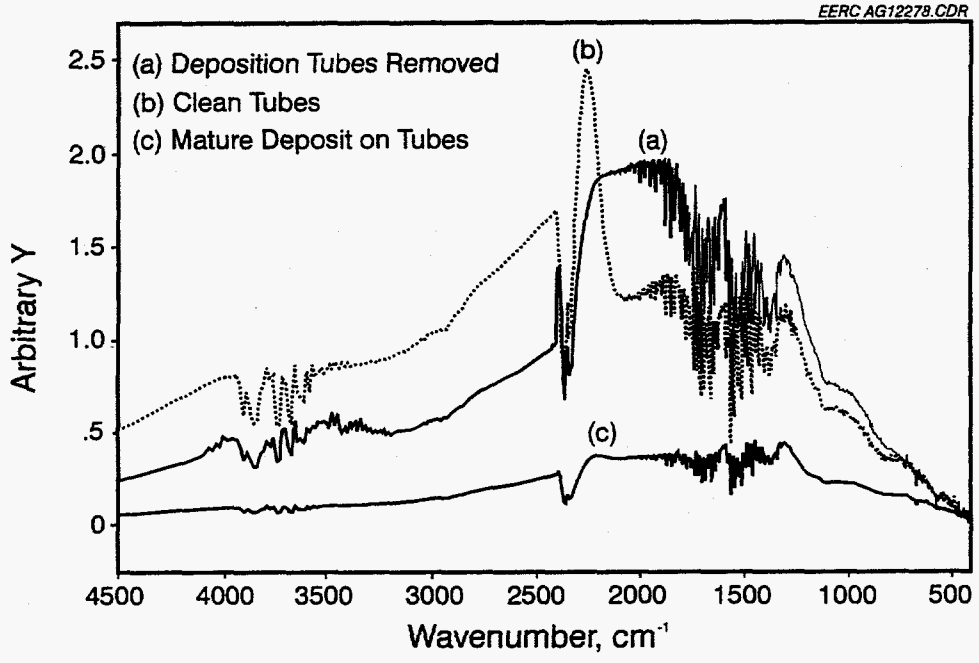

Figure 6. Infrared emission spectra of furnace duct.

ratio of the intensities at λ_1 and λ_2, namely $I_{\lambda 2}/I_{\lambda 1}$, one has an indicator of deposit thickness, since the intensity of λ_2 decreases with increasing deposit thickness. The baseline wavelength at λ_1 is used to account for changes in the ambient infrared radiation. Figures 7 and 8 show the evolution of deposit growth during the pilot-scale tests. Figure 7 illustrates the deposit evolution during a test fired with Antelope coal under normal operating conditions. Figure 8 depicts data taken during a run firing Illinois No.6 coal. The flame temperature during this run was about 95°C (200°F) higher than normal operating conditions (1200°C [2200°F]), and some problems occurred with the coal feeder that contributed to greater fluctuations in the run conditions. The fluctuating conditions may be one reason for the increased variability of the data shown in Figure 8.

The data presented in Figures 7 and 8 represent the evolution of deposit thickness. However, this measurement is confounded by accumulation of very thin deposits on the IESP lens. We have partially corrected for this by taking the ratio of intensity of the wavelength of interest, λ_2, to the intensity of a baseline wavelength, λ_1. Taking the ratio of the intensities at these two wavelengths in this way compensates for the loss of throughput for the objective lens because of the thin layer of deposits formed. Even with loss of lens throughput, there is strong evidence that the intensity observed at λ_2 is correlated with deposit thickness for the following reasons: First, the spectra in Figure 6 show that when the deposition tube (Spectrum a) is removed, the relative intensity at λ_2 is reduced, and when a clean tube is placed in the view of the IESP, the infrared intensity is strongly peaked at λ_2. These findings indicate observed infrared radiation, which correlates to clean deposition tubes. Second, when a mature deposit is present on the deposition tube, the relative intensity is reduced to almost its original value (relative to the surrounding spectral region) at λ_2. Finally, during the course of the final testing (21 June), the deposit was observed falling off the deposition probe twice. During each of these events, the ratio of intensities ($I_{\lambda 2}/I_{\lambda 1}$) increased, indicating a change in deposit thickness (Figure 8).

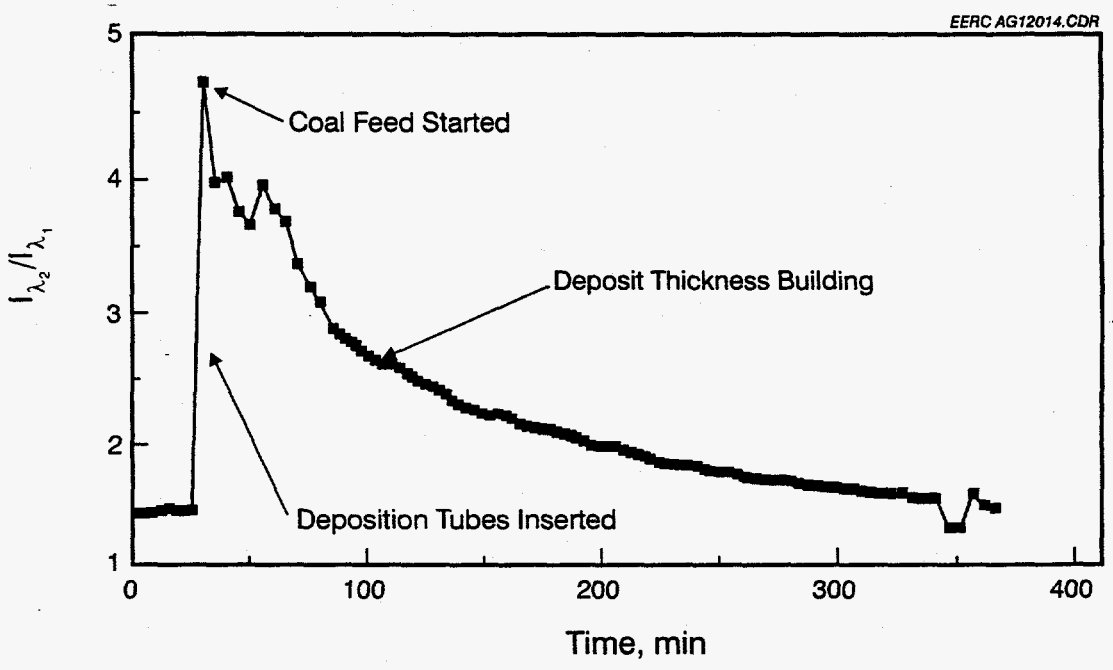

Figure 7. Two-color infrared measurement at 10.0 μm (λ_1) and 4.4 μm (λ_2). Data collected on April 26, 1995 (Antelope).

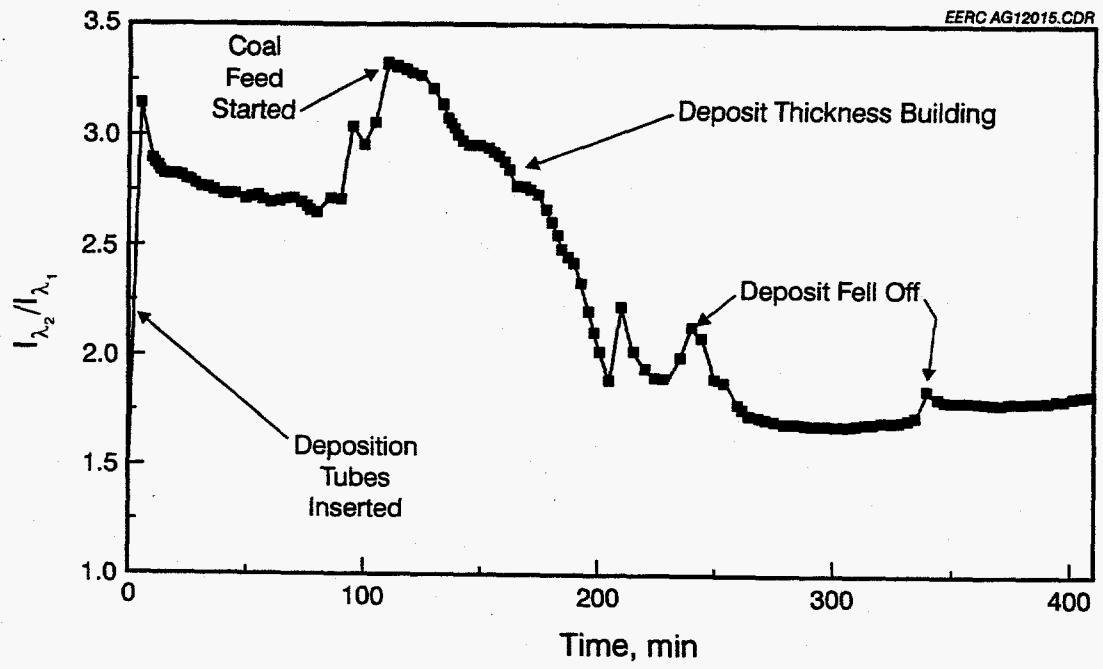

Figure 8. Two-color infrared measurement at 10.0 μm (λ_1) and 4.4 μm (λ_2). Data collected on June 21, 1995 (Illinois No. 6).

5.0 SUMMARY

Data collected using the IESP indicate that the current instrument configuration offers promise in application as a deposit thickness monitor, as evidenced by the data presented in Section 4.0. No information was obtainable on deposit chemistry during formation using this configuration of the IESP. However, several improvements in the instrument can be made to make it more effective in the measurement of deposit chemistry.

6.0 RECOMMENDATIONS

The capability of FT-IR for remotely monitoring deposit thickness has been demonstrated. After some refinement of the optical interface and development of turnkey software, further investigation of the infrared emissions of ash deposits can be undertaken. The development of the FT-IR technique coupled with the IESP can be continued to advance capabilities for the determination of deposit chemistries in situ. The following improvements can be made in the FT-IR–IESP system:

- Addition of a blackbody reference source as a baseline reference for collecting chemical information from deposit emissions

- Modification of the IESP to decouple vibrations from the combustion system to the FT-IR spectrometer

- Modification of the IESP optics to reduce the effects of background infrared radiation from furnace walls

In addition, for the application of remote IR measurements to deposit thickness, a simple optical instrument can be developed using the concept of a two-wavelength measurement, as described in Section 4.0. The new instrument will be much less complicated to construct and operate than an FT-IR spectrometer. A unit could be built as a hand-held device similar to an optical pyrometer.

7.0 PAPERS AND PRESENTATIONS

The following papers and presentations were a result of this work:

- An invited lecture given by T. F. Wall and co-authored by L. L. Baxter, S.P. Bhattacharya, B. C. Young, and A. A. Grisanti, entitled Ash Deposit Properties and Radiative Transfer in Coal-Fired Plants – Current Understanding and New Developments was presented at the Engineering Foundation Conference, Application of Advanced Technology to Ash-Related Problems in Boilers, held at Waterville Valley, New Hampshire, July 16–22, 1995.

- An invited paper, "Ash Deposit Properties and Radiative Transfer in Coal-Fired Plants – Current Understanding and New Developments" authored by T.F. Wall, S.P. Bhattacharya, L.L. Baxter, B.C. Young, and A.A. Grisanti was presented by Professor Terry Wall at the 3rd International Symposium on Coal Combustion Science and Technology, September 18–21, 1995, Beijing, China.

- A technical paper on the work will be submitted to the 26th International Symposium on Combustion in Naples, Italy, August 1996.

8.0 REFERENCES

1. Wall, T.F.; Bhattacharya, S.P.; Zhang, D.K.; Gupta, R.P. "The Properties and Thermal Effects of Ash Deposits in Coal-Fired Furnaces: A Review," *In* Engineering Foundation Conference on the Impact of Ash Deposits in Coal-Fired Furnaces; Taylor and Francis Inc., 1993.

2. Wall, T.F.; Baxter, L.L.; Richards, G.; Harb, J. "Ash Deposits, Coal Blends, and the Thermal Performance of Furnaces," *Journal of Fuel Processing Technology*, **1995**.

3. Solomon, P.R.; Markham, J.R.; Best, P.E.; Yu, Z.Z. "Radiative Properties of Ash and Slag," Advanced Fuel Research, Inc; 1990.

4. Richards, G.H.; Harb, J.N.; Baxter, L.L.; Bhattacharya, S.P.; Gupta, R.P.; Wall, T.F. "Radiative Heat Transfer in PC Fired Boilers - Development of the Absorptive/Reflective Character of Initial Deposits of Walls," Unpublished, 1994.

5. Pang, L.S.K.; Vassallo, A.M.; Phong-Anant, D.; Wilson, M.A. "A Study of Slag in Laboratory, Pilot, and Commercial Scale Furnaces Using FTIR Microscopy, Electron Microscopy and NMR Spectroscopy," *Fuel Processing Technology* **1993**, *33*, 13–32.

6. Markham, J.R.; Solomon, P.R.; Best, P.E. "An FT-IR Based Instrument for Measuring Spectral Emittance of Material at High Temperature," *Rev. Sci. Instrum.* **1990,** *61*, 3700–3708.

7. Markham, J.R.; Best, P.E.; Solomon, P.R.; Yu, Z.Z. "Measurements of Radiative Properties of Ash and Slag by FT-IR Emission and Reflection Spectroscopy," *J. Heat Transfer* **1992**, *114*, 458–464.

8. Goodwin, D.G.; Mitchner, M. "Infrared Optical Constants of Coal Slags: Dependence on Chemical Composition," *J. Thermophysics* **1989,** *3*, 53–60.

9. Clark, G.A.; Holmes, M.J; Vecci, S.J.; Bailey, R.T. "In Situ Measurements of Coal Ash Deposit Optical Properties," Alliance Research Center Report; 1989.

10. Baxter, L.L.; Richards, G.H.; Ottesen, D.K.; Harb, J.N. "In Situ, Real-Time Characterization of Coal Ash Deposits Using Fourier Transform Infrared Emission Spectroscopy," *Energy & Fuels* **1993,** *7*, 755–760.

11. Ahluwalia, R.K.; Im, K.H. "Spectral Radiative Heat-Transfer in Coal Furnaces Using a Hybrid Technique," *J. Institute of Energy* **1994,** *67*, 23–29.

12. Vassallo, A.M.; Cole-Clarke, P.A.; Pang, L.S.K.; Palmisano, A.J. "Infrared Emission Spectroscopy of Coal Minerals and Their Thermal Transformations," *Applied Spectroscopy* **1992,** *46*, 73–78.

13. Vassallo, A.M.; Finnie, K.S. "Infrared Emission Spectroscopy of Some Sulfate Minerals," *Applied Spectroscopy* **1992**, *46*, 1477–1482.

APPENDIX A

DESCRIPTION OF COMBUSTION TEST FACILITIES AND PROCEDURES

DESCRIPTION OF FACILITIES AND PROCEDURES

Research programs have been under way at the Energy & Environmental Research Center (EERC) for more than 25 years to study ash fouling of boiler heat-transfer surfaces in coal-fired utility boilers. A 550,000-Btu/hr pulverized-coal pilot plant test furnace was constructed in 1967 to evaluate the influence of variables, including ash composition, excess air, gas temperature, and tube wall temperatures on ash fouling. Results from this work have shown a strong correlation between ash characteristics and degree of fouling.

The research capabilities of the combustion test facility (CTF) have been enhanced and expanded to provide information on a wide range of combustion-related issues. The many research applications of this pilot-scale combustion equipment over the years have included the following:

- Determining ash-fouling rates and the strength, composition, and structure of fouling deposits.
- Applying sophisticated analytical methods to characterize input coal, ash, and deposits and to correlate coal and ash properties with deposit growth rates and strength development.
- Evaluating the effectiveness of ash-fouling additives.
- Studying particle-size distribution and velocity prior to deposition on convective section heat-transfer surfaces.
- Evaluating combustion characteristics of coal–water fuels.
- Studying high-temperature baghouse operation and performance.
- Evaluating sorbent injection for SO_x control.
- Assessing integrated particulate and SO_x–NO_x control.
- Studying NO_x control using selective catalytic reduction and disposable catalysts.
- Evaluating slagging potential in a simulated wet-bottom firing mode.
- Performing flame stability tests for comparing a particular fuel at full load and under turndown conditions.

COMBUSTION TEST FACILITY

An isometric drawing of the EERC CTF is shown in Figure A-1. The furnace capacity is approximately 75 lb/hr (550,000 Btu/hr) of pulverized lignite. The combustion chamber is 30 inches in diameter, 8 feet high, and refractory-lined for combustion testing of low-rank coals.

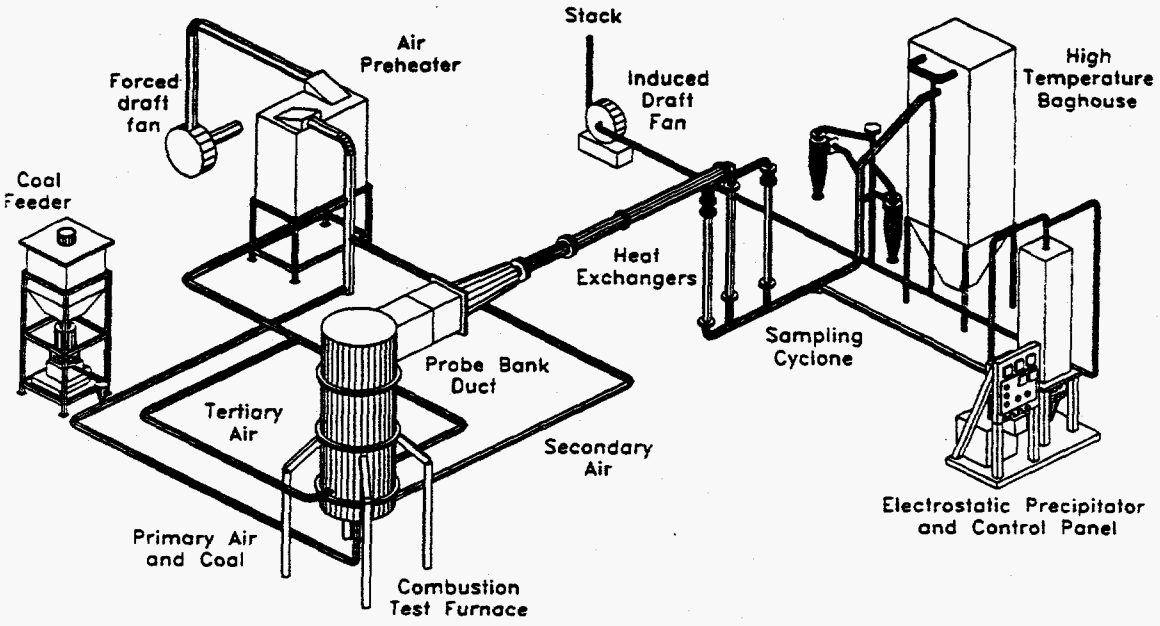

Figure A-1. Combustion test facility and auxiliary systems.

The furnace diameter may be reduced to 26 inches to elevate the temperature entering the convective pass. Furnace exit gas temperatures as high as 2400°F have been achieved during combustion testing in this mode. Most tests are performed using the standard configuration (30-inch inside diameter), with the furnace exit gas temperature maintained at approximately 2000°F for each combustion test.

Coal is pulverized remotely in a hammer mill pulverizer, targeted to a size of 70% less than 200 mesh. The coal is then charged to a microprocessor-controlled weight loss feeder from a transport hopper. Combustion air is preheated by an electric air heater. The pulverized coal is screw-fed by the gravimetric feeder into the throat of a venturi section in the primary air line to the burner. Heated secondary air is introduced through an annular section surrounding the burner. Heated tertiary air is added through two tangential ports located in the furnace wall about 1 foot above the burner cone. The percentages of the total air used as primary, secondary, and tertiary air are usually 10%, 30%, and 60%, respectively. (An adjustable swirl burner, which uses only primary and secondary air with a distribution of approximately 15% and 85%, respectively, was used during flame stability testing). Flue gas passes out of the furnace into a 10-inch-square duct that is also refractory lined. Located in the duct is a vertical probe bank designed to simulate superheater surfaces in a commercial boiler.

Figure A-2 shows the construction of the ash-fouling test probe bank, which is located in a hinged door to facilitate inspection and cleaning. The three fouling probes used during this combustion test were constructed of 1.66-inch-outside-diameter Type 304 stainless steel pipe and were cooled with compressed air. Each probe has two thermocouples embedded in its upstream edge to measure metal temperature. One of the

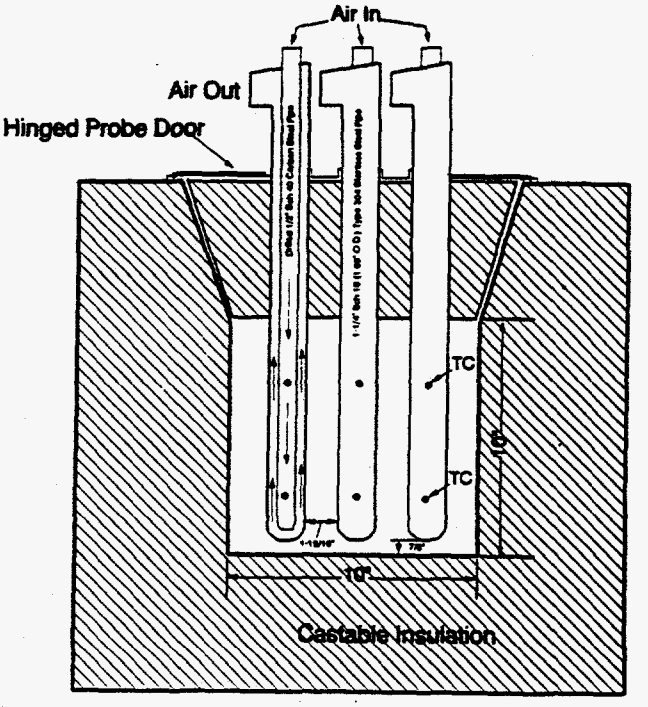

Figure A-2. Detail of probe bank construction.

thermocouples on each probe is attached to a temperature recorder–controller that regulates the cooling air to the probe. The surface temperature of each probe was maintained at 1000°F. The gas velocity between the tubes is normally about 25 ft/s when low-rank coals are fired. The gas temperature entering the probe bank is normally maintained at 2000°F.

After leaving the probe duct, the flue gas passes through a series of water-cooled heat exchangers before being discharged through either an electrostatic precipitator (ESP) or a baghouse.

General Test Method

The relative fouling or other tendencies of test coals are determined by burning coal samples under specified conditions. When starting with a cold furnace, the following 13.25-hour test program is normally used:

	Hours
Preheat on gas	8.00
100% coal firing	5.25
Total	13.25

The coal feed rate is commonly adjusted to keep the flue gas temperature entering the upper duct to the probe bank at 2000°F, with 25% excess air. Coal samples are taken periodically to form a composite sample. Oxygen, carbon dioxide, nitrous oxides, carbon

monoxide, and sulfur dioxide in the flue gas are continuously monitored by recording analyzers. The operating conditions and procedures described above are those normally used when the ash-fouling tendencies of low-rank western coals are studied.

The test furnace has numerous ports that permit observation of the probes and the furnace burner zone during the test run. These ports can also be used for installation of additional test probes, auxiliary measurements, photography, or injection of additives.

At the completion of the test period, the probe door is carefully opened and photographs are taken of the deposit. The deposit is then removed from the probes in two fractions, an inner and an outer layer, and each is weighed and analyzed separately. Normally, the inner white layer weighs less than 10 grams, as compared to 100 to 500 grams for the outer sintered deposit.

The weight of ash deposited on the probe bank during a standard test is used to rank the coal for its relative fouling potential. To ensure that the pilot-scale test results are meaningful for evaluation of ash-fouling potential in full-scale utility boilers, calibration tests were previously conducted with low-rank coals known to produce low and high fouling when used in utility boilers. Comparisons of ash fouling have been made from tests conducted at a number of power stations throughout the western United States: Monticello (Texas Utilities), Big Brown (Texas Utilities), Four Corners (Arizona Public Service Company), St. Clair (Detroit Edison Company), Jim Bridger (Pacific Power and Light), Big Stone (Otter Tail Power Company), Leland Olds (Basin Electric Power Cooperative), and San Miguel (San Miguel Electric Cooperative). Based on these tests, the ash deposit buildup rate on the probe bank was found to be a good indicator of fouling potential. The relationship between deposit weight and a fuel's fouling potential is generally categorized as indicated below:

Deposit Weight, grams	Relative Fouling Potential
0–150	Low
150–300	Medium
Above 300	High

Deposit Strength Tests

The weight of the ash deposit from the probe bank has proven to be a good indicator of the fouling potential for most coals tested in the EERC CTF. Heavy deposits in the 5.25-hour test indicate high deposition rates, which can usually be related to potential ash-fouling problems in utility boilers. However, the deposition rate does not provide an indication of the ease of removal of deposits by sootblowing. Methods to measure deposit tenacity and strength have been reviewed at the EERC, and strength test methods have been developed that appear to provide reliable, reproducible results (1).

Deposit strength is initially assessed by means of the strength rating factor (SRF). This factor is determined from observations made by a pilot plant operator during removal of ash deposits from the probe bank. Deposit hardness and breakability is rated from 1 to 10, with "1" indicating "soft and crumbly" and "10" meaning "hard and unfragmented."

The probe deposit can also be subjected to a laboratory deposit strength evaluation procedure developed at the EERC, which utilizes a drop impactor technique. A known weight is dropped with a measured impact on the sliced face of a 1-inch-long deposit sample. After the drop test, the sample is sieved in a sonic sifter through a series of six screens ranging in size from 5.66 to 0.21 mm. The percentage of each size is determined and, using the procedure from the ASTM Tumbler Test (ASTM Method D441-45), the dust index, friability, and mass mean diameter of the crushed deposit sample are determined. The dust index is indicative of the tendency of the deposit to form dust on impaction. The mass mean diameter is the average size of the fragmented particles after the drop test. An impact resistance value (IRV) is calculated, which adjusts the results of the impactor tests for the test parameters under which they were obtained. The calculation was developed by analysis of a large body of data obtained by this procedure.

Furnace Wall Slag Probes

The combustion test facility at the EERC was originally designed for tests of fouling potential of low-rank coals. As a result, the nominal design values of heat input (550,000 Btu/hr), FEGT (2000°F), and excess air levels (25%) reflect utility industry experience on such fuels. More recently, efforts were made to evaluate slagging potential in the CTF. A slag probe was designed, constructed, and positioned close to the flame region of the furnace, just above the flame. The slagging test probe was water-cooled, to enable monitoring and maintaining surface metal temperatures between 500° and 800°F.

FLAME STABILITY TESTING

Flame stability is assessed by observation of the flame and its relation to the burner quarl as a function of secondary air swirl and operating conditions at full load and under turndown conditions. An International Flame Research Foundation (IFRF)-type adjustable secondary air swirl generator (shown in Figure A-3) uses primary and secondary air at approximately 15% and 85% of the total air, respectively, to adjust swirl between 0 and a maximum of 1.9. Swirl is defined as the ratio of the radial (tangential) momentum to axial momentum imparted to the secondary air by movable blocks internal to the burner and is used to set up an internal recirculation zone (IRZ) within the flame that allows greater mixing of combustion air and coal. Swirl is imparted by moving blocks to set up alternate paths of radial flow and tangential flow, creating a spin on the secondary air stream that increases the turbulence in the near-burner zone. At the fully open position of the swirl block, the secondary air passes through the swirl burner unaffected, and the momentum of this stream has only an axial component (the air enters the combustion chamber as a jet). As the angle of the blocks changes, the air begins to spin or "swirl" and the radial component to the momentum is established, creating the IRZ in the near-burner region. It is the ratio of this radial component of the momentum to the axial component that establishes the quantity defined as "swirl."

The adjustable swirl burner used by the EERC during flame stability testing consists of two annular plates and two series of interlocking wedge-shaped blocks, each attached to one of the plates. The two sets of blocks can form alternate radial and tangential flow channels, such that the air flow splits into an equal number of radial and tangential streams which combine further downstream into one swirling flow as shown in Figure A-4. By a simple rotation of the movable plate, radial channels are progressively

closed and tangential channels opened so that the resulting flux of angular momentum increases continuously, between zero and a maximum value. This maximum swirl depends on the total air flow rate and the geometry of the swirl generator. Swirl can be calculated from the dimensions of the movable blocks (the ratio of the tangential and radial openings of the blocks) or from the measurement of the velocity of the air stream (obtaining both radial and axial components). The following description of that calculation is provided by Beer and Chigier (2):

> When rotating motion is imparted to a fluid upstream of an orifice, the fluid flow emerging from the orifice has a tangential velocity component in addition to the axial and radial components of velocity encountered in nonswirling jets. The presence of the swirl results in the setting up of radial and axial pressure gradients which, in turn, influence the flow field. In the case of strong swirl, the adverse axial pressure gradient is sufficiently large to result in reverse flow along the axis, setting up the internal recirculation zone.

In swirling free jets or flames, both axial flux of the angular momentum (G_φ) and the axial thrust (G_x) are conserved. These can be written as

$$G_\varphi = {}_0\int^R [(Wr)\,\rho U 2\pi r]\,dr = \text{const}$$

$$G_x = {}_0\int^R [U\rho U 2\pi r]\,dr + {}_0\int^R [p 2\pi r]\,dr = \text{const}$$

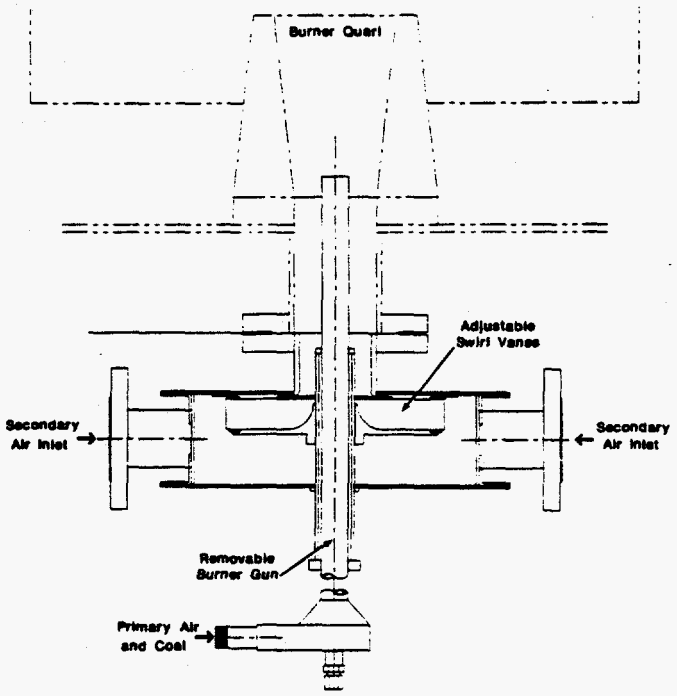

Figure A-3. IFRF adjustable swirl burner.

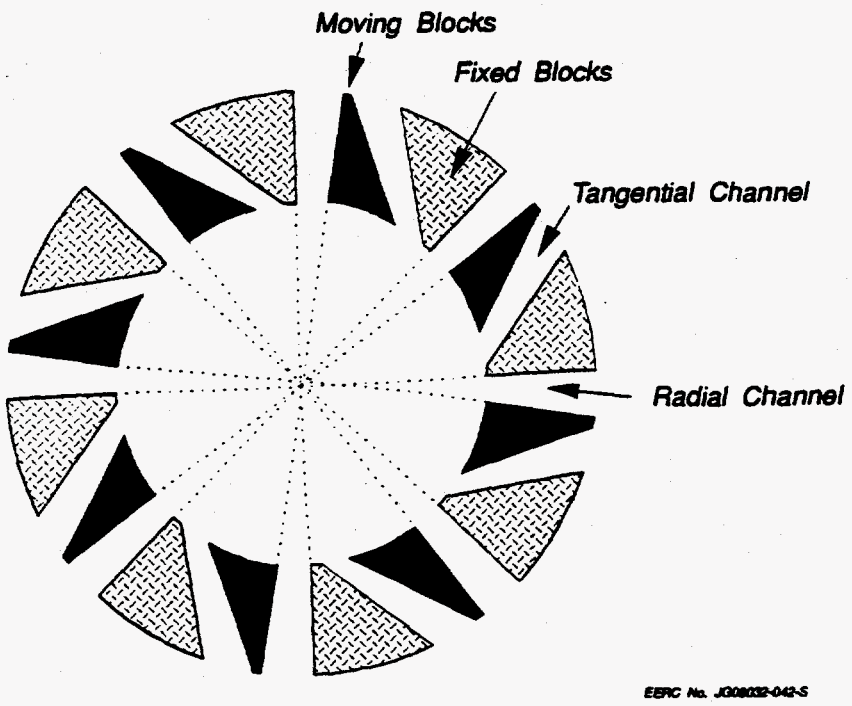

Figure A-4. Cross section of movable block assembly.

where, U, W and p are the axial and tangential components of the velocity and static pressure, respectively, in any cross section of the jet. Since both these momentum fluxes can be considered to be characteristic of the aerodynamic behavior of the flame, a nondimensional criterion based on these quantities can describe the swirl intensity as

$$S = G_\varphi/G_x R \quad (R = \text{exit radius of the burner nozzle}).$$

Experiments have shown that the swirl number S was the significant similarity criterion of swirling jets produced by geometrically similar swirl generators. Other similarity criteria which take account of nonisothermal conditions and of confinement of jet flow by walls can also be applied in conjunction with the swirl number. The calculation of swirl in other types of swirl generators, such as the air registers on a utility boiler, are also described by Beer and Chigier (2), though not mentioned here.

Secondary air swirl is used to stabilize the flame. In the absence of swirl, loss of flame may result, increasing the risk of dust explosion. As swirl is applied to the combustion air, coal particles are entrained in the IRZ, increasing the heating rate of the particles, leading to increased release of volatiles and char combustion. The flame becomes more compact and intense as swirl is increased to an optimum level, which is characterized in the EERC test facility as the point at which the flame makes contact with the burner quarl. Increasing swirl beyond this level can pull the flame into the burner region, unnecessarily exposing metal burner components to the intense heat of the flame and possible combustion in the coal pipe.

Increasing swirl to provide flame stability and increased carbon conversion can also affect the formation of NO_x. The high flame temperatures and increased coal–air mixing associated with increased swirl create an ideal situation under which NO_x may form. In full-scale burners with adjustable vanes, swirl is often increased to reach the optimum condition and then decreased slightly to reduce the production of NO_x.

General Test Method

The general test method sets the burner at its maximum level of swirl and monitors system parameters such as fuel feed rate, excess air, gaseous emissions (CO_2, CO, SO_x, and NO_x), combustor static, and air flow rates. Photographs of the flame and burner zone are then taken through a sight port in the furnace proper just above the burner cone using standard 35-mm film. Flame temperature is also measured using a high-velocity thermocouple (HVT) at a set location in the furnace, and heat flux is monitored using a baseline heat flux probe at the same location. An ash sample is collected at each swirl setting to establish carbon burnout. The swirl setting is then reduced until the flame is visually observed to lift off the burner quarl. At this point, the flame is characterized as unstable under full load conditions (between 600,000 and 650,000 Btu/hr firing rate). Photographs are again taken to record the flame at this setting, temperature and heat flux measurements are taken, and an ash sample is taken once again. Once flame liftoff is established, the optimum swirl setting is located by visual observation of the flame, and measurements are recorded once again.

Flame stability under turndown conditions is characterized by firing the test fuel at reduced load (typically one-half to three-quarters of the full load rate), maintaining the same primary air flow, and adjusting the secondary air flow to meet excess air requirements. The procedure described above is then used to establish flame stability at reduced load.

FLY ASH PARTICULATE CHARACTERIZATION

Fly ash samples are obtained by various means at the inlet and outlet of the pilot plant ESP or baghouse, as shown in Figure A-1. EPA Method 5 is used to establish particulate concentrations in the flue gas. High-volume sample extraction and the pilot plant control device collection hoppers can provide large samples for study. Particulate sizing and laboratory ash resistivity techniques, used to characterize the fly ash from each test, are described below.

Five-Stage Cyclone System

A five-stage cyclone system, shown in Figure A-5, was used to determine the size distribution of particulate entering the ESP. The system consists of five cyclones and a backup filter connected in series to provide five equally spaced particle-size cuts on a logarithmic scale from 0.1 to 10 μm. The nominal flow rate for the system is 1.0 acfm. The five-stage cyclone system was designed to operate in-stack, but is operated out-of-stack (particulate-laden flue gas is isokinetically extracted from the stack using a sampling probe) at the EERC due to the small pipe diameters associated with the pilot-scale combustion equipment.

Laboratory Resistivity Unit

Bulk electrical resistivity measurements are made with an apparatus designed and built according to the American Society of Mechanical Engineers Power Test Code 28 that provides control of temperature and flue gas environment for the ash samples being tested. Temperature control is maintained by an electrically heated oven (Figure A-6). The oven can be heated to a maximum of 800°F in approximately one-half hour and can maintain any temperature between room temperature and 800°F. Flue gas components (O_2, CO_2, SO_2, and N_2 from compressed gas cylinders) are metered with rotameters to match the flue gas concentrations in which the fly ash was collected. Humidity is provided by bubbling gas through a humidity bath maintained at a precisely controlled temperature. The outlet gas is saturated with water vapor at the given temperature. Sulfur dioxide and CO_2 do not go through the humidity bath, but enter the simulated flue gas stream just prior to the oven.

Fly ash resistivity measurements are made using a movable disk electrode, as shown in Figure A-7. This electrode was designed to put a pressure of 10 g/cm^2 on a layer of ash 5 mm thick. The ash sample container and the electrode are made of sintered stainless steel of 25-μm porosity to allow contact between the ash and the flue gas.

A high-voltage supply with a range of 0 to 1200 volts is wired to the sample pan electrode. Current passing through the sample layer from the sample pan to the measuring electrode is measured by an electrometer capable of reading currents from 10^{-14} to 10^{-1} amperes.

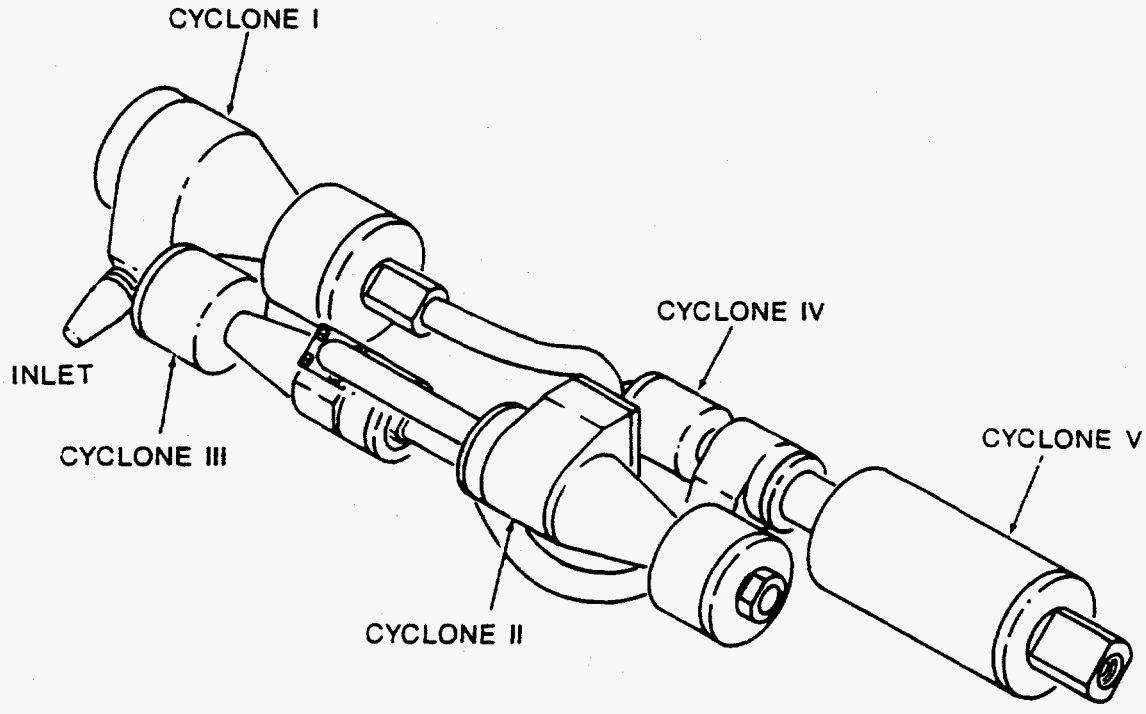

Figure A-5. Five-stage cyclone sampling system.

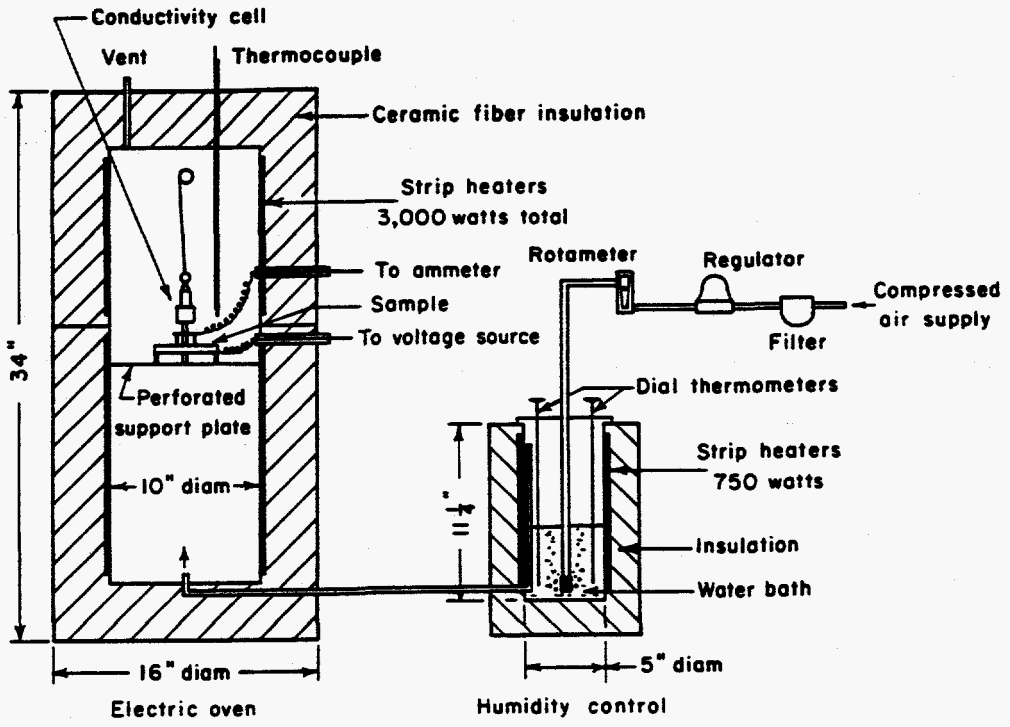

Figure A-6. Schematic of laboratory resistivity apparatus.

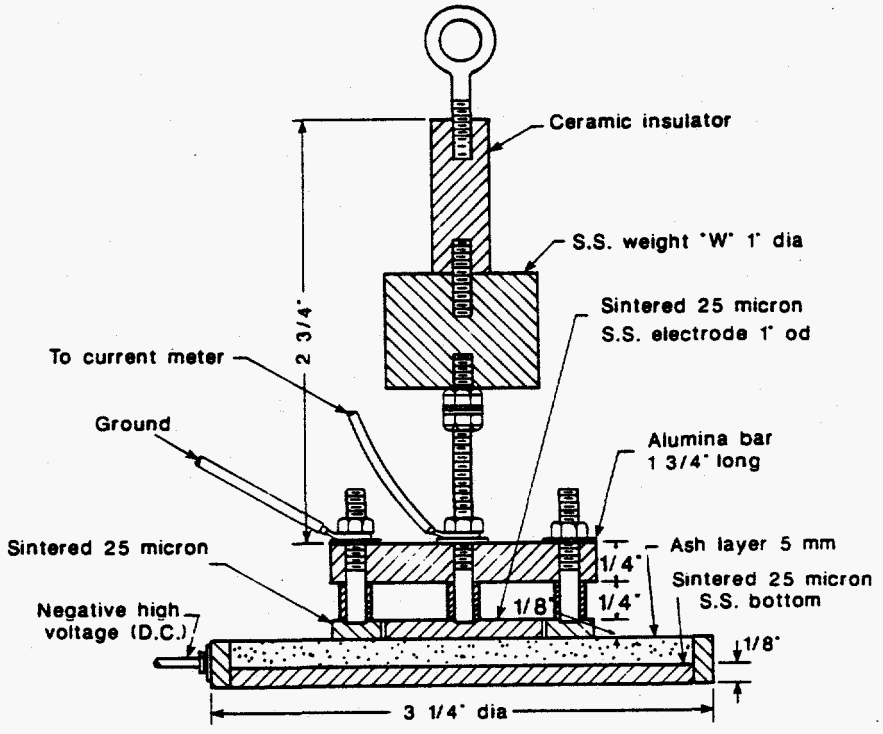

Figure A-7. Resistivity-measuring electrode.

A uniform ash layer is introduced to the conductivity cell, and the electrode is carefully lowered onto the ash layer. The oven door is then closed, and the temperature is set to 200°F. After the oven has maintained the designated temperature for at least 40 minutes, a 750-volt source is applied to the 0.5-cm ash layer. This produces a field strength of 1.5 kV/cm, which is used for all measurements. The current through the ash layer is measured with a high-sensitivity electrometer. The temperature of the oven is increased to the next higher temperature, after which there is a 40-minute waiting period to ensure that the ash layer has a uniform temperature. The test voltage is then applied, the current reading is recorded, and the temperature is increased to the next setting. Analysis duration is normally 8 to 10 hours to complete one set of readings from 200° to 750°F.

The fly ash resistivity is then calculated using the equation:

$$\rho = \frac{VA}{IL}$$

In this expression, V is the applied voltage, which is held constant at 750 volts. A is the area of the one-inch-diameter inner electrode, which is also constant at 5.07 cm^2. L is the thickness of the ash layer, which is 0.5 cm, and I is the measured current in amperes. For a given test, the data are presented as a plot of fly ash resistivity versus temperature

ANALYTICAL PROCEDURES

Coal Analysis

The coal is analyzed to determine the proximate, ultimate, and heating value analyses. The particle-size distribution is also determined for each combustion test sample. Descriptions of these analyses are as follows:

- Proximate analysis to determine moisture, ash, and volatile matter content is performed with a Fisher 490 coal analyzer. Fixed carbon is calculated by difference as the final remaining constituent.

- Ultimate analysis is performed using a Perkin-Elmer Model 240 elemental analyzer to determine CHN concentrations and a Leco sulfur analyzer for sulfur content. The level of chlorine in the coal is determined by ASTM Method D2361. Ash content is determined by ASTM Method D3174. Oxygen in the coal is calculated by difference as the final remaining constituent.

- Gross caloric value is measured by ASTM Method D2015 using a Parr adiabatic calorimeter and master controller.

- Particle-size distributions are determined by sieve analysis according to ASTM Method D410.

Inorganic and Mineral Component Analysis

Concentrations of major mineral oxides in the coal ash (Al_2O_3, SiO_2, Na_2O, MgO, CaO, P_2O_5, K_2O, Fe_2O_3, TiO_2, and SO_3) are determined by x-ray fluorescence (XRF). The ash samples are prepared using the ASTM D3174 procedure in which the sample is heated to 1382°F in air for 15 hours (a larger sample analyzed by the EERC lab requires additional drying time). Analysis is performed using a Kevex x-ray spectrometer.

Fusion temperatures of the ash are determined under oxidizing and reducing conditions, in accordance with ASTM Method D1857, using a Preier–Mineco electric tube furnace.

Advanced Coal Analyses

A sample of the test coal is also analyzed by chemical fractionation and computer-controlled scanning electron microscopy (CCSEM) to aid in understanding ash behavior. The characteristics of fly ash or ash deposits are dependent on two basic factors: 1) the types, abundance, and associations of the inorganic constituents in the original fuel; and 2) combustion conditions. In order to understand the mechanisms and processes occurring among inorganic components during combustion, a precise and accurate knowledge of the inorganic materials entering the combustion system must be obtained.

Conventional ASTM ash analysis was developed for high-rank coals in which the primary inorganic constituents are minerals. Low-rank coals contain a complex mixture of inorganic components, including cations bound to the organic acid groups and clays, organically coordinated inorganic elements, and discrete mineral phases. The EERC advanced method of coal analysis is a two-part analysis designed to quantitatively determine not only what inorganic elements are present but also their mode of occurrence. The first part of the EERC advanced coal analysis uses the chemical fractionation technique to quantitatively determine the modes of occurrence of inorganics. The second part of the method uses CCSEM to quantify the amounts and sizes of minerals present.

Chemical Fractionation

Chemical fractionation is used to quantitatively determine the modes of occurrence of the inorganic elements in coal, based on the extractability of the elements in solutions of water, 1 molar ammonium acetate, and 1 molar hydrochloric acid. The flow diagram shown in Figure A-8 illustrates the technique. A 75-gram sample of −325-mesh vacuum-dried coal is stirred with 160 mL of deionized water to extract water-soluble minerals such as sodium chloride. After being stirred for 24 hours at room temperature, the water–coal mixture is filtered. The filtered coal is dried, and a portion is removed to be tested by XRF to determine the percent of each element remaining. The residues are then mixed with 160 mL of 1 molar ammonium acetate (NH_4OAc) and stirred at 70°C for 24 hours to extract the elements associated with the coal as ion-exchangeable cations present primarily as the salts of organic acids. The ammonium acetate extractions are performed two more times to effect complete removal of the ion-exchangeable cations. After the third ammonium acetate extraction, a sample of the dried residue is analyzed by XRF. The remaining residue of the ammonium acetate extractions is then stirred with 1 molar hydrochloric acid (HCl) at 70°C for 24 hours to remove the elements held in coordination complexes within the organic structure of the coal, as well as acid-soluble minerals such

as carbonates, oxides, and sulfates. The residue is then analyzed by XRF. The hydrochloric acid extraction is repeated once. The elements remaining in the coal after the chemical fractionation extractions are determined by difference. The nonextractable elements are associated in the coal as silicates, aluminosilicates, sulfides, and insoluble oxides.

CCSEM Analysis

Size and composition of mineral grains in the coal were determined by computer-controlled scanning electron microscopy (CCSEM), a program used in conjunction with the EERC JEOL scanning electron microscope (SEM) and microprobe system. The program is used to characterize inorganic components in samples of coal, char, and inorganic combustion products. The CCSEM system uses a computer to control the operation of the SEM in order to determine the size, quantity, distribution, and association of mineral grains and other particulate matter. The CCSEM analysis system uses an annular backscattered electron detector to locate and size the particles. The backscattered electron detector distinguishes compounds based on the atomic number of their elements. Therefore, particles such as mineral grains appear brighter than the coal or epoxy matrix in which they are mounted. This allows the electron beam to detect the particles by noting contrast differences.

When a particle is detected, the particle center is automatically located, a series of eight diameters about the center of the particle are measured, and the perimeter, area, and shape factor of the particle are calculated. The CCSEM analysis for the coal samples is performed using a magnification of 240x. Particles less than 1 micron in average diameter are not included in the analysis, since 1 micron is the lower limit for the energy-dispersive spectra (EDS) analysis.

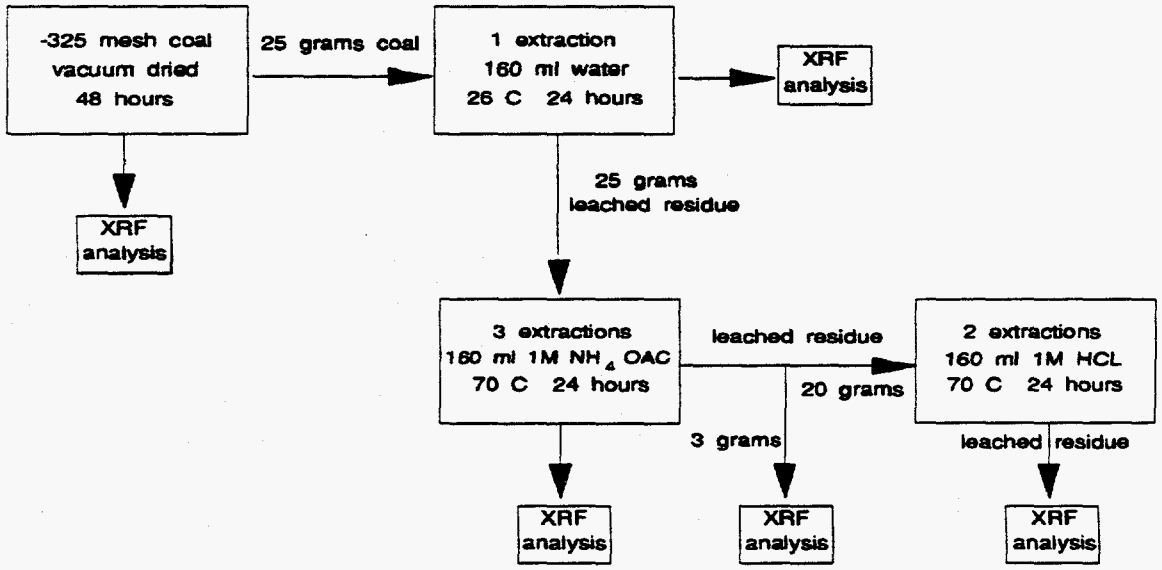

Figure A-8. Flow chart of the EERC chemical fractionation procedure.

The electron beam is then relocated to the center of the particle, and an EDS is taken for 2 seconds. Energy photon counts are accumulated for each element present and normalized to 100%. The CCSEM system can analyze for Na, Mg, Al, Si, P, S, Cl, K, Ca, Fe, Ba, and Ti. All information obtained by the CCSEM program is automatically stored in a microcomputer print file. These data are imported into a spreadsheet where phases are identified by the relative proportions of elements in each sized particle. Size distributions are also tabulated.

Ash Deposit Characterization

Chemical compositions of probe deposit and fly ash samples are determined by means of XRF. X-ray diffraction (XRD), which allows the identification of major crystalline forms, is used to support more quantitative SEM techniques in evaluating ash deposition phenomena. Identification, selection, and analysis of critical regions of the deposits are accomplished using SEM techniques.

SEMPC Analysis

A scanning electron microscopy point count technique (SEMPC) is used to quantify the phases present in the deposit. The SEM microprobe system is a powerful tool that can be used to examine the microscopic features of deposits and fly ash and provide chemical analysis of points as small as 1 micron in size. The system is automated and computer controlled, which increases data manipulation and data storage capabilities. The SEMPC technique was developed at the EERC to systematically and quantitatively determine the distribution of phases in ash deposits and fly ash. The SEMPC technique provides information on the degree of interaction and melting of the deposited ash components and the abundance of crystalline, amorphous, and unreacted ash particles. The data obtained from the technique are critical in identifying the components in ash deposits that are responsible for deposit growth and strength development. In addition, viscosity distribution profiles can be calculated for the amorphous or liquid phases using SEMPC data. This information provides insight into the propensity of a particular ash to form a strong deposit.

The procedure for SEMPC analysis involves preparing a cross section of the sample by mounting the ash deposit sections in epoxy. The epoxy block is sectioned to expose the ash deposit material. The exposed section is then polished to provide a very smooth surface for examination with the SEMPC technique.

The polished sample is placed in the SEM, and a compositional analysis is obtained from a series of 250 grid points across approximately 35 mm^2 of the sample. The Tracor Northern 5500 computer system differentiates between epoxy and deposit material and stores the chemical information. The stored chemical information is transferred to a microcomputer that identifies and quantifies the amorphous and crystalline components in the deposit. The crystalline components are readily identified as minerals based on chemical composition and molar ratios. The amorphous component is classified as either derived phases or unclassified material. Derived phases resemble their coal mineral precursor. Unclassified material has no crystalline structure and shows no molar ratios that conform to mineral formulas stored in the SEMPC program.

REFERENCES

1. Honea, F.I. "Studies of Ash Fouling Potential and Deposit Strength in the GFETC Pilot Plant Test Furnace," In *Fouling and Slagging from Impurities in Combustion Gases;* Bryers, R.W., Ed.; Engineering Foundation: New York, 1983; pp 117–141.

2. Beer, J.M.; Chigier, N.A. *Combustion Aerodynamics;* John Wiley & Sons: New York, 1972; pp 100–146.

APPENDIX B

ENGINEERING DRAWINGS OF IESP

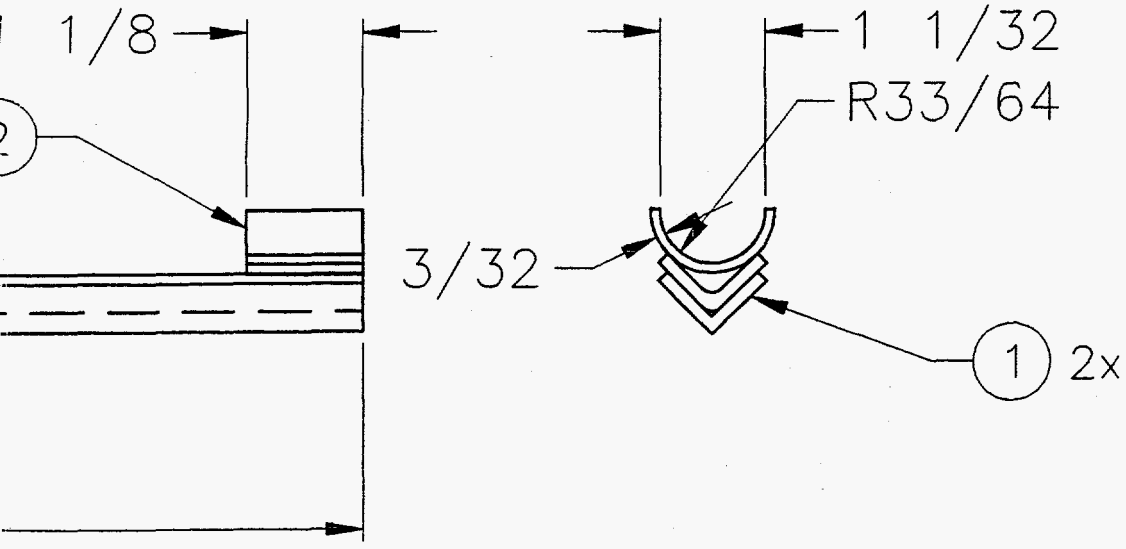

	1	3	–	PLATE, 1/16	C.S.		
	1	2	--	PLATE, 3/32	C.S.		
	2	1	–	L3/4 x 3/4 x 1/8	C.S.		
$\frac{-2}{QTY}$	$\frac{-1}{QTY}$	ITEM	PART NO	DESCRIPTION	MATERIAL SPEC	Q.C.	DATE

ENERGY AND ENVIRONMENTAL RESEARCH CENTER

GRAND FORKS, NORTH DAKOTA, U.S.A.
UND–EERC PROPRIETARY DESIGN DRAWING

CRADLE, IESP PROBE

DRAWN BY: DMB	ESS CHK: WRK	DATE: 10-17-95	W: 386 E: –
DO NOT SCALE FROM DRAWING	ENGR: DAC	DATE: 17 OCT 95	FUND NO: 4721
	CLIENT:	DATE:	REV: –
UNLESS SPECIFIED ALL DIMENSIONS IN INCHES	EERC S.O.	DATE:	SCALE: 1:2
TOLERANCES: FRACTIONAL ± 1/16; 3 PLC. DEC. ± 0.005; 2 PLC. DEC. ± 0.30; 1 PLC. DEC. ± 0.1; ANGULAR ± 2-1/2	MGR: BG	DATE:	SHEET 1 OF 1
	APVD:	DATE:	PRESSURE TEST DRAWING LEVEL: –
	FINAL ASSY: –	NEXT ASSY: 2276	DWG. NO: 2279

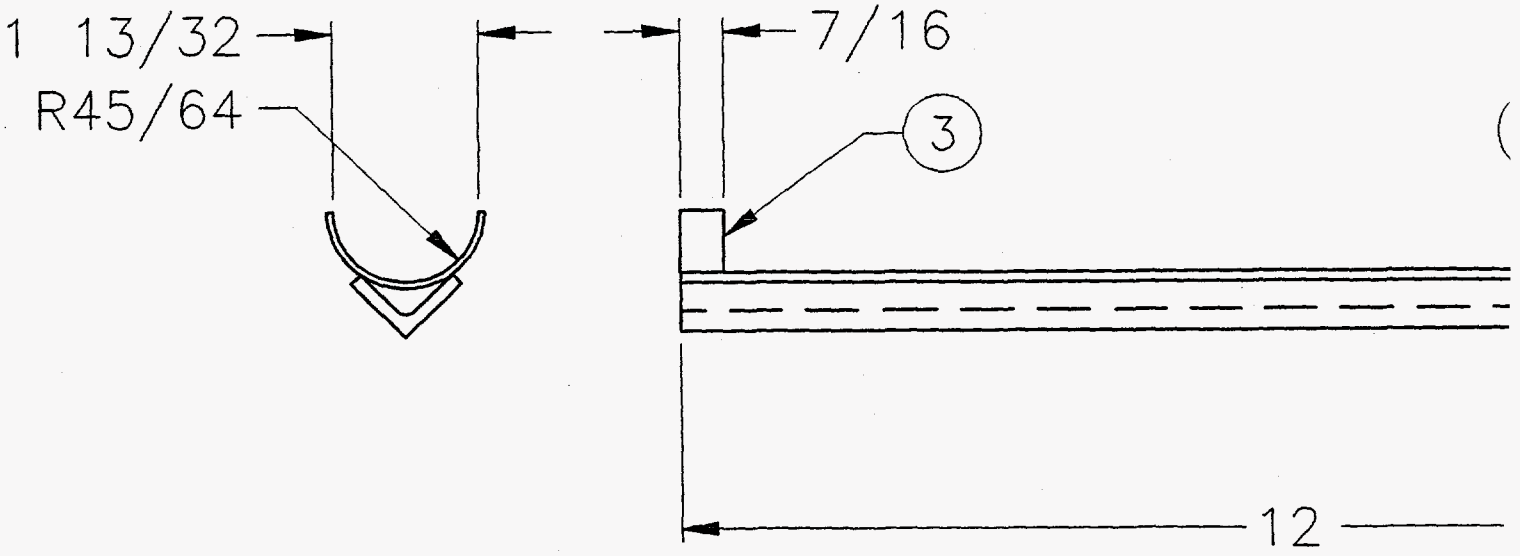
1 13/32
R45/64
7/16
3
12

GENERAL NOTES:

1. USE WPS NO. 9 UNLESS OTHERWISE NOTED.
2. CERTIFIED WELDING IS REQUIRED AS PER ASME B31.3 EXCEPT AS NOTED.

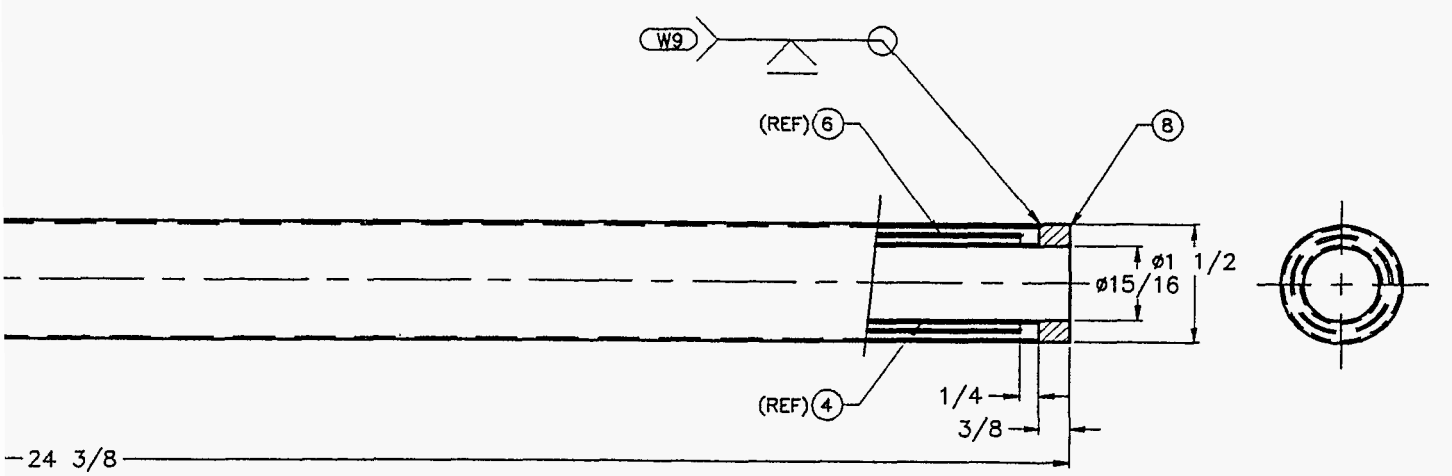

-2 QTY	-1 QTY	ITEM	PART NO	DESCRIPTION	MATERIAL SPEC	Q.C.	DATE
	1	8	–	ROUND, ø1-1/2" x 3/8"	A276-316		
	1	7	–	ROUND, ø1-1/2" x 1/8"	A276-316		
	1	6	–	TUBE, ø1-1/4 x .035	A269-TP316		
	1	5	–	ROUND, ø1-1/4"	A276-316		
	1	4	–	TUBE, ø1" x .035	A269-TP316		
	3	3	2267?	INLET/OUTLET COUPLING, IESP PROBE	–		
	1	2	2283	THERMOCOUPLE HEAD, IESP PROBE	–		
	1	1	–	TUBE, ø1-1/2" x .035	A269-TP316		

ENERGY AND ENVIRONMENTAL RESEARCH CENTER

GRAND FORKS, NORTH DAKOTA, U.S.A.
UND-EERC PROPRIETARY DESIGN DRAWING

PROBE ASSEMBLY, IESP PROBE

DRAWN BY: DMB	ESS CHK: OK	DATE: 10-17-95	W: 386 E: –
DO NOT SCALE FROM DRAWING	ENGR: ABG	DATE: 17 OCT 95	FUND NO: 2276
UNLESS SPECIFIED ALL DIMENSIONS IN INCHES	CLIENT:	DATE:	REV: –
TOLERANCES: FRACTIONAL ± 1/16; 3 PLC. DEC. ± 0.005; 2 PLC. DEC. ± 0.30; 1 PLC. DEC. ± 0.1; ANGULAR ± 2-1/2°	EERC S.O.	DATE:	SCALE: 1:1
	MGR:	DATE:	SHEET 1 OF 1
	APVD:	DATE:	PRESSURE TEST DRAWING LEVEL: –
	FINAL ASSY: 2276	NEXT ASSY: 2276	DWG. NO: 2277

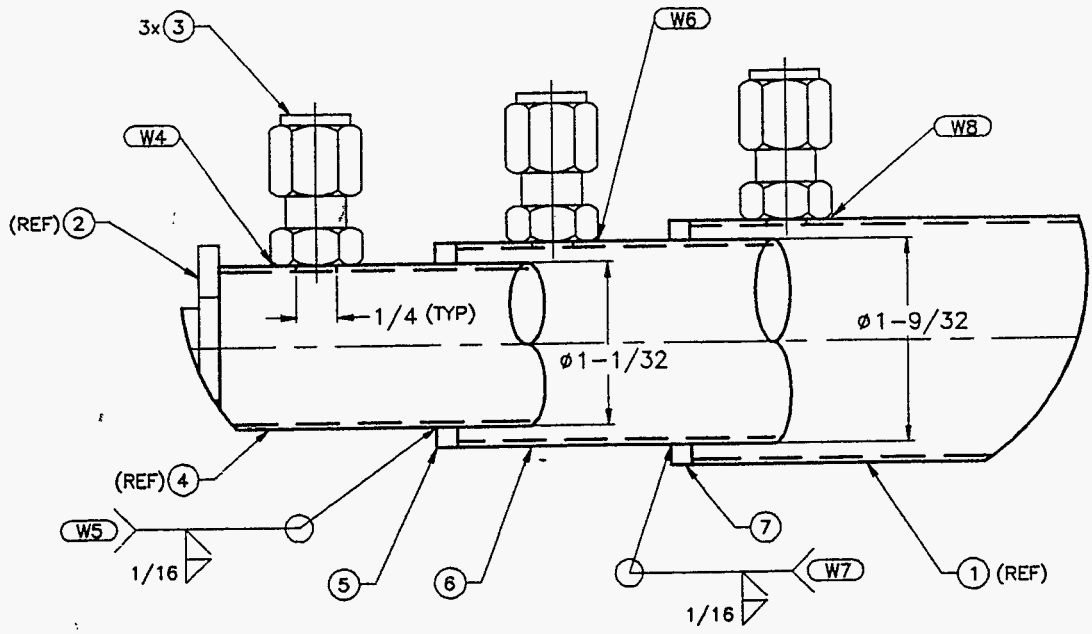
3x 3
W6
W4
W8
(REF) 2
1/4 (TYP)
ø1-1/32
ø1-9/32
(REF) 4
W5
1/16
5
6
7
W7
1/16
1 (REF)

DETAIL-A

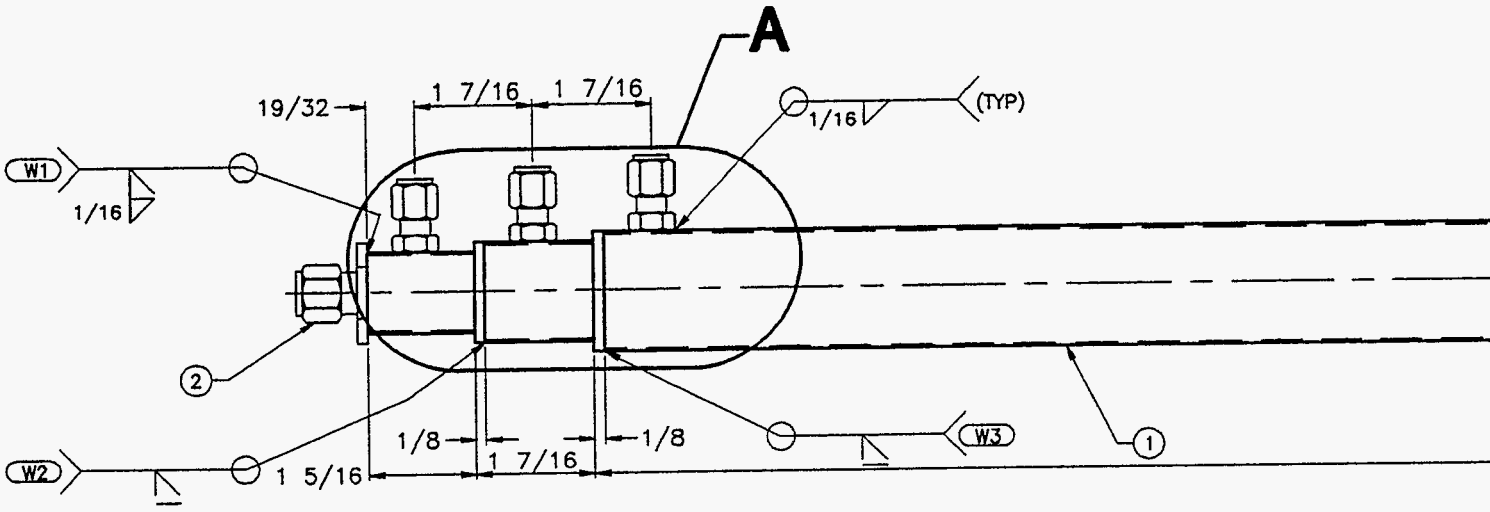
A
19/32
1 7/16
1 7/16
1/16 (TYP)
W1
1/16
2
1/8
1/8
1 7/16
W3
W2
1 5/16
1

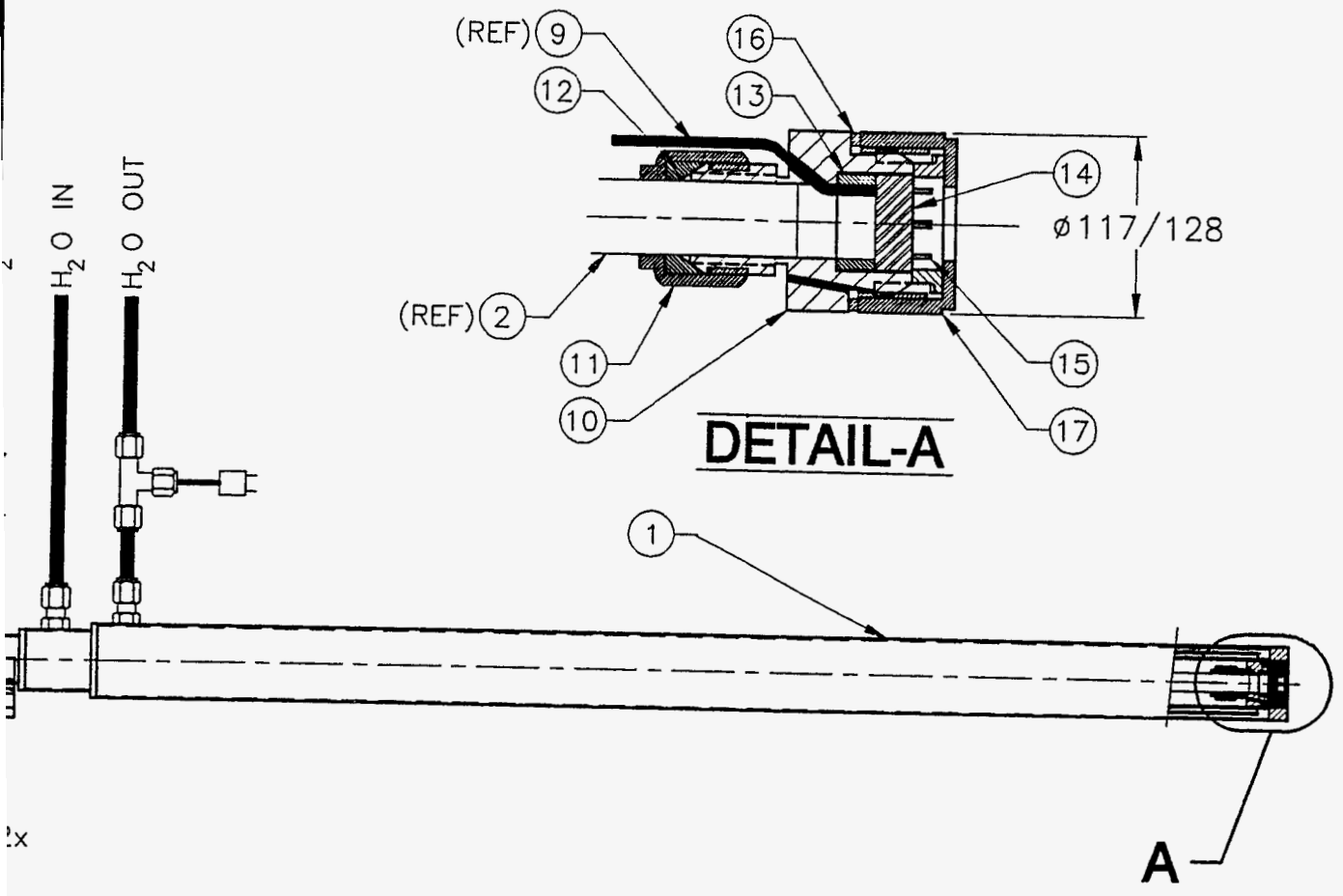

	1	17	–	NUT, HEX, CONNECTOR (PARKER)	316 SS		
	1	16	–	ROUND, ø7/8 OD x ø3/4 ID x 3/64	PTFE		
	1	15	2281	END, LENS HOLDER, IESP PROBE	–		
	1	14	CUSTOM	LENS, PLANO-CONVEX, 125 mm focal dist (IR OPTICAL)	CdTe		
	1	13	–	TUBE, ø31/64 OD x ø1/4 ID x 3/16	PTFE		
	1	12	–	FERULE, 1/4" (PARKER)	–		
	1	11	–	NUT, 1/4" CONNECTOR (PARKER)	316 SS		
	1	10	2280	BODY, LENS HOLDER, IESP, PROBE	–		
	2	9	–	THERMOCOUPLE	–		
	2	8	–	PIPE CLAMP, SCREW	304 SS		
	1	7	2279	CRADLE, IESP PROBE	–		
	1	6	AOT-8	8", OPTICAL CONDUIT (AXIOM)	–		
	1	5	AOT-22	22", OPTICAL CONDUIT (AXIOM)	–		
	1	4	AOP-8	8", 90° PARABOLIC MIRROR ASSEMBLY (AXIOM)	–		
	1	3	AOP-2	2", 90° PARABOLIC MIRROR ASSEMBLY (AXIOM)	–		
	1	2	SPECIAL	OPTICAL CONDUIT, 1/4" (AXIOM)	AU COATED		
	1	1	2277	PROBE ASSEMBLY, IESP PROBE	–		
SUB QTY	ASSY QTY	ITEM	PART NO	DESCRIPTION	MATERIAL SPEC	Q.C.	DATE

ENERGY AND ENVIRONMENTAL RESEARCH CENTER

GRAND FORKS, NORTH DAKOTA, U.S.A.
UND–EERC PROPRIETARY DESIGN DRAWING

PROBE ASSEMBLY, IESP PROBE

DRAWN BY: DMB	ESS CHK: [illegible] DATE: 10-17-95	W: 386	E: –
DO NOT SCALE FROM DRAWING	ENGR: AAG DATE: 10/26/95	FUND NO: 2276	
UNLESS SPECIFIED ALL DIMENSIONS IN INCHES	CLIENT: DATE:	REV: –	
TOLERANCES: FRACTIONAL ± 1/16; 3 PLC. DEC. ± 0.005; 2 PLC. DEC. ± 0.30; 1 PLC. DEC. ± 0.1; ANGULAR ± 2-1/2	EERC S.O. DATE:	SCALE: 1:1	
	MGR: [illegible] DATE:	SHEET 1 OF 1	
	APVD: DATE:	PRESSURE TEST DRAWING LEVEL: –	
	FINAL ASSY: 2276 NEXT ASSY: 2276	DWG. NO: 2276	

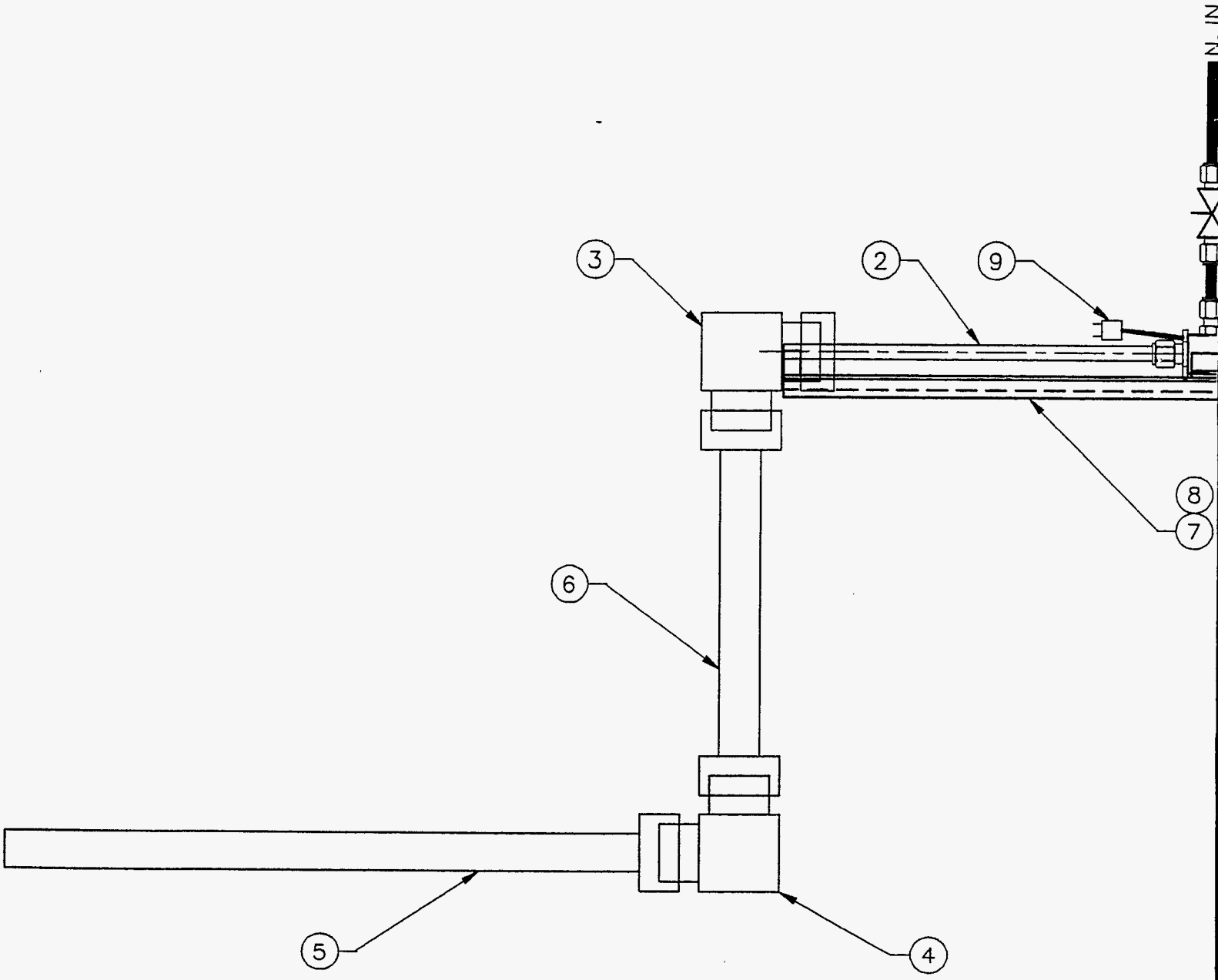
3
2
9
8
7
6
5
4

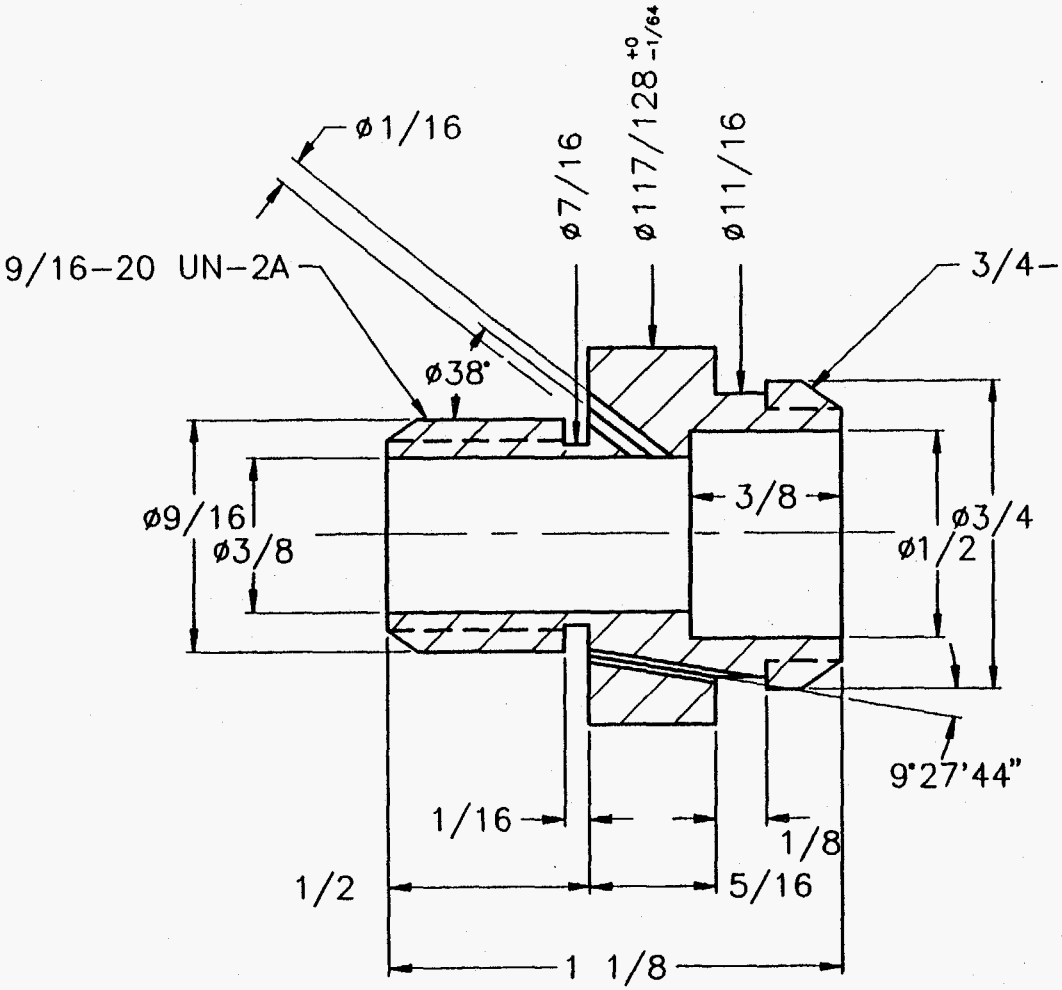

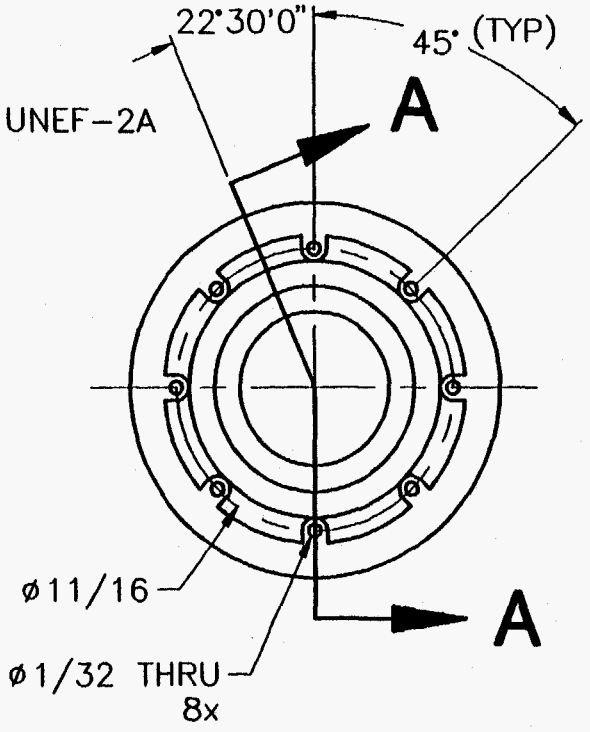

SECTION A-A

QTY	QTY	ITEM	PART NO	DESCRIPTION	MATERIAL SPEC	Q.C.	DATE
	1	1	-	ROUND, ø 1	316 SS		

ENERGY AND ENVIRONMENTAL RESEARCH CENTER
GRAND FORKS, NORTH DAKOTA, U.S.A.
UND-EERC PROPRIETARY DESIGN DRAWING

BODY, LENS HOLDER, IESP PROBE

DRAWN BY: DMB	ESS CHK: [illegible]	DATE: 10-17-96	W: 386 E: -
DO NOT SCALE FROM DRAWING	ENGR: A.B.L.G.	DATE: 12 OCT 96	FUND NO: 4721
UNLESS SPECIFIED ALL DIMENSIONS IN INCHES	CLIENT:	DATE:	REV: -
TOLERANCES: FRACTIONAL ± 1/16; 3 PLC. DEC. ± 0.005; 2 PLC. DEC. ± 0.30	EERC S.O.	DATE:	SCALE: 2:1
	MGR: [illegible]	DATE:	SHEET 1 OF 1
	APVD:	DATE:	PRESSURE TEST DRAWING LEVEL: -

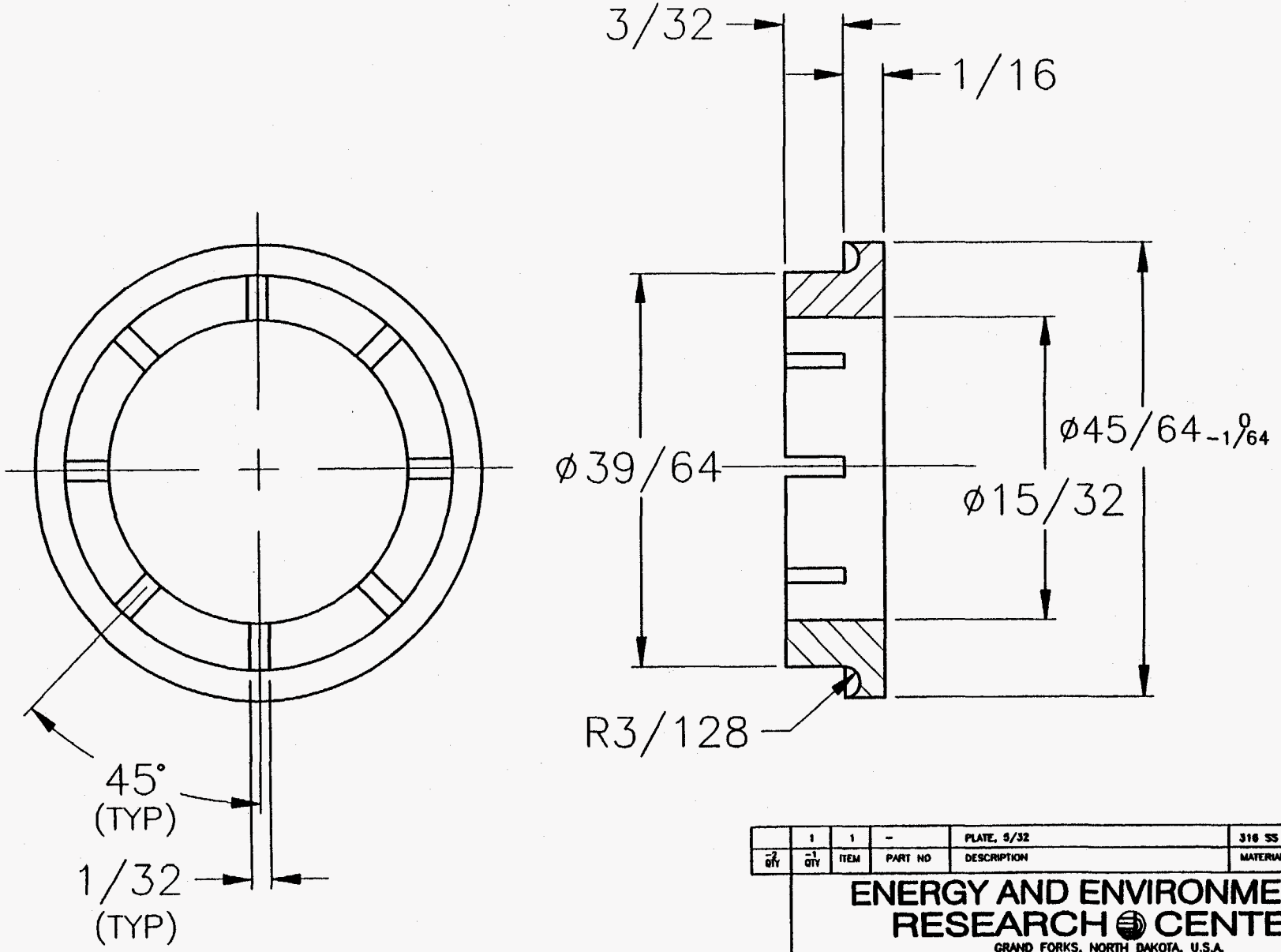

2 QTY	1 QTY	ITEM	PART NO	DESCRIPTION	MATERIAL SPEC	Q.C.	DATE
	1	1	-	PLATE, 5/32	316 SS		

ENERGY AND ENVIRONMENTAL RESEARCH CENTER

GRAND FORKS, NORTH DAKOTA, U.S.A.
UND-EERC PROPRIETARY DESIGN DRAWING

END, LENS HOLDER, IESP PROBE

DRAWN BY: DMB	ESS CHK: URK	DATE: 10-17-95	W: 386 E: -
DO NOT SCALE FROM DRAWING	ENGR: A.A.G.	DATE: 17 oct 95	FUND NO: 4721
UNLESS SPECIFIED ALL DIMENSIONS IN INCHES	CLIENT:	DATE:	REV: -
TOLERANCES: FRACTIONAL ± 1/16; 3 PLC. DEC. ± 0.005; 2 PLC. DEC. ± 0.30; 1 PLC. DEC. ± 0.1; ANGULAR ± 2-1/2	EERC S.O.	DATE:	SCALE: 4:1
	MGR: B.M.	DATE:	SHEET 1 OF 1
	APVD:	DATE:	PRESSURE TEST DRAWING LEVEL: -
	FINAL ASSY: 2276	NEXT ASSY: 2278	DWG. NO: 2281

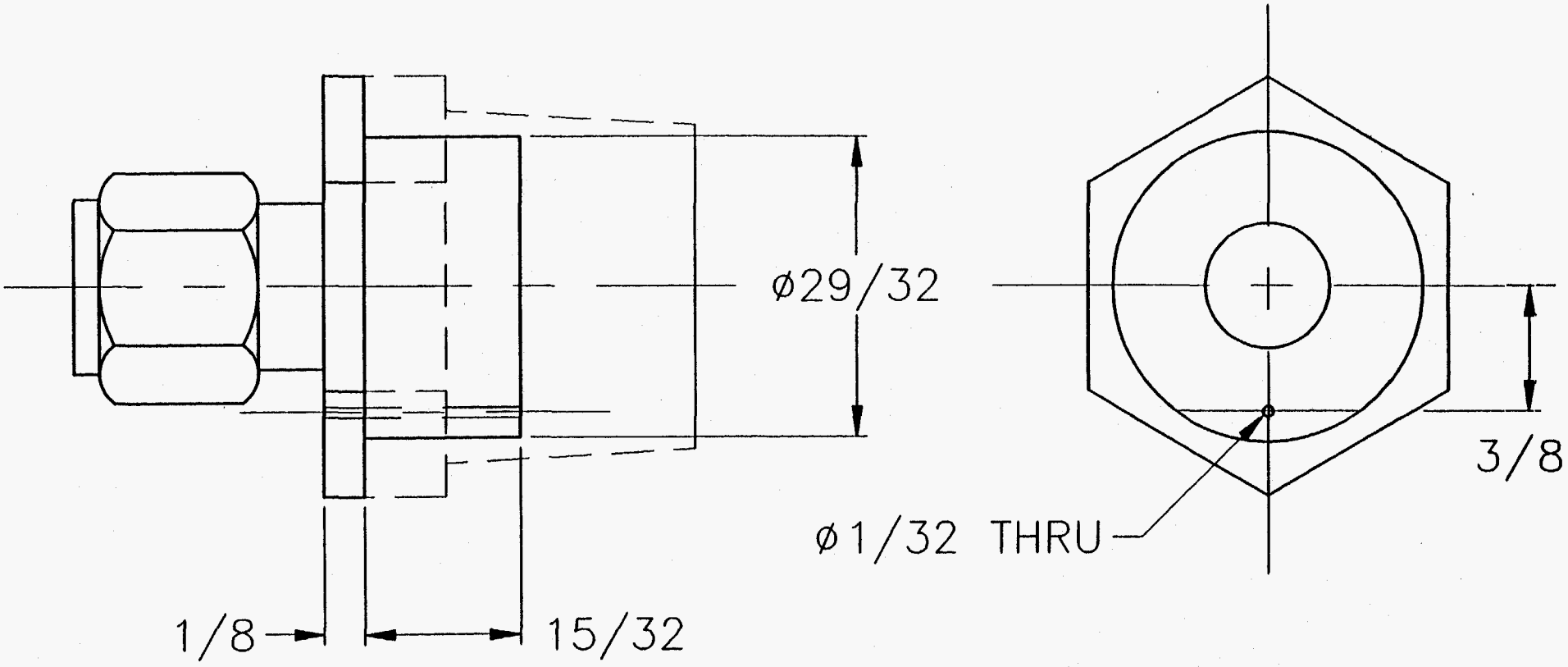

-2 QTY	-1 QTY	ITEM	PART NO	DESCRIPTION	MATERIAL SPEC	Q.C.	DATE
	1	1	SS-600-1-12	CONNECTOR, MALE, 3/8"-3/4" (SWAGELOK)	316 SS		

ENERGY AND ENVIRONMENTAL RESEARCH CENTER

GRAND FORKS, NORTH DAKOTA, U.S.A.
UND-EERC PROPRIETARY DESIGN DRAWING

THERMOCOUPLE HEAD, IESP PROBE

DRAWN BY: DMB	ESS CHK: CRT	DATE: 10-17-95	W: 386 E: -
DO NOT SCALE FROM DRAWING	ENGR: AAG	DATE: 17 OCT 95	FUND NO: 4721
UNLESS SPECIFIED ALL DIMENSIONS IN INCHES	CLIENT:	DATE:	REV: -
TOLERANCES: FRACTIONAL ± 1/16; 3 PLC. DEC. ± 0.005; 2 PLC. DEC. ± 0.30; 1 PLC. DEC. ± 0.1; ANGULAR ± 2-1/2	EERC S.O.	DATE:	SCALE: 2:1
	MGR: BJH	DATE:	SHEET 1 OF 1
	APVD:	DATE:	PRESSURE TEST DRAWING LEVEL: -
	FINAL ASSY: 2278	NEXT ASSY: 2277	DWG NO: 2283

APPENDIX C

EMISSION SPECTRA OF PURE MINERALS

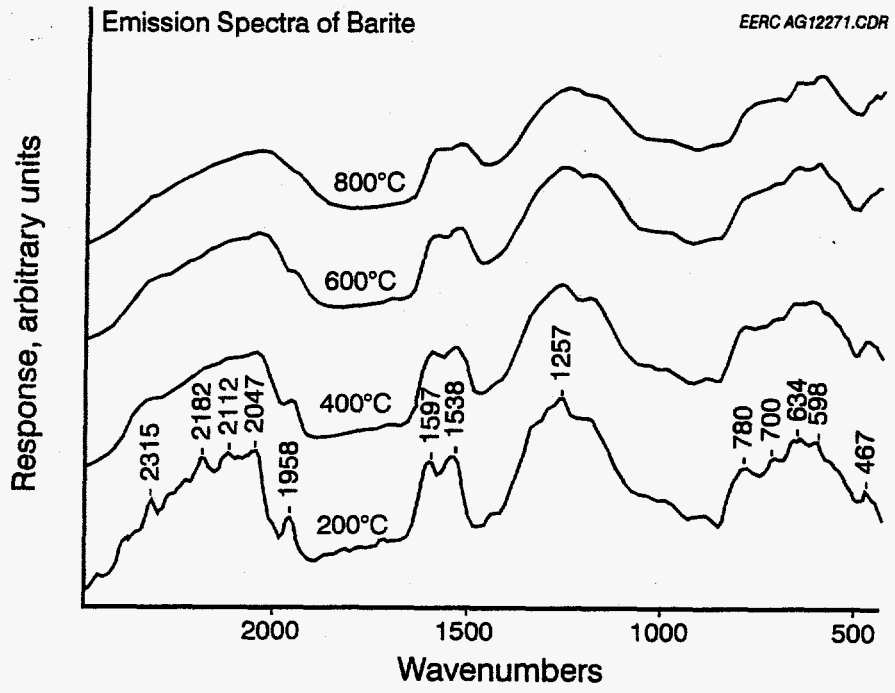
Emission Spectra of Barite
EERC AG12271.CDR
Response, arbitrary units
800°C
600°C
400°C
200°C
2315
2182
2112
2047
1958
1597
1538
1257
780
700
634
598
467
2000
1500
1000
500
Wavenumbers

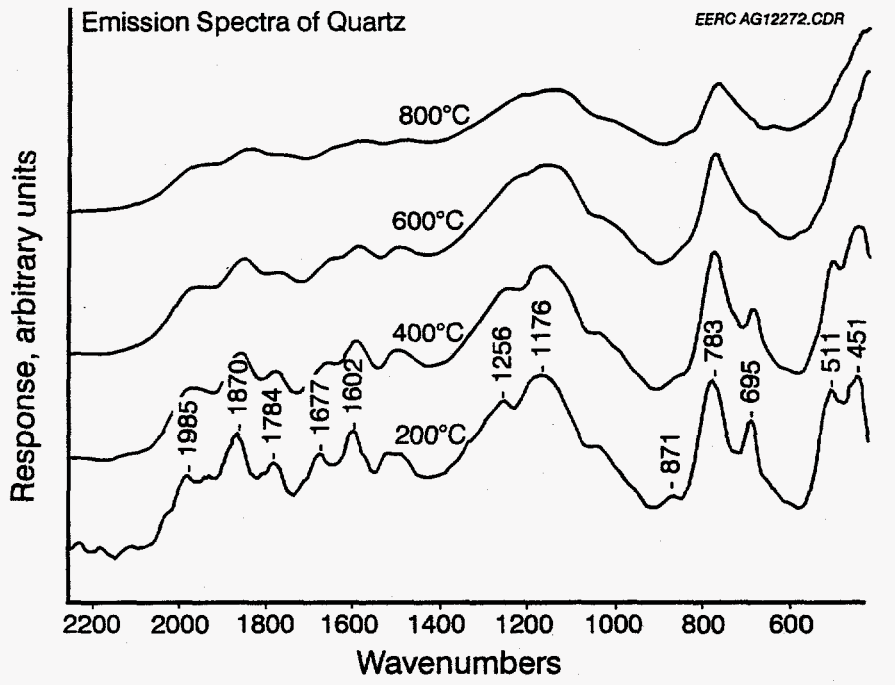
Emission Spectra of Quartz
EERC AG12272.CDR
Response, arbitrary units
800°C
600°C
400°C
200°C
1985
1870
1784
1677
1602
1256
1176
871
783
695
511
451
2200
2000
1800
1600
1400
1200
1000
800
600
Wavenumbers

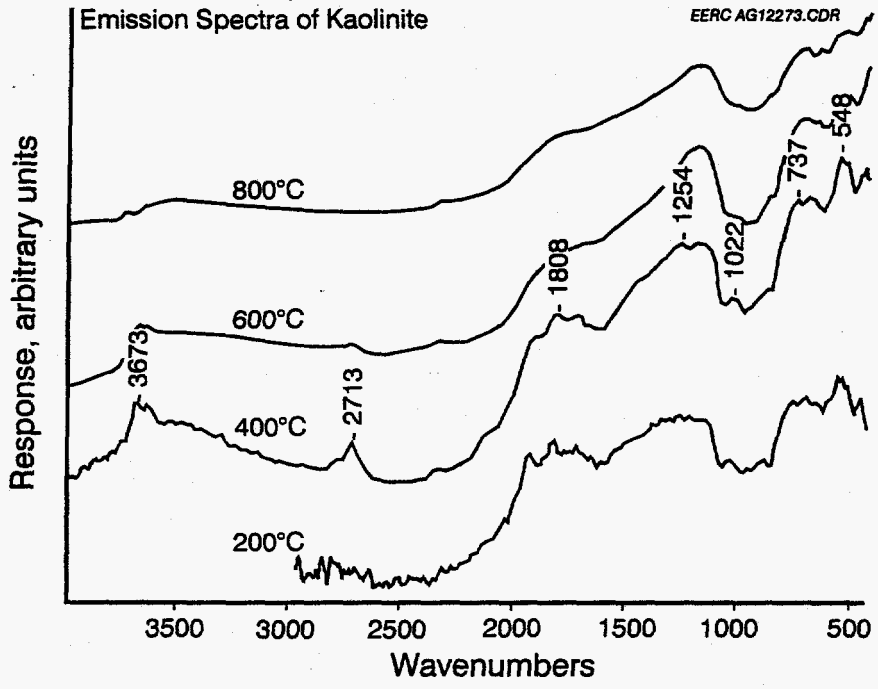
Emission Spectra of Kaolinite
EERC AG12273.CDR
Response, arbitrary units
800°C
600°C
400°C
200°C
3673
2713
1808
1254
1022
737
548
3500
3000
2500
2000
1500
1000
500
Wavenumbers

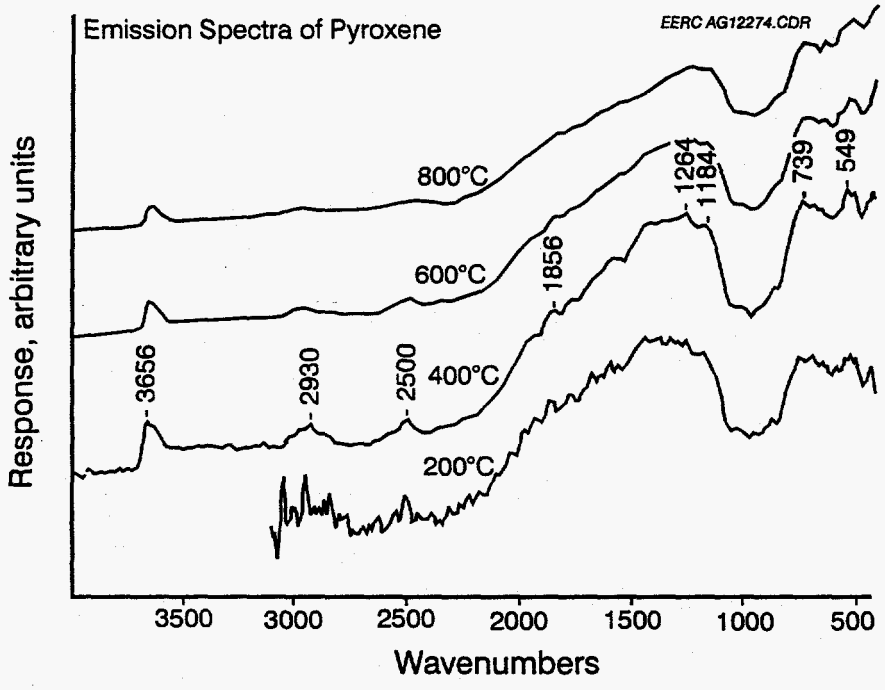
Emission Spectra of Pyroxene
EERC AG12274.CDR
Response, arbitrary units
800°C
600°C
400°C
200°C
3656
2930
2500
1856
1264
1184
739
549
3500
3000
2500
2000
1500
1000
500
Wavenumbers

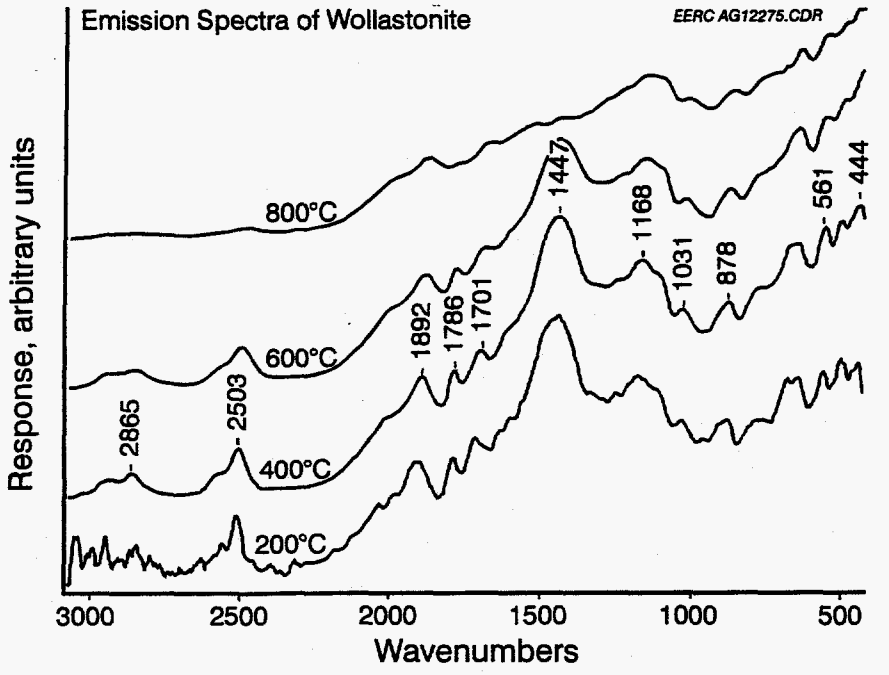
Emission Spectra of Wollastonite
EERC AG12275.CDR
Response, arbitrary units
800°C
600°C
400°C
200°C
2865
2503
1892
1786
1701
1447
1168
1031
878
561
444
3000
2500
2000
1500
1000
500
Wavenumbers

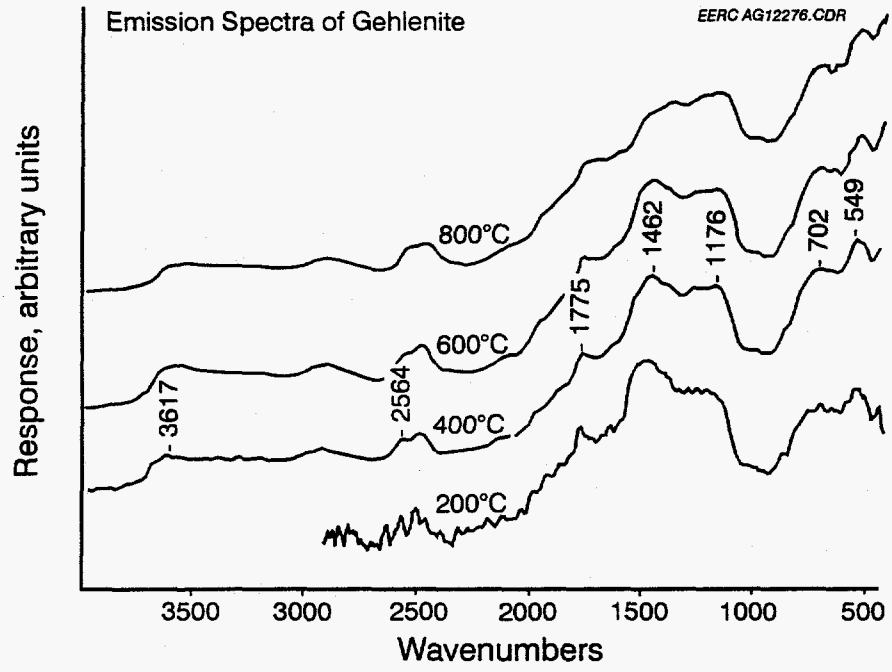
Emission Spectra of Gehlenite
EERC AG12276.CDR
Response, arbitrary units
800°C
600°C
400°C
200°C
3617
2564
1775
1462
1176
702
549
3500
3000
2500
2000
1500
1000
500
Wavenumbers

APPENDIX D

LITERATURE REVIEW

SPECTROSCOPIC MONITORING OF FIRESIDE DEPOSITS FROM COAL COMBUSTION - LITERATURE REVIEW

1.0 INTRODUCTION

For several decades measurements of the radiative properties of ash deposits have reported dependencies on the deposit morphology and chemistry (1). In addition it is known that many chemical species found in deposits emit in characteristic bands. Recent spectroscopic studies on samples of fly ash and deposits together with in-situ measurements at laboratory, pilot scale and industrial scale have now indicated the technical possibilities of monitoring deposits (1). The information provided relates to aspects of the deposit chemistry, its physical structure and radiative heat transfer properties. This information may be used to monitor the progressive character of deposits in utility boilers as they initiate, grow and develop strength and to assist in decisions related to boiler operation such as soot-blowing.

The report presents this information, much of which has been extracted from Wall et al. (1), and provides recommendations on the potential application of spectroscopic techniques.

2.0 BACKGROUND

2.1 The Mechanisms of Heat Transfer to and Through Ash Deposits

The average temperature of the gases within a furnace can be determined by a heat balance whereby the heat released by combustion is equated to the sensible heat level of the flue gases together with the heat transferred to the sink. The heat transfer is considered here in isolation but its relation to the other variables through the heat balance should not be forgotten. For example, as deposits build up so as to restrict heat transfer the gas temperature will increase thereby increasing the possibility of further reactions between the ash constituents at elevated temperature.

In a furnace the thermal energy transfer from flame gases (at temperature T_f) to the exterior surface of the ash deposits (at temperature T_s) is by radiative transfer and convection (convection usually of secondary importance in the furnace regions but dominant in the superheater region). The transfer through the deposit and tube is by conduction and then by convection the contained steam. Figure 1 illustrates the process (2). Equating the net radiative transfer at the surface (per unit area of surface) to the heat conducted through the deposit, taking a flame emissivity of unity (for a large furnace), neglecting the thermal resistance of the tube and steam film gives (using notation in Figure 1):

$$Q = H - R - \varepsilon E = \alpha H - \varepsilon E \qquad (1)$$

so that

$$Q = \frac{k}{x}(T_s - T_t) = \alpha\sigma T_f^4 - \varepsilon\sigma T_s^4 \qquad (2)$$

where T_t is the tube temperature.

This equation considers only the radiative transfer between the flame gases and the deposit surface. In practical furnaces convective transfer is a minor (<5%) heat transfer mechanism. The equation also considers the deposit as a surface radiator whereas, in fact, incident radiation will be absorbed somewhat within the deposit (say, to a depth of 1 mm). The thermal conductivity (k) therefor includes both conductive and radiative mechanisms. The properties determining heat transfer are therefore the thermal conductivity (k), absorbance (α) and emittance (ε). In many cases, the deposit layer is sufficiently thin so that $T_f^4 \gg T_S^4$ and the surface emission (the last term in Equation (2)) is small. The only radiative property of importance is then the absorbance of the deposit surface.

2.2 The Radiative Properties

There is an upper limit to the amount of radiative energy that can be emitted by a body (3, 4). A body emitting at this rate is known as a blackbody, and is also perfect absorber. The rate of energy emitted into hemispherical space, per unit wavelength interval, from a blackbody is known as the spectral blackbody flux density $e_B(\lambda,T)$, given by Planck's law.

Integration of the spectral flux density over all wavelengths at a fixed temperature yields the total blackbody radiation flux density, or emissive power, E_B.

$$E_B(T) = \int_{\lambda=0}^{\infty} e_B(\lambda,T)\,d\lambda \qquad (3)$$

This integral has been evaluated as

$$E_B(T) = \sigma T^4 \qquad (4)$$

The most commonly defined radiative property of a surface is its emissivity ε - the ratio of its emission rate to that from the blackbody at the same temperature ($\varepsilon = E/E_B$). A grey surface is one for which the emissivity is independent of wavelength and therefore of temperature, but the "effective" emissivity of a deposit depends on the spectral distribution of emissivity (ε_λ) and the surface temperature. The absorptivity α and reflectivity ρ are defined as the fractions of the radiation incident which are absorbed and reflected. For an opaque surface the reflectivity is complementary to the absorptivity. The spectral properties are related by $\varepsilon_\lambda = \alpha_\lambda = 1 - \rho_\lambda$.

Radiation properties are designated as total if they refer to the entire wavelength spectrum. Total emissivity ($\varepsilon_\lambda(T_S)$), spectral blackbody flux density ($e_B(\lambda,T_S)$) and emissive power $E_B(T_S)$, as

$$\epsilon_t(T_s) = \frac{1}{E_B(T_s)} \int_{\lambda=0}^{\infty} \varepsilon_\lambda(T_s) e_B(\lambda, T_s)\, d\lambda \tag{5}$$

Total absorptivity α_t is also defined in terms of spectral absorptivity $\alpha_\lambda(T_S)$ and spectral incident flux density $H_\lambda(T_f)$ as

$$\alpha_t(T_s,\ T_f) = \frac{\int_{\lambda=0}^{\infty} \alpha_\lambda(T_s) H_\lambda(T_f) dUB\lambda}{\int_{\lambda=0}^{\infty} H_\lambda(T_f) d\lambda} \tag{6}$$

Total absorptivity is defined therefore as a function of both surface temperature T_s and source radiation temperature T_f. Kirchoff's law states that the total emissivity and total absorptivity of a surface in radiative equilibrium with its surroundings are the same when there is not net radiative transfer from the surface. The spectral emissivity $\varepsilon_\lambda(T_s)$ and spectral absorptivity $\alpha_\lambda(T_s)$ are equal, even though there may be net transfer as long as absorptivity is insensitive to a wide variation in the intensity of irradiation (3). It was also noted that, strictly speaking, Kirchoff's law holds for monochromatic radiation in a particular direction and for each component of polarization (4). Applying Kirchoff's law, substitution of $\varepsilon_\lambda(T_s)$ for $\alpha_\lambda(T_s)$ therefore allows calculation of total absorptivity from the spectral emissivity distribution as follows:

$$\alpha_t(T_s,\ T_f) = \frac{\int_{\lambda=0}^{\infty} \varepsilon_\lambda(T_s) H_\lambda(T_f) d\lambda}{\int_{\lambda=0}^{\infty} H_\lambda(T_f) d\lambda} \tag{7}$$

Some implications of considerable practical importance for total properties arise from the way spectral properties vary with wavelength. If ε_λ does not vary with wavelength, then it follows that ε_t does not vary with temperature. The converse is not necessarily true, but in practice invariance of the total emissivity with temperature usually implies that ε_λ is constant. From Kirchoff's law, it

then follows that total absorptivity is equal to total emissivity, i.e., $\alpha_t = \varepsilon_t$ = constant. This is so for a grey body. Some real materials approximate this condition (e.g., heavily oxidised metal surfaces), but dielectric materials generally so not (3). A significant feature of dielectrics - which include ash deposits - is a region of low spectral emissivity at short wavelengths (up to 2 or 3 μm), followed by a region of high emissivity at longer wavelengths, which is usually strongly banded. The effect of this spectral distribution on total emissivity or absorptivity is to cause α_t or ε_t to decrease with increasing flame or surface temperature respectively. The reason for this is that whilst the emission (or absorption) regions of such materials remain relatively fixed with respect to spectral position as temperature increases, the region of maximum energy of the Planck's function moves towards the low (short wavelength) spectral emissivities, at high T_s or T_f, respectively, from Eqs. 6 and 7.

2.3 Significance of Spectral Effects for Particulate Ash Deposits

Measurements of the banded spectral emittance by Wall and Becker (5) allow the significance of the variation noted above of emittance with wavelength to be estimated. Fig. 2 gives illustrative values, and indicates that at wavelengths less than 6 μm ash deposits have a low emittance (and therefore high reflectance). The spectral data can be converted to total emittance [$\varepsilon_t(T_s)$] values using Eq.(6) and total absorbances values [$\alpha_t(T_s,T_f)$] using Eq.(7). The results are given on Fig. 3. The reduction of ε and α with temperature is evident.

The significance of the spectral character is illustrated on Fig. 4. The absorbed radiative energy is $\int H_\lambda \alpha_\lambda d\lambda$ and is weighted to the shorter wavelengths where (as seen on Fig. 2), α_λ is low. The emitted radiation is $\int e_\lambda \alpha_\lambda d_\lambda$ and is weighted to higher wavelengths where ε_λ is high. As a consequence the total absorptivity is less than the total emissivity.

$$\alpha_t(T_s,T_f) < \varepsilon_t(T_s) \qquad (8)$$

3.0 DATA FOR THE PROPERTIES

3.1 Total Emittance

Most of the published radiative property data is for total emittance rather than for the spectral emittance relevant to spectroscopic techniques. As this data does provide insights into the influence of deposit character on properties, it is reviewed briefly here.

Figs. 5 and 6 present estimates of total emittance for powdery ash layers and sintered and fused ash layers respectively, with Table 1 giving the sources of the data. The following points which are relevant to the spectral character of deposits are noted.

a) *For layer of powdered ash*, as shown in Fig. 5, emittance decreases with temperature as noted in Section 2. As previously noted this is a consequence of the spectral region of low emittance at low wavelengths. The trend is apparent for all samples, even for some powders (e.g., Fe_2O_3) that appear to be dark to the eye and therefore good absorbers in the optical spectrum.

b) *For sintered, fused and slag* layers are characterized by a total emittance greater than that of powders. The data for slags (set 2 on Fig. 6) indicates total emittance values between 0.9 and 1.0, with no obvious temperature dependence. This is consistent with a spectral emittance with little spectral variation.

3.2 Thermal Conductance

The thermal conductivity of ash deposits depends on the chemical composition, the physical state and texture, and the temperature of the deposit (6). At the high temperatures encountered in furnaces, radiation through the deposits is generally included in the values for the thermal conductivity (7), i.e., the effective thermal conductivity. Ash deposits may be divided into the following four categories (8) which define the physical state: relatively loose deposits; bonded deposits; slag deposits; and bonded slag deposits. Loose deposits are ash particles which adhere mechanically to surfaces and are easily removed. Bonded and bonded slag deposits are formed over long periods. Clearly, deposits are not uniform and the various bands will have different resistances to heat transfer.

The physical structure of deposits has a dominant effect on measurements as shown on Fig. 7 (7). The effects are best described in terms of the heating cycle used to obtain the particular results. The measurements are seen to be fairly independent of temperature below a temperature (usually 900°–1200°C) at which sintering occurs. Further heating above this temperature softens the sample and improves the contact between particles. After fusion, the sample has a higher thermal conductivity on cooling than the original particulate sample as it was heated. The chemical and physical changes therefore cause the thermal conductivity measurements to be irreversible over the heating and cooling cycle. The higher the temperature at which the cooling cycle starts, the higher the thermal conductivity on cooling.

The thermal conductivity of coal ash is compared with that of the powdered and fused oxides on Fig. 8. The particulate (region 1) as is seen to have a thermal conductivity below that of the oxides. The data of Mulcahy et al. (9) and Boow and Goard (10) clearly shows an increase of thermal conductivity with mean particle size as well as a decrease with porosity, the effect of particle size being greater. Silica ratio is important at high temperatures (7), where strong sintering and fusion can occur. However the thermal conductivity of actual furnace deposits (curve 2) is many times that of the particulates and is closer to that of the sintered or fused ash which, in turn, is close to the data for refractory bricks. A large variation in the reported values for the thermal conductivities of coal ash deposits is evident.

It has been mentioned above that the thermal conductivity of oxide mixtures is approximately weighted to the mass proportions of the oxides. However, for coal ash this correlation is not apparent probably because the ash is not composed of the oxides, even though an ash analysis which is obtained by analysis of the elements is generally reported in terms of equivalent oxides. That is, compounds such as glasses and salts are present, in addition to oxides. Anderson et al. (7) has also claimed that a simple correlation between the coal ash and its oxide components is not possible. For silica ratios greater than unity mixtures of the oxides show a continuous increase of thermal conductivity with temperature, indicating a significant contribution of silica. Some measurements show that the rate of increase of the thermal conductivity of coal ashes with temperature is greater than that for the pure oxides or bricks. This may be due to a temperature

related error in the hemispherical pyrometer method used for the coal ash and other uncertainties in the measurements (2), as data reported by Anderson et al. (7) indicate that the rate of increase is less than that for silica.

The data covering low porosities from Wain et al. (11) on Fig. 9 is for slags of differing chemical compositions and degree of crystallinity. The two variables of greatest importance are seen to be porosity and temperature. The data covering high porosities from Anderson et al. on Fig. 9 is for flyash and slag; experiments A and B were for flyash of size 13.5 and 25.5 μm; C, D, and E for crushed slags of different diameter and I for slag. The bars plotted on Fig. 9 cover the data in the temperature range 300°–900°C, with estimates increasing with temperature. Also indicated is the range of porosity for packings of monosize spheres. It is apparent that the thermal conductivity is increased by more than an order of magnitude over the range of porosity of the measurements. It may also be speculated that the porosity is indirectly related to deposit density, so that Fig. 9 may also have been plotted in terms of density.

The effective thermal conductivity of ceramics are also known to be influenced by their porous character (12), particularly when radiative transfer is significant. Other factors such as grain boundaries, mineralogical inhomogeneities, the distribution of phases, crystallographic orientations of grains and grain-grain interfaces have also been noted in these studies. Ash deposits have yet to be characterized in such detail although the effects mineralogical composition have been identified.

4.0 THE INFLUENCE OF THE DEPOSITION SEQUENCE, CHEMICAL AND PHYSICAL PROPERTIES

The data on total heat transfer properties may be used to estimate trends in properties as deposits initiate, grow and mature with the association of these properties on the chemical and physical character of the deposits. These associations provide insight for the way in which spectroscopic measurements may be interpreted.

Wall et al. (1) provide these speculations, which are given in Fig. 10. For a deposit-free wall (or tube), the absorbance is high, say 0.8. The initial deposit layer (b) is likely to be fine condensible salts or fine ash transported by the thermophorosis mechanism. For a particulate layer of 2 μm particles the absorbance may be less than 0.3. As the fine layer thickens and results in the collection of larger particles (which rebound from a thin layer) a layer of coarse ash © develops with an absorbance of, perhaps, 0.4–0.5. As this particulate layer builds to a greater thickness (d), the absorbance will not change but the conduction coefficient (k/x) will continue to reduce. During the development of this particulate layer, the temperature difference over the deposit, and therefore the temperature of its surface, will continuously increase. Sintering and fusion will result. Also a thick deposit is likely to leave an irregular (rough) surface. Therefore (e) both α and k/x will increase. Once the thickness builds, and temperature increases further, a liquid slag will develop. α and k will increase (f), and k/x may increase or decrease compared to its value for the sintered deposits. As shown by the horizontal arrows on Fig. 10, an intermediate steady state may develop during the deposit growth. For example, if the deposit does not sinter appreciably, the erosion rate of the deposit by large particles may balance the deposition rate and a permanent particulate character will result.

The spectral region of low emittance would therefore be expected to be present during all but the final (slagged) state indicated on Fig. 10.

5.0 PREVIOUS SPECTROSCOPIC STUDIES

Several recent studies have reported measurements of the spectral emittance of sampled ash and deposits in the laboratory, with in-situ measurements in pilot-scale and full scale combustors. Together with an understanding of the theoretical trends expected as deposits change their physical character as they mature - from powdery, to sintered, to a molten state - these allow an evaluation of the practical use of spectroscopic techniques.

Solomon and coworkers (12) have reported hemispherical spectral emittance measurements on samples of powdery ash and collected slag using an FTIR spectrometer. Measurements were made for powdered fly ash and the same ash, after heating to a fused state, and also a sintered slag sample, both heated to a molten state and crushed to a powder. The results, presented on Fig. 11, show a continuous increase in spectral emittance as a powder sinters, fuses and melts in the spectral region below 8 μm. The degree of sintering, and to what extent the surface is particle-like or glass-like, therefore controls the emittance in this region. They conclude that radiative properties depend on the surface morphology of the deposit with a minimal influence of chemical composition.

Baxter and coworkers (13) have measured the spectral emission of deposits formed on a rotating tube during a three hour period using an FTIR spectrometer. With increasing exposition time the estimated spectral emittance changes from that for a clean tube to that for an opaque ash layer, as shown on Fig. 12. The change in emittance at wavelengths greater than 7 μm is due to the changing chemical species on the deposit surface with spectral structure obvious on Fig. 12, which is related to the existence of sulfates and clays. The results are for initial deposits approximately 20–30 μm thick and indicate that information may be derived on the chemical nature of such deposits. Fig. 13 gives spectra for deposits which grow to a greater thickness, indicating that the banded spectra is lost as deposits thicken. This may be due to surface roughness. Also apparent on Fig. 13 is a progressive increase on emissivity at wavelengths less than 6 μm where Solomon and coworkers observed an influence of sintering.

As might be expected, experiments in pilot-scale and full scale combustors are more difficult to interpret. Clark et al. (14) report in-situ measurements in a pilot-scale combustor using a grating monochromator sighed onto a slag panel with deposits grown for periods up to 52 hours. The spectral in-situ measurements show wide variations in values at particular wavelengths, and it is not clear how the effects of reflected radiation is avoided. Measurements on powdery ash deposit samples showed a region of low emittance at low wavelengths as observed by Solomon, see Fig. 14. No banded structure was observed for the relatively mature deposits which were observed. The objective of the work was to prove an increase in emittance as deposits mature, this was achieved.

A series of papers report spectral emittance measurements for ash from Powder River Basin coals (15). It would appear the results are for powdered ash using an FTIR technique in the laboratory and a region of low emittance again corresponds to that observed by Solomon. In-situ

emittance results as low as 0.22 are also reported, but the details of the experimental technique are not given.

Recent theoretical predictions by Wall et al. (1) and Markam et al. (12) allow an interpretation of the above experimental results to be made. For a homogeneous smooth slab (which approximate a slag layer), spectral emittance predictions are 0.9 or greater, in agreement with measurements. Predictions for particulate layers given on Fig. 15 are based on the scattering of incident radiation by fine particles. Two predictions are given, the first for iron containing ash particles given on Fig. 15 predicts that the low wavelength region ($< 6\ \mu m$) observed in many studies on powders will be related to the fineness of the ash. Fine ash particles are more efficient scatters of radiation and therefore are characterized by low emittance estimates in this region. Predictions for a layer of $CaSO_4$ particles given on Fig. 16 show a banded spectra with features similar to that found in experiments (13).

6.0 THE POTENTIAL APPLICATIONS OF SPECTROSCOPIC TECHNIQUES

6.1 Identification of Deposit Character and Radiative Properties

The previous section has indicated that three types of properties might be identified by the emissive or reflective spectra from deposits, these being:

- Identification of aspects of *chemical character* (for example, salt and silicates)
- Identification of *physical character* (powdered, sintered, fused or molten)
- Measurement of *radiative properties* (emittance, absorbance or reflectance), and possibly temperature

The chemical character measurements may therefore yield information on the elements and compounds which are preferentially deposited, the identification of the physical character may monitor the changes associated with the development of strength in deposits. Both aspects may be used in strategies for optimizing cleaning (soot blowing) cycles in a practical plant. The on-line measurement of radiative properties will assist in the monitoring of the thermal performance of furnaces, and identifying coals and/or blends associated with performance problems. The properties monitored will clearly be those of the outer layers of the deposit, as determined by its transparency, but probably less than a depth of 0.5 mm.

6.2 Interpretation of Spectra

The previous experimental work and theoretical predictions allow us to identify the spectral features which may provide information on the three properties. These features include the presence of bands which are characteristic of molecular bonds and spectral effects associated with the interaction of electromagnetic radiation with the deposit, which is related to the physical character of the deposit. The spectral regions of interest depend on the particular property and are summarized on Table 2.

The infrared spectra of a vast number of minerals and pure compounds are known, with banded structure related to the bonding of the elements. For example, Vassallo and Finnie (16) have shown the similarity in spectra from sulfates. These features, together with those for clay minerals, are evident on Figs. 12 and 13.

It is not clear, at present, if the banded spectra suitable for extracting chemical information will be evident once deposits assume an irregular surface and reaction between the species have occurred. Indeed, this issue is to be investigated experimentally during the present study.

It is believed that the above understanding is sufficient to allow spectra to be interpreted even though chemical and physical properties influences may overlap, or occur together during deposit growth. Changes in spectra observed as deposits grow will clearly be easier to interpret than a single spectra.

6.3 Measurements of Reflected or Emitted Radiation

As is apparent in Fig. 1, the radiation leaving the deposit surface, which may be detected by an FTIR, comprises reflected and emitted beams. For most practical situations the magnitude of the incident radiation from the flame or hot furnace gases, and therefore the reflected radiation, exceeds the emitted radiation. This will certainly be so for initial deposits, and until the deposit surface temperature increases with deposit growth. For mature thick deposits the leaving radiation will comprise both reflected and emitted radiation.

For deposit covered tubes in the ash fouling furnace duct of the EERC, calculations predict that the leaving radiation will be comprised of 86–90% of reflected radiation, 10–20% emitted radiation. This necessitates the measurement of both incident as well as leaving radiation to estimate reflectivities. A similar conclusion was reached by Shaw and Smouse (17) who decided to shroud the incident energy so that only emitted energy was detected.

6.3.2 Measurement Geometry

For measurements taken in either pilot-scale or full-scale combustors, geometric effects are expected to influence measured spectra. Deposits may approximate diffuse reflectors and emitters – radiation is independent of direction – however the incident radiation is commonly direction dependent. Consider the geometry depicted for the measurements on Figure 17, with a measurement system comprising a probe having an acceptance angle of 40° sighting onto tubes from a number of locations. At location 1, the system will see tubes and refractory, at location 2, two tubes and location 3, one tube only. The incident radiation from the furnace and that reflected from the refractory walls of the duct, will bathe the front surfaces of the tubes. The rear of the tubes will see only refractory. The reflected radiation from tubes will therefore depend on the view the measurement system has of the tubes. Measurements onto tube banks in practical systems will have similar problems.

The only geometry which may avoid these problems would be that of a large furnace with a probe having optics such that it sighted onto a wall from a distance. This appears to be the approach attempted by the cleaning advisor available from the Diamond Power Speciality Company, which is used to monitor the reflectance of walls adjacent to sootblowers.

Due to the above geometrical problems, the following approach to interpretation of on-line spectra is recommended.

1. Note *changes in spectra* with time and relate these changes in deposit chemistry and morphology.

2. Note *spectral features* (particularly bands) and relate these to deposit chemistry.

These changes and features, it is believed, should indicate the physical and chemical processes during ash deposited, and the processes leading to strength development. These should be sufficient for a deposit monitor used to assist scheduling for soot-blowing. In order to assist in the interpretation of spectra deposits, deposits should also be collected and analyzed to check conclusions made based on the spectra. Removable metal coupons, on which deposits are collected, could also be attached to tubes. Emission FTIR spectra measurements on these deposits would be compared to the on-line spectra.

6.4 Potential and Necessity for the Measurement of Conductive Properties

The measurement of the thermal conductivity (k) of a deposit is based on one-dimensional heat transfer, as described by Eq. 2 in total radiation terms. The measurement of Q, (say, by heat flux meter), T_s (by thermocouple or spectroscopic technique, see Markahm et al.[12]) and x therefore allows estimates of k. Alternatively Q may be estimated by the radiative balance represented by the extreme RHS of this equation, necessitating the measurement of incident and reflected radiation.

Again geometrical problems arise. Although multi-dimensional heat transfer data can be theoretically related to the thermal conductivity of the medium via analysis using mathematical models, we are not aware of this having been attempted. For the 'wedge' shaped deposits found growing from the stagnation point of tubes the heat transfer process is multidimensional. For the reasons outlined in the previous section, it is believed that the data from a deposit monitor need not be interpreted in terms of the transport properties involved. Rather, changes monitored as deposits grow should be satisfactory.

7.0 CONCLUSIONS

Several recent studies, both theoretical and experimental, indicate that measurements of the spectral radiation leaving a deposit surface is related to the chemical and physical nature of the deposits. Measurements of the spectra and changes (with time) may therefore be interpreted to provide information on this character and possibly the radiative properties of the deposit. Different spectral regions may provide information on the physical and chemical character. This character is related to the deposit tenacity and strength and therefore may be used to optimize cleaning (soot-blowing) cycles.

The determination of radiative properties (such as absorptivity and reflectively) is complicated by the geometry of the measurements and the need to measure incident radiation as well as leaving (reflected and emitted) radiation.

8.0 REFERENCES

1. Wall, T.F., Bhattacharya S.P., Zhang D.K., Gupta R.P., He X., Prog. Energy Combust Sci. (in press).

2. Wall T.F., Lowe A., Wibberley L.J. and Stewart I, McC, Prog. Energy Combust Sci., Vol, 5 pp 1-29, 1979.

3. Hottel, H.C. and Sarofim, A.F. Radiative transfer, McGraw-Hill, 1967.

4. Brewster, M.Q., Thermal radiative transfer and properties, John Wiley, 1992.

5. Wall T.F. and Becker H.B., J. Eng. Gas Turbine Power, Vol. 106, p771, 1984.

6. Jakob M. And Hawkins G.A., Elements of heat transfer, John Wiley & Sons, New York, 1957.

7. Anderson D.W., Viskanta R. And Incropera F.P., Journal of Eng. For Gas Turbines and Power, Vol. 109, p215, 1987.

8. Ots A.A. et al, Teploenergetica, Vol. 20, p2, 1973.

9. Mulcahy M., Boow J. And Goard P.R.C., J. Inst Fuel, Vol. 39, p385, 1966.

10. Boow J. and Goard P.R.C., J. Inst. Fuel, Vol. 42, p412, 1969.

11. Wain S.E., Livingston W.R., Sanyal A. And Williamson J., in Inorganic transformation and ash deposition during combustion, (Ed. Steven A. Benson), Engineering Foundation, p459, 1991.

12. Markham J.R., Best P.E., Solomon P.R. and Yu Z.Z., J. Heat Transfer, Vol. 114, p458, 1992.

13. Richards G.H., Harb J.H., Baxter L.L., Bhattacharaya S., Gupta R.P., Wall T.F., Radiative Heat Transfer in PC Fired Furnaces - Development of the Absorptive/Reflective Character of Initial Ash Deposits (to be presented at 25th (Int) Symp. Combustion, Irvine, 1994).

14. Clark G.A. er al, In-situ Measurements of Coal Ash Deposit Optical Properties, US DOE Report, DOE/PC/79902-77, 1989.

15. Carter H.R., Kokoal C.G., Garrabrent M.A., ASME Paper 92-JPGC-Pwr 35, 1992.

16. Vassallo A.M., Finnie K.S., Infrared Emission Spectroscopy of some Sulfate Minerals, Applied Spectroscopy, 46 (10), 1477-1482, 1992.

17. Shaw and Smouse.

Table 2 Summary of data source for emittance

Figure Notation	Sample description: Size (μm)	Composition (%): SiO_2	Al_2O_3	Fe_2O_3	CaO	MgO	Na_2O	K_2O	SO_3	References and methods	Remarks
Powdery ash deposits (Figure 21)											
1-1	~4.5				ND					Street & Twamley[34], two colour pyrometery	•
1-2	~3.5				ND						•
2-1	ND				ND					Mitor and Konopel'ko[35] emission method	**
2-2	ND				ND						**
3-1	as	41.0	26.0	13.3	8.94	2.31	3.11	0.92	0.72	Mulcahy et al[27]-hemi-	•
3-2	received				as above					spherical pyrometer method	•
3-3	(<422)				as above					water cooled probe deposits	•
3-4	211-422	45.0	23.7	5.00	25.0	0.00	0.00	0.00	0.00	crushed synthetic slags	•
3-5	104-211				as above						•
3-6	53-104				as above						•
3-7	< 44				as above						•
3-8	53-104	47.4	23.7	0.20	23.7	0.00	0.00	0.00	0.00	Synthetic slag for	•
3-9	53-104	50.0	25.0	0.00	25.0	0.00	0.00	0.00	0.00	Fe_2O_3 effect	•
3-10	as	Leigh Creek SA. open cut coal: Blend D								Combust. chamber deposits	•
3-11	received	as above								primary superheater deposits	•
3-12	(<422)	as above								electrostatic precipitator dep.	•
3-13		Leigh Creek SA. open cut coal: Lobe C west								ash prepared in laboratory	•
3-14		Garrick SM, Prospecting tunnel, Qld									•
3-15		Victoria Tunnel, Lambton, NSW									•
4-1	as	58.0	28.0	2.90	1.20	0.50	1.30	2.70	2.40	Godridge & Morgan[36]	•
4-2	received	42.0	27.0	7.50	8.60	2.20	1.50	2.90	1.10	hemispherical method	•
4-3		46.0	29.0	7.80	8.50	2.20	1.60	3.20	1.30		•
4-4		47.0	30.0	1.40	11.0	2.70	0.80	2.30	2.40		•
4-5		54.0	30.0	3.80	3.90	0.80	0.80	1.50	4.40		•
4-6	120	62.0	26.0	4.80	3.60	1.30	0.40	1.00	1.10		•
4-7	33	57.0	33.0	2.50	2.00	0.40	0.90	1.70	2.60		•
4-8	6.5	62.0	30.0	2.10	1.80	0.30	0.90	1.70	0.90		•
SiO_2	ND	(pure oxides and sulfates)								Wall et al [2]	
Al_2O_3	15-80										
Fe_2O_3	ND										
CaO	3-5										
MgO	90-120										
$CaSO_4$	ND										
Na_2SO_4	63-90										
Sintered and fused (slag) layers (Figure 22)											
1-1					ND					Goetz[7], hemisph. method	**
1-2					ND					pilot scale furnace deposits	**
2-1		52.2	11.0	23.7	7.22	0.00	0.00	2.23	2.56	Markham et al[8], FTIR	**
2-2		52.2	11.0	23.7	7.22	0.00	0.00	2.23	2.56	emittance measurements	**
2-3		59.3	11.1	21.0	4.96	0.00	0.05	2.04	0.09		**
2-4.1		56.2	18.2	14.7	4.13	1.47	2.76	1.47	0.12	ε_λ data integrated using	**
2-4.2					as above					Eq. (5) at sample surface	**
2-4.3					as above					temperatures	**
2-4.4					as above						**
2-5		70.6	17.1	2.53	4.32	0.00	2.11	1.55	0.94		**
2-6					as above						**

Note: ND - Not Determined; • - normal emittance; ** - hemispherical emittance.

TABLE:2: Suggested character - spectra relationships

Deposit	Illustrative properties monitored	Analysis of spectra which is necessary	Relevant Wavelength region (μm)	References
1. Chemical character	Salts (SO_4^{--}, CO_3^{--}), aluminosilicates	Identified by location (μm) of bands in spectra	8 - 20	Baxter (1992, 1993)
2. Physical character	Transformation of Powdery deposits to sintered/fused deposits and molten slags	The magnitude, and trends with time, at spectral region outside bands of 1	< 8	Richards et al (1994)
3. Radiative properties	Emissivity, absorptivity, reflectivity, emissive power, temperature	Spectral radiation is integrated w.r.t black body function to obtain properties	Full thermal spectrum required, say, 1.5-15 μm	Wall et al (1993)

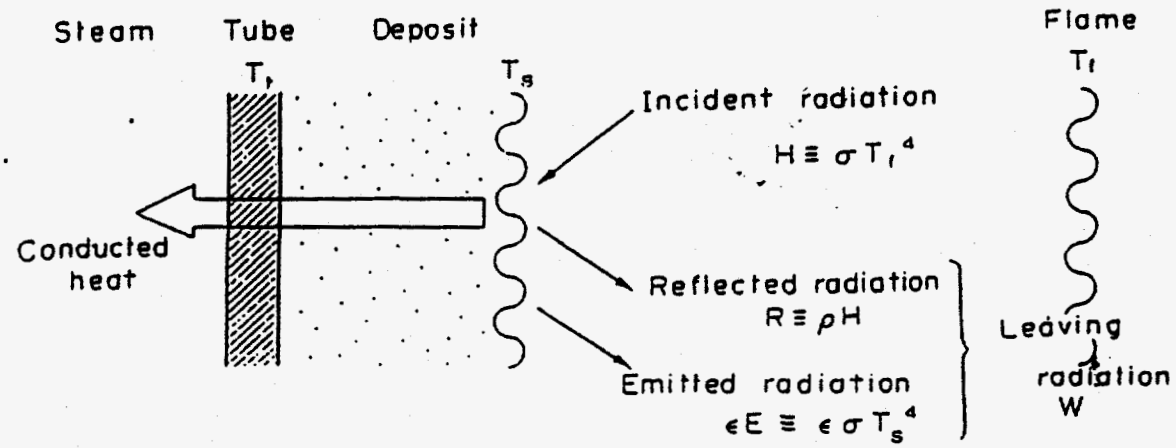
Steam
Tube
Deposit
Flame
T_f
T_t
T_s
Incident radiation
$H \equiv \sigma T_f^4$
Conducted heat
Reflected radiation
$R \equiv \rho H$
Leaving radiation
W
Emitted radiation
$\epsilon E \equiv \epsilon \sigma T_s^4$

Fig 1

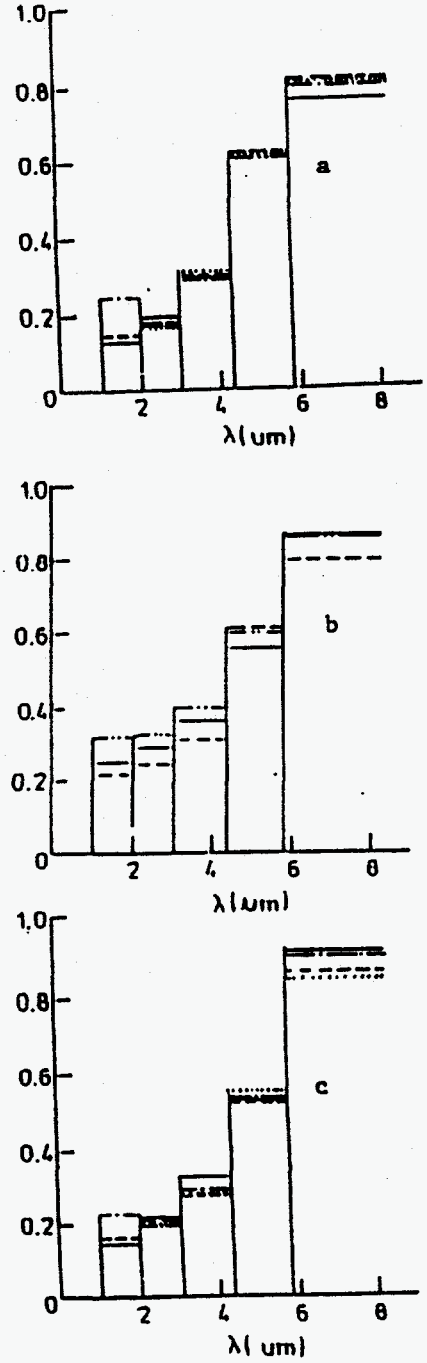

WE NEED FIGURE LEGEND, PLEASE.

Fig 2

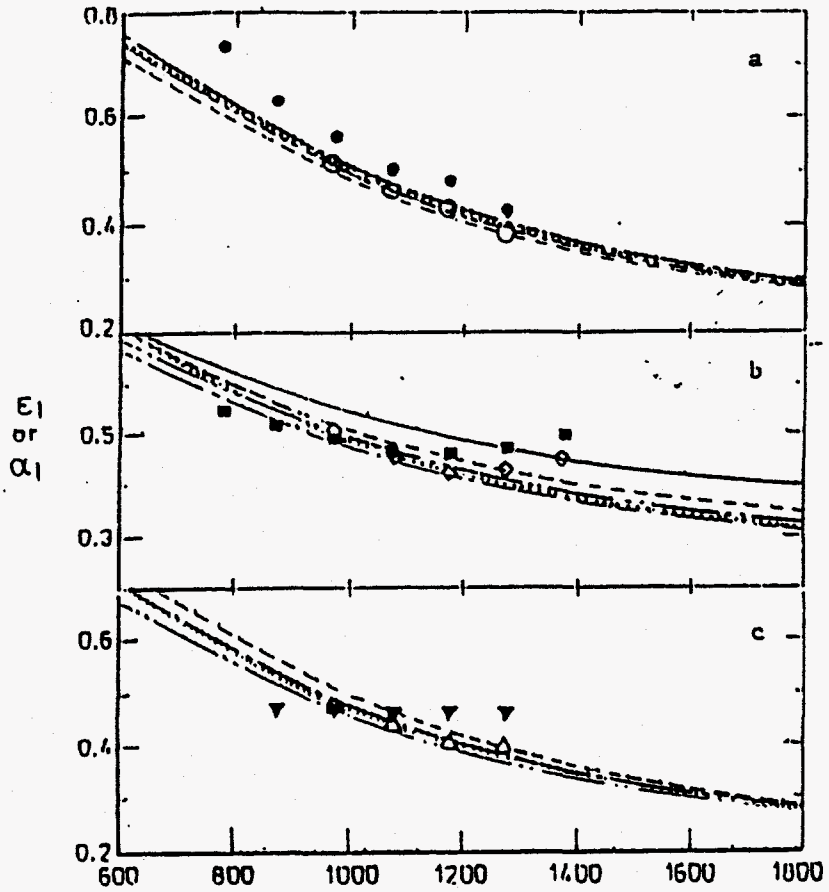
0.8
0.6
0.4
0.2
a
b
c
ε_1 or α_1
0.5
0.3
0.6
0.4
0.2
600
800
1000
1200
1400
1600
1800
SOURCE TEMPERATURE T_F, K. for α_1
ASH TEMPERATURE T_s, K. for ε_1

Fig 3

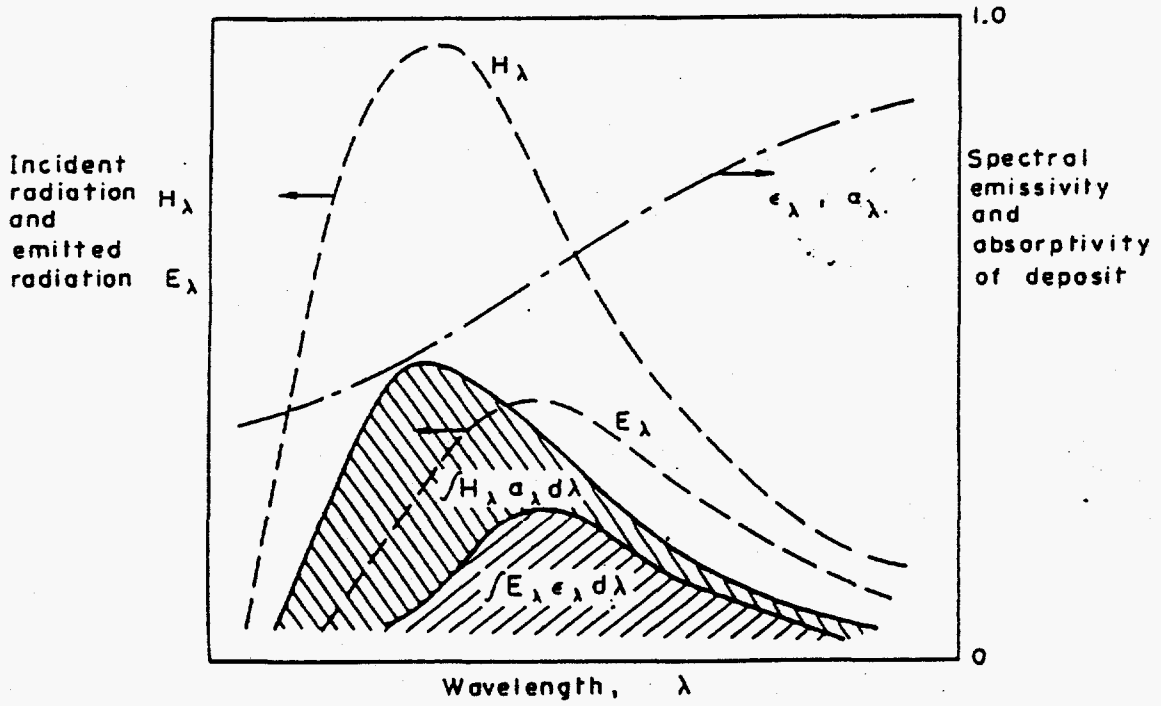
1.0
H_λ
Incident radiation and emitted radiation H_λ E_λ
ϵ_λ , a_λ
Spectral emissivity and absorptivity of deposit
E_λ
$\int H_\lambda a_\lambda d\lambda$
$\int E_\lambda \epsilon_\lambda d\lambda$
0
Wavelength, λ

Fig 4

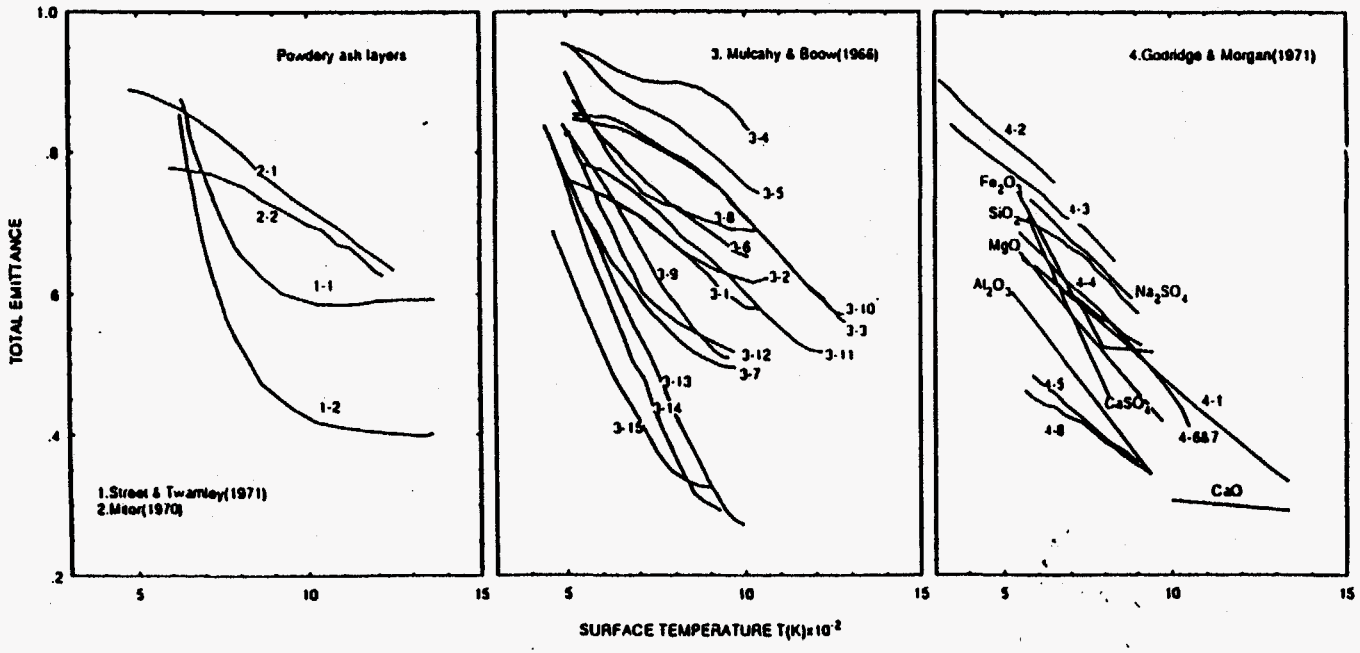
Powdery ash layers
2-1
2-2
1-1
1-2
1.Street & Twamley(1971)
2.Mean(1970)
3. Mulcahy & Boow(1966)
3-4
3-5
3-8
3-6
3-9
3-2
3-1
3-10
3-3
3-11
3-12
3-7
3-13
3-14
3-15
4.Goodridge & Morgan(1971)
4-2
Fe_2O_3
SiO_2
MgO
Al_2O_3
4-3
4-4
Na_2SO_4
4-5
$CaSO_4$
4-1
4-6&7
4-8
CaO
TOTAL EMITTANCE
1.0
.8
.6
.4
.2
5
10
15
SURFACE TEMPERATURE T(K)x10^{-2}

Fig 5

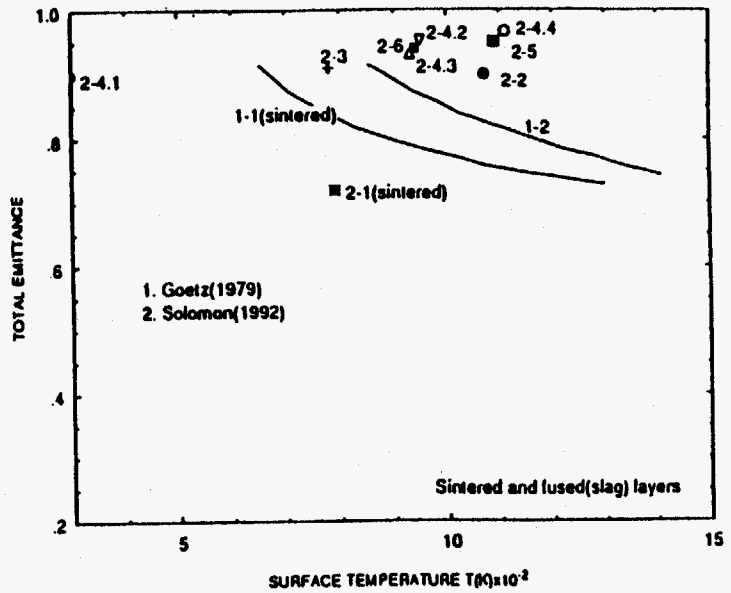

Fig 6
Page 22
Fig 6

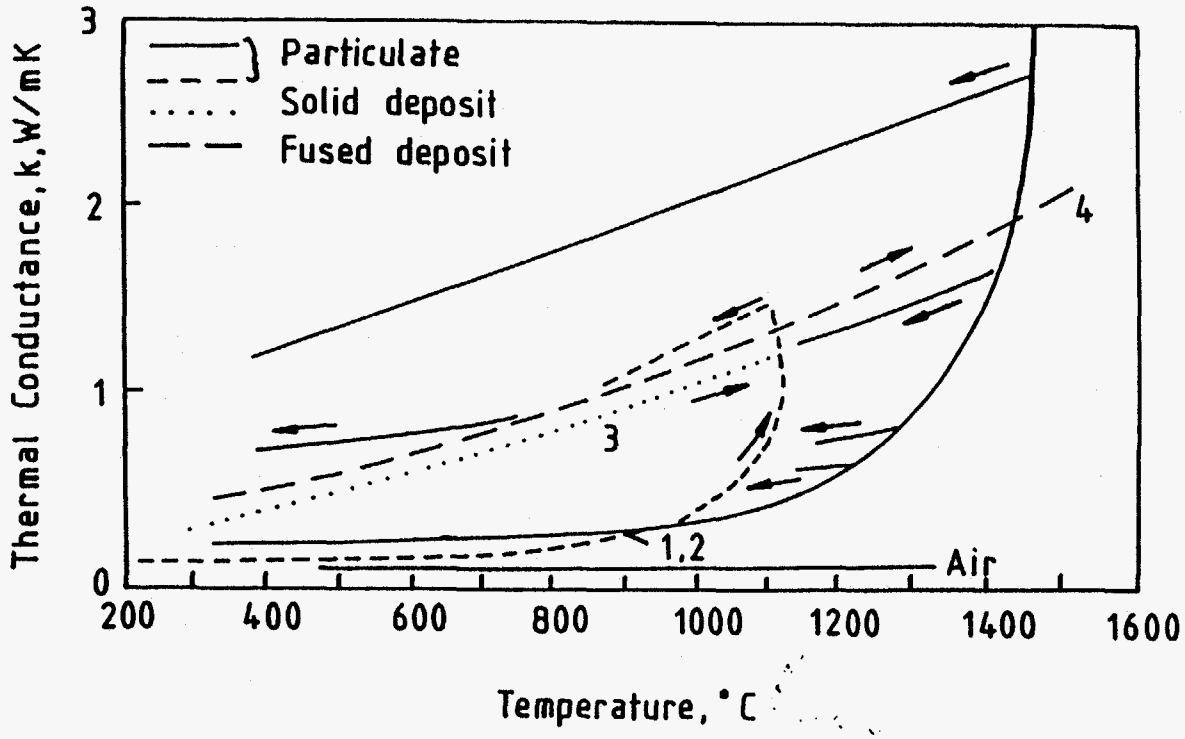
Particulate
Solid deposit
Fused deposit
Thermal Conductance, k, W/mK
Temperature, °C
3
2
1
0
200
400
600
800
1000
1200
1400
1600
4
3
1,2
Air

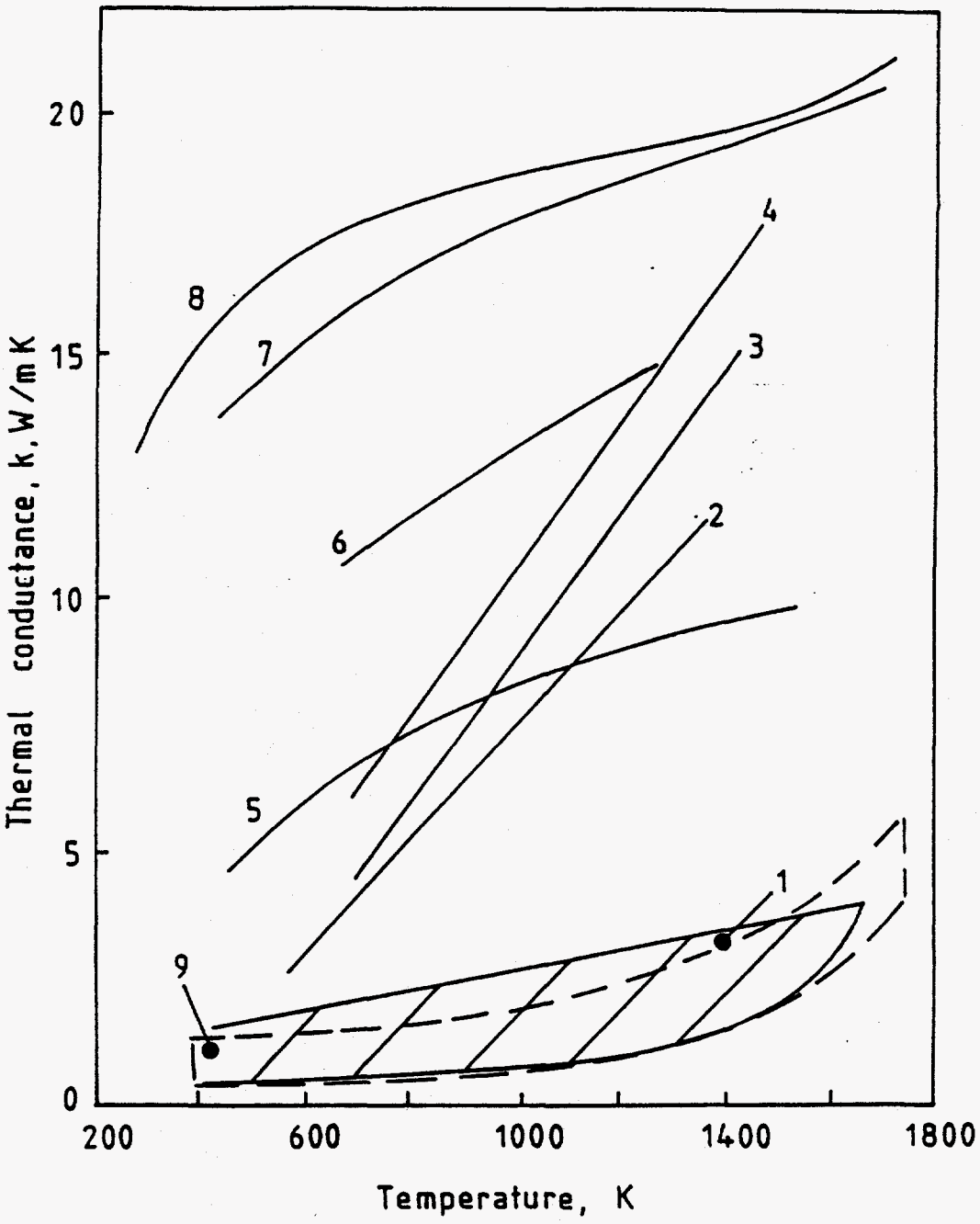

Fig 8

~~Fig 16~~

~~Fig 8~~

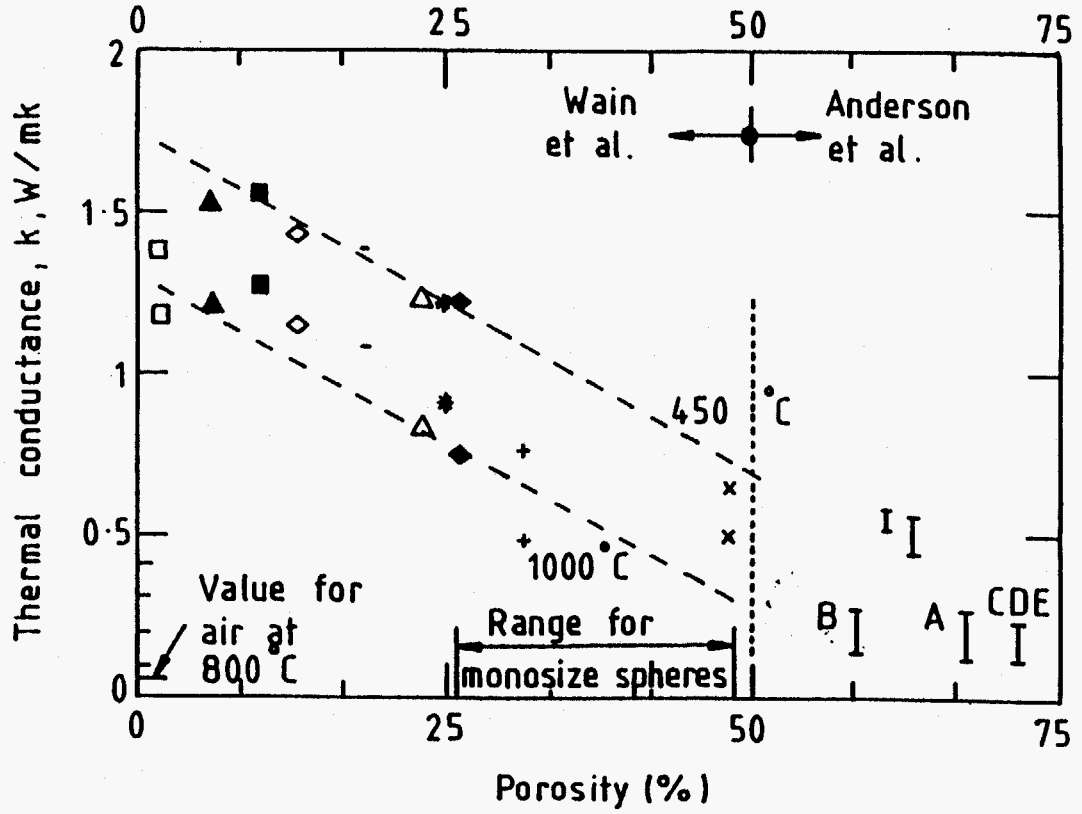
Thermal conductance, k, W/mk
Porosity (%)
0
25
50
75
2
1·5
1
0·5
0
Wain et al.
Anderson et al.
450 °C
1000 °C
Value for air at 800 °C
Range for monosize spheres
I
B
A
CDE

Fig 5

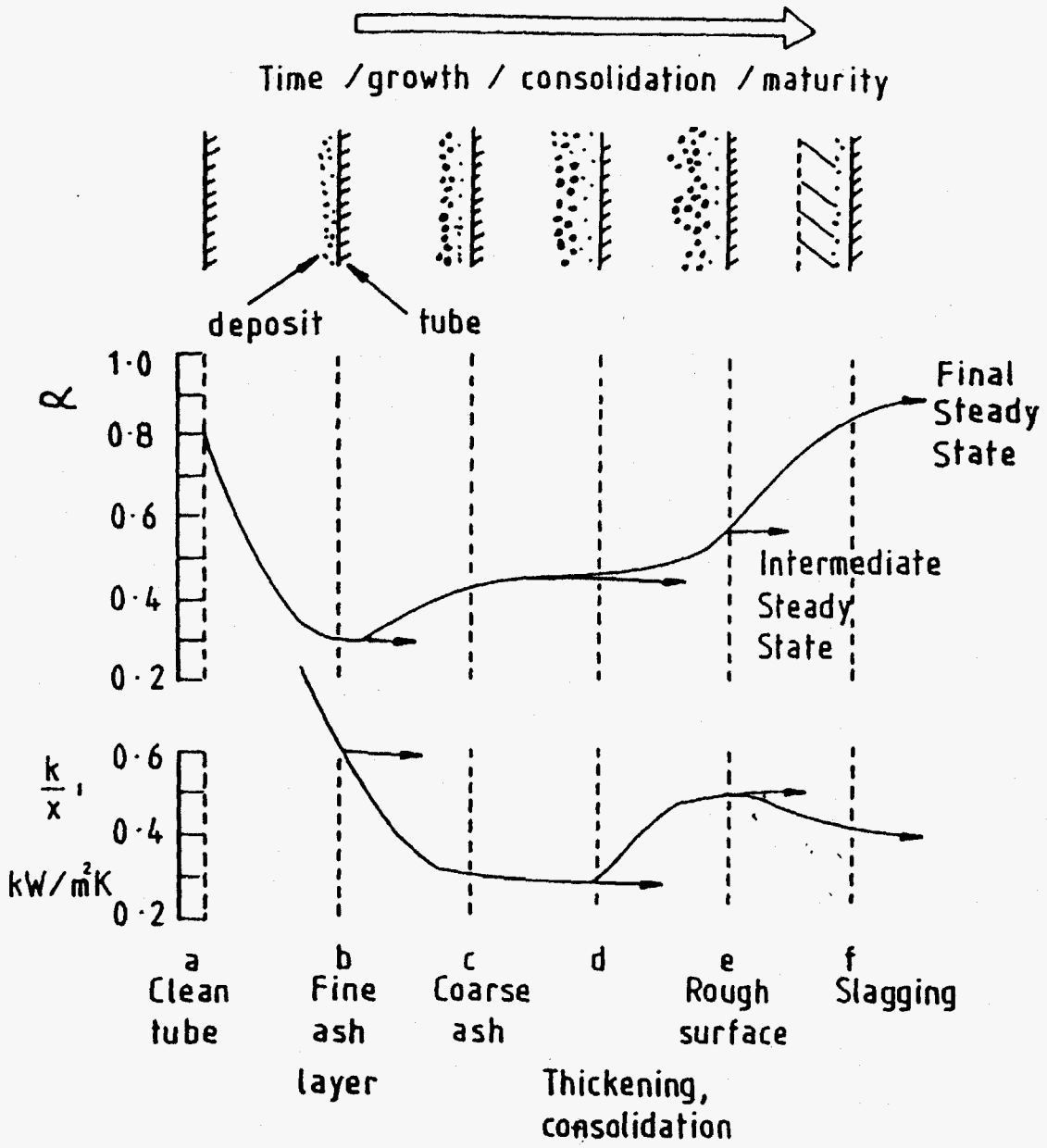
Time /growth / consolidation / maturity
deposit
tube
α
1·0
0·8
0·6
0·4
0·2
Final Steady State
Intermediate Steady State
k/x,
kW/m²K
0·6
0·4
0·2
a
Clean tube
b
Fine ash layer
c
Coarse ash
d
e
Rough surface
f
Slagging
Thickening, consolidation

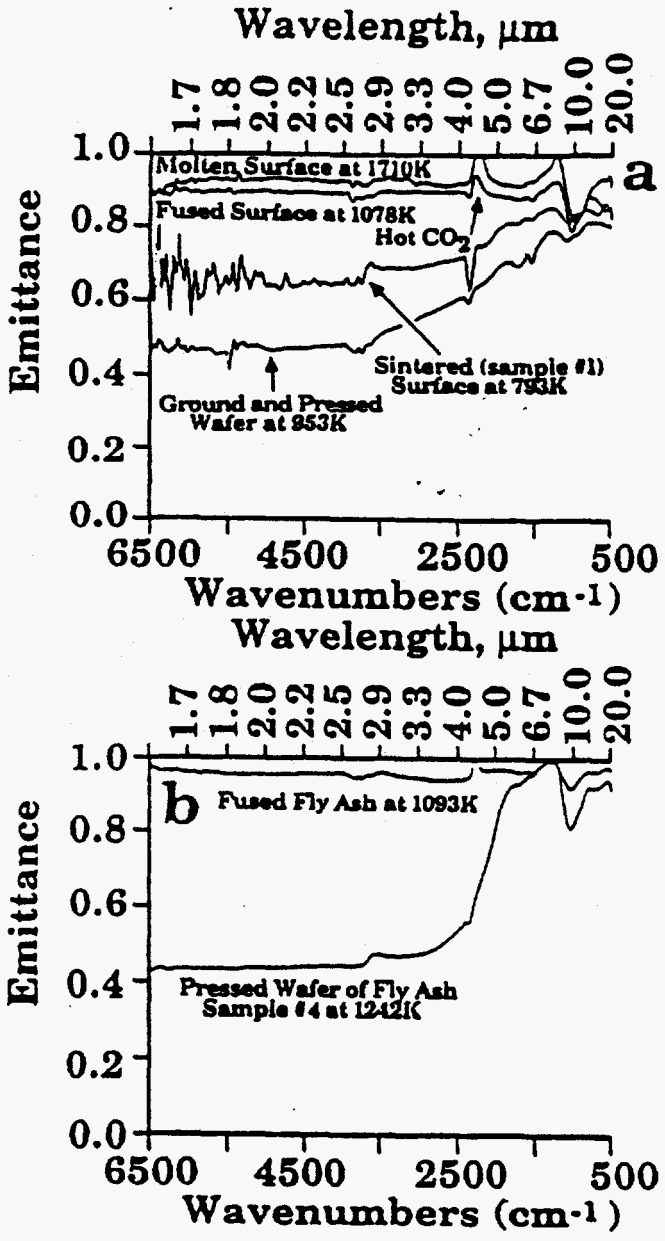

Fig. 4 Measured spectral emittance for (*a*) sintered slag deposit (sample #1) compared to the material after grinding and pressing into a wafer; and after thermally fusing the material, and (*b*) powdery ash (sample #4) compared to the emittance after thermally fusing the material

Fig 11

position (see Table 2). This indicates that the morphology of the deposit surface dominates the emittance characteristics.

Analysis of Growing Deposits. The influence that particle-like deposits will have on the emittance of a surface was readily demonstrated. The measurements technique was also applied to show the change in spectral emittance (and hence, in heat absorption rate) for a surface as the ash deposit thickness was increased. Measurements were performed on a heavily oxidized stainless steel surface after subjecting it to impaction with the

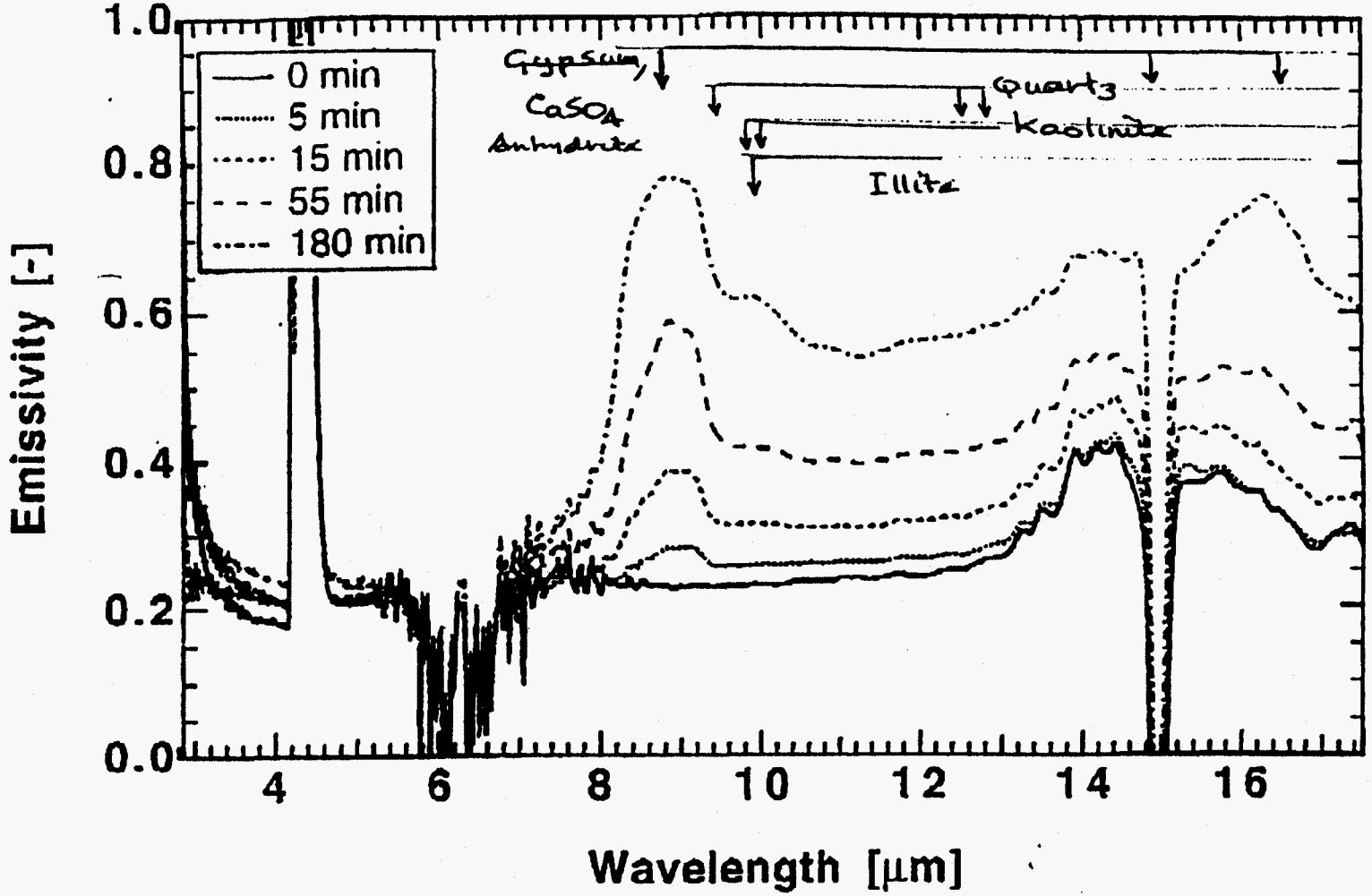

Fig 12 : Spectra from deposit from Antelope coal with bands indicated for particular species from Vassallo and Finlayson

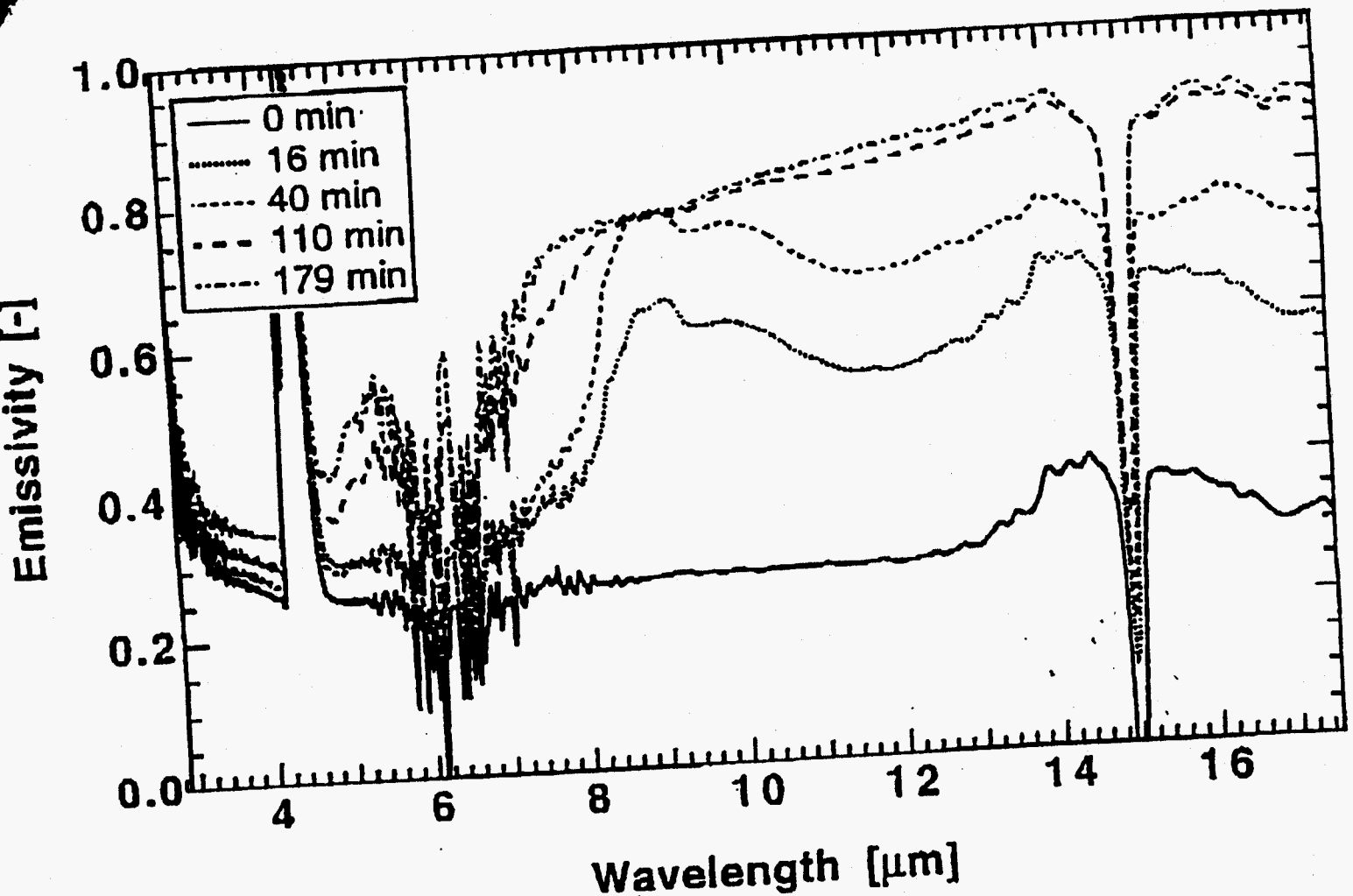
0 min
16 min
40 min
110 min
179 min
Emissivity [-]
Wavelength [µm]
1.0
0.8
0.6
0.4
0.2
0.0
4
6
8
10
12
14
16

Laboratory Spectral Emittance Measurements

Powdery Deposit Sample on Oxidized SS Plate

Temperature = 856 Deg. F

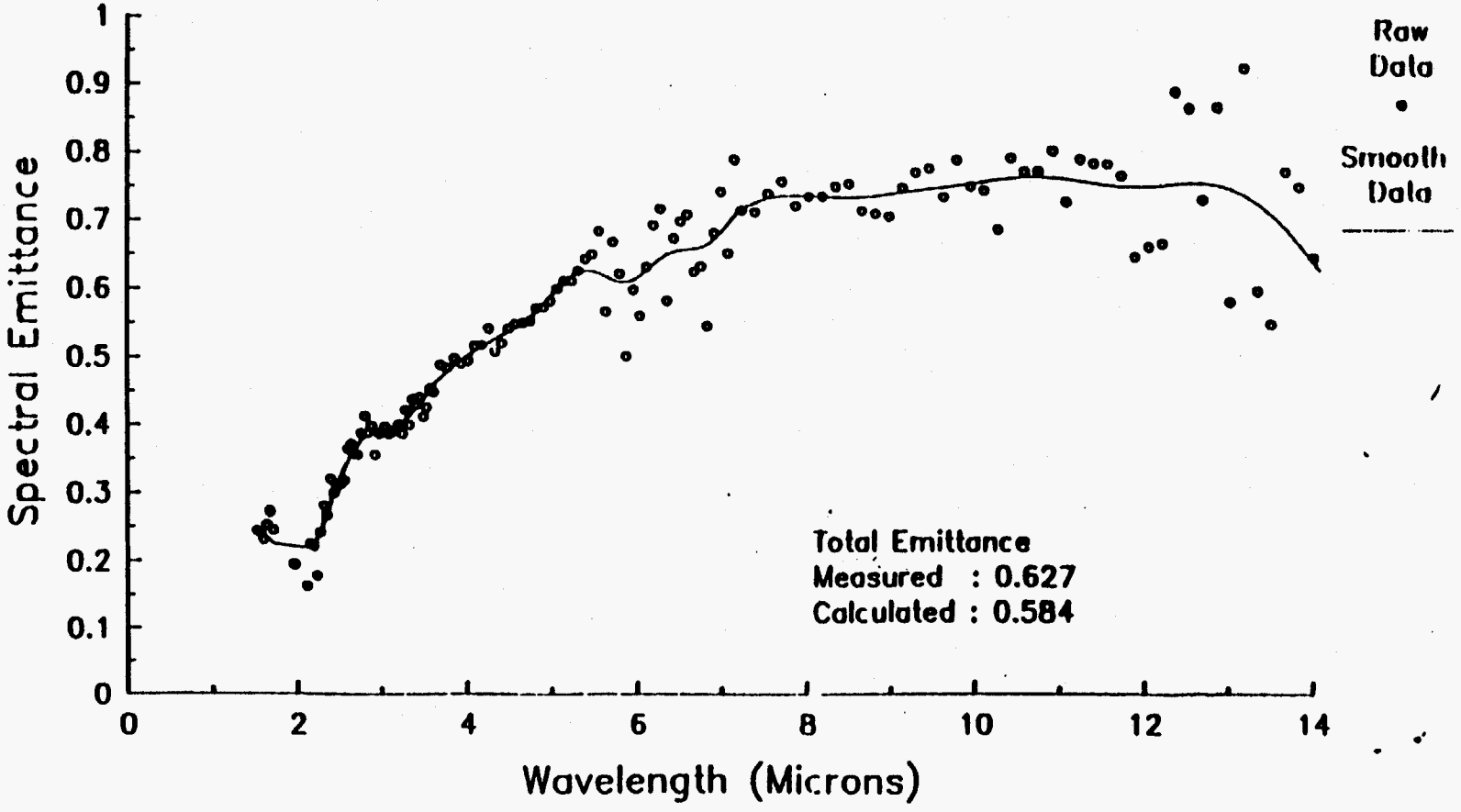

Babcock & Wilcox a McDermott Company
Research and Development Division
Alliance Research Center

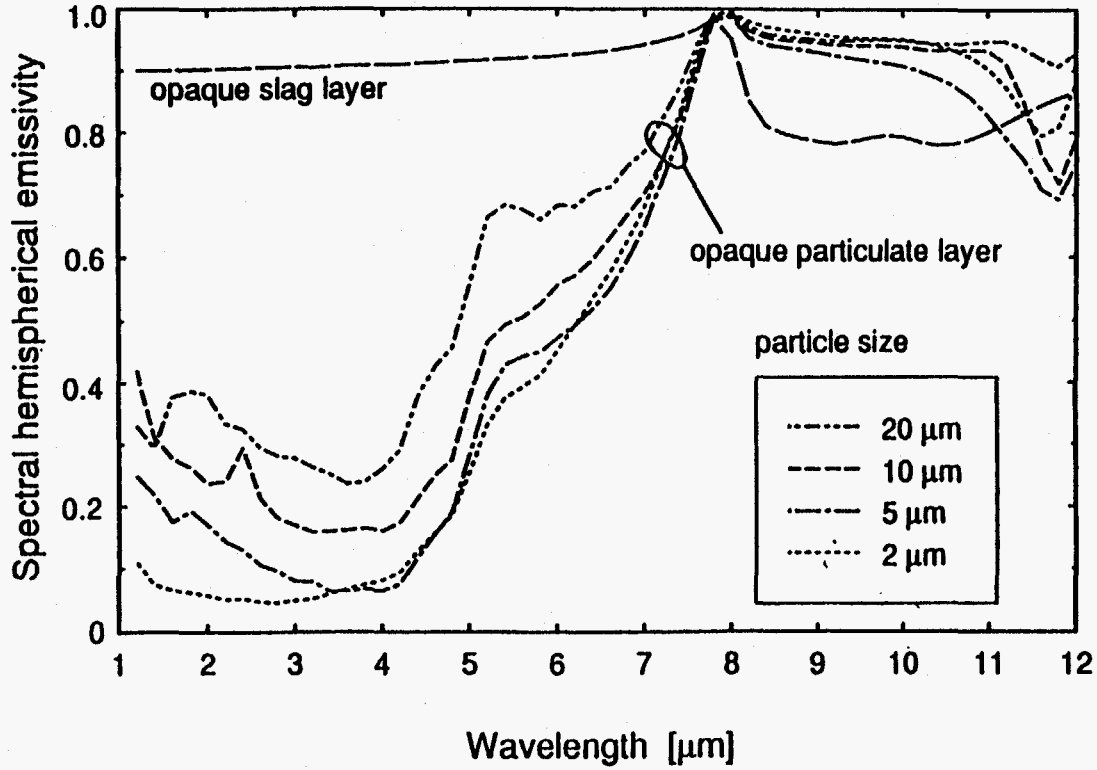
Spectral hemispherical emissivity
1.0
0.8
0.6
0.4
0.2
0
1
2
3
4
5
6
7
8
9
10
11
12
Wavelength [μm]
opaque slag layer
opaque particulate layer
particle size
20 μm
10 μm
5 μm
2 μm

Fig 15

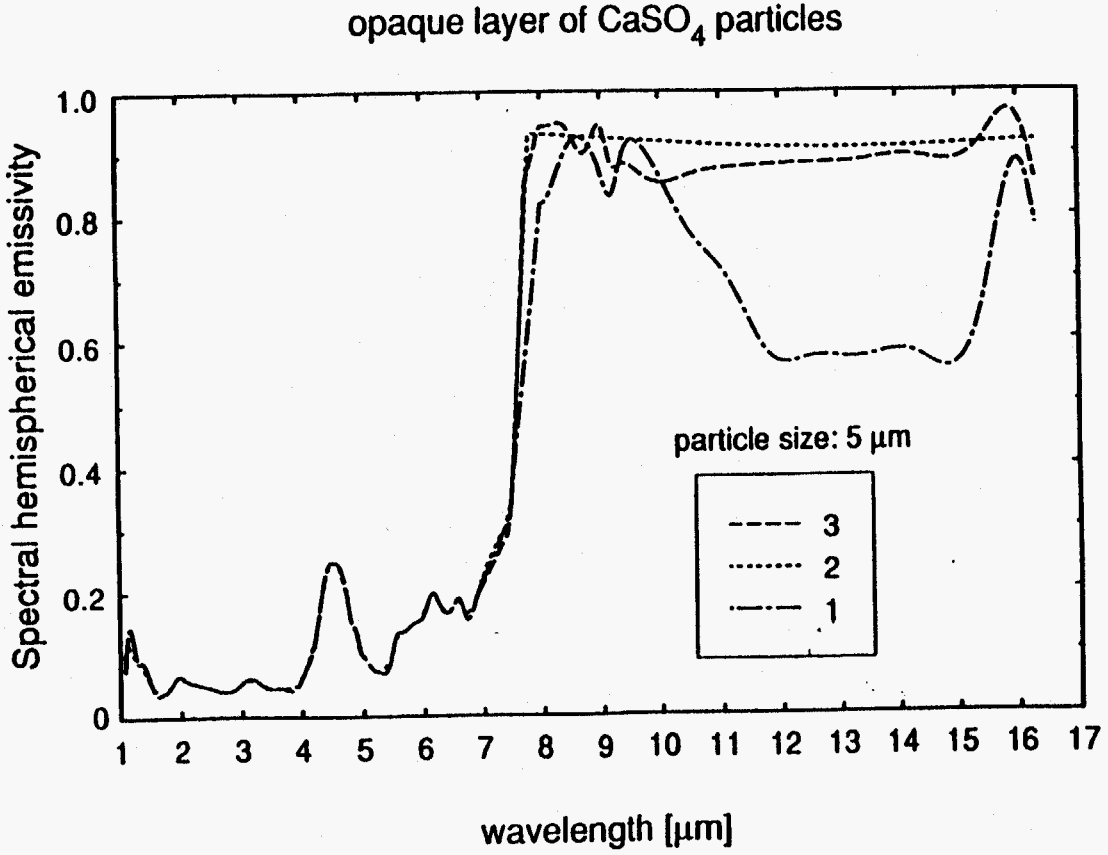
opaque layer of $CaSO_4$ particles
Spectral hemispherical emissivity
1.0
0.8
0.6
0.4
0.2
0
1 2 3 4 5 6 7 8 9 10 11 12 13 14 15 16 17
wavelength [μm]
particle size: 5 μm
3
2
1

Fig 16

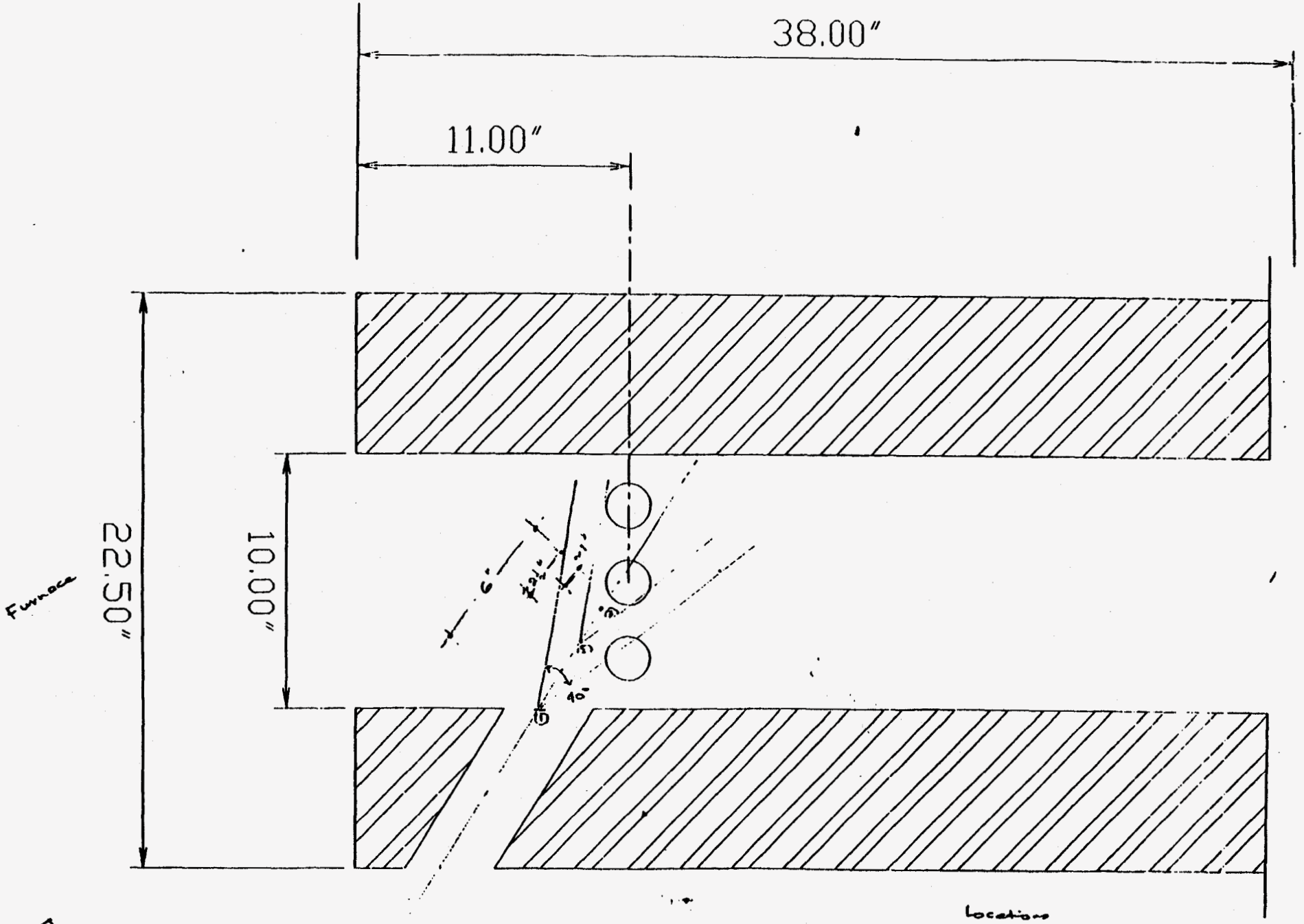

Locations

1. At hole opening.
2. Where tubes only are seen
3. Sight on angled tubes.

APPENDIX E

COAL AND ASH ANALYSES

TABLE 1

Proximate and Ash Analyses of Antelope Subbituminous and Illinois No. 6 Bituminous Coals

Sample	Antelope Subbituminous		Illinois No. 6 Bituminous	
Proximate Analysis	As-Received	Moisture-Free	As-Received	Moisture-Free
Moisture, wt%	27.8	--	3.4	--
Volatiles, wt%	32.8	45.4	40.5	42.0
Fixed C, wt%	34.8	48.2	45.3	46.9
Ash, wt%	4.6	6.4	10.8	11.1
Ash Analysis	% Elemental	Oxide % of Ash	% Elemental	Oxide % of Ash
Silica, SiO_2	15.0	32.0	23.6	50.4
Aluminum Oxide, Al_2O_3	8.2	15.5	10.2	19.4
Ferric Oxide, Fe_2O_3	2.8	4.0	13.2	18.8
Titanium Oxide, TiO_2	0.5	0.9	0.5	0.8
Phosp. Pentoxide, P_2O_5	0.7	1.6	0.2	0.6
Calcium Oxide, CaO	20.3	28.4	3.5	4.9
Magnesium Oxide, MgO	4.0	6.6	0.7	1.2
Sodium Oxide, Na_2O	0.8	1.0	2.8	3.7
Potassium Oxide, K_2O	0.4	0.4	1.5	1.8
Sulfur Trioxide, SO_3	3.8	9.5	1.2	3.1
Total, wt%	56.4	100.0	57.4	104.6

TABLE 2

XRD Analysis of Ash Deposits

Coal	Phases	Mineral Name	Nominal Composition
Antelope	Major	Quartz	SiO_2
		Melilite	$Ca_2(Mg,Al)(Al,Si)_2O_7$
	Minor	Anhydrite	$CaSO_4$
		Periclase	MgO
		Calcium Aluminum Oxide	$CaAl_2O_4$
		Calcium Magnesium Silicate	$Ca_5MgSi_3O_{12}$
		Plagioclase	$(Ca,Na)(Al,Si)_4O_8$
		Wollastonite	$CaSiO_3$
		Dolomite	$CaMg(CO_3)_2$
	Amorphous	Unidentified (small amount)	
Illinois No. 6	Major	Hematite	Fe_2O_3
	Minor	Quartz	SiO_2
		Mullite	$Al_6Si_2O_{13}$
		Merwinite	$Ca_3Mg(SiO_4)_2$
	Amorphous	Unidentified (large amount)	

TABLE 3

XRF Analysis of Feed Coal and Ash Deposits

	Antelope Subbituminous		Illinois No. 6 Bituminous	
Compound	Feed % Elem.	Dep. % Elem.	Feed % Elem.	Dep. % Elem.
Silica, SiO_2	15.0	14.8	23.6	24.4
Aluminum Oxide, Al_2O_3	8.2	6.4	10.2	9.7
Ferric Oxide, Fe_2O_3	2.8	4.5	13.2	13.6
Titanium Oxide, TiO_2	0.5	0.7	0.5	0.4
Phosp. Pentoxide, P_2O_5	0.7	0.2	0.2	0.0
Calcium Oxide, CaO	20.3	27.2	3.5	2.9
Magnesium Oxide, MgO	4.0	3.6	0.7	0.5
Sodium Oxide, Na_2O	0.8	0.1	2.8	0.0
Potassium Oxide, K_2O	0.4	0.2	1.5	1.7
Sulfur Trioxide, SO_3	3.8	1.0	1.2	0.0
Total	56.4	58.6	57.4	53.3